UNIVERSITÀ DI PARMA

UNIVERSITA' DEGLI STUDI DI PARMA

DOTTORATO DI RICERCA IN INGEGNERIA INDUSTRIALE

CICLO XXV

Innovative solutions for the optimization of heat transfer processes in food industry

Coordinatore:

Chiar.mo Prof. Gianni ROYER CARFAGNI

Tutor:

Chiar.ma Prof. Sara RAINIERI

Co-tutor:

Chiar.mo Prof. Ing. Fabio BOZZOLI

Dottorando: Dr. Matteo MALAVASI

Anni Accademici 2019 /2020 – 2021/2022

List of contents

CHAPTER 1: Introduction: Thermal processes in food industry and their optimization 1

References 11

PART I:

TRIPLE TUBE HEAT EXCHANGER FOR FOOD INDUSTRY 15

CHAPTER 2: Thermal aspects of three tube heat exchangers 18

2.1 Heat exchangers in food industry 18

2.2 Three tube heat exchangers 23

CHAPTER 3: Inverse heat transfer problems (IHTPs) and parameter estimation 30

CHAPTER 4: Thermal characterisation of Triple Tube Heat Exchangers by parameter estimation approach 48

4.1 Heat exchanger model 48

4.2 Parameter estimation and sensitivity analysis for the characterisation of TTHE behaviour 57

4.3 Application of the parameter estimation procedure to synthetic data 63

4.4 Application of the parameter estimation approach to experimental data 74

4.5 Parameter estimation extension: 4 and 6 parameters 83

CHAPTER 5: Closure 95

References 97

PART II:

FERMENTER FOR OENOLOGICAL INDUSTRY 103

CHAPTER 6: Thermal aspects in oenological production 107

6.1 Alcoholic fermentation in winemaking process 107

6.2 Thermal control of the fermentation phase in wine industry 111

6.3 Heat pipes 117

CHAPTER 7: Application of a thermosiphon heat pipe to a wine fermenter: feasibility study 124

7.1 Experimental setup: the fermenter tank 125

7.2 Experimental setup: the ideal thermosyphon heat pipe (ITHP) 126

7.3 Experimentally setup: test conditions 129

7.4 Results 133

7.5 Closure 140

CHAPTER 8: Implementation of a real thermosyphon heat pipe (HP) 141

8.1 Design and realization of a preliminary HP 142

8.2 Verification of the heat transfer limits of the HP 144

8.3 Characterization of the performances of the HP 147

8.4 Closure 153

CHAPTER 9: Solutions for achieving the correct thermal sizing of the innovative cooling system 155

9.1 Solution 1: calculation of the optimal number of HPs 155

9.2 Solution 2: development of a model of the HP for its thermal sizing inside the fermenter 161

CHAPTER 10: Development of an innovative tool for estimating the heat release curve during wine fermenting processes 173
10.1 The estimation of heat release during oenological fermentation 173
10.2 Experimental setup and estimating model 175
10.3 Results 180
CHAPTER 11: Conclusions 185
References 189

PART III: CORRUGATED PIPES FOR FOOD INDUSTRY 197

CHAPTER 12: Wall corrugation in pipes for food heat exchanger 201
12.1 Heat transfer enhancement 201
12.2 Corrugated pipes 206
CHAPTER 13: Average and local analysis of the effect of different corrugations on pipes wall in turbulent regime 213
13.1 Pipes tested 213
13.2 Experimental setup for average analysis 215
13.3 Experimental setup for local analysis 218
CHAPTER 14: Results 230
14.1 Average results 230
14.2 Local results 237
CHAPTER 15: Closure 250
References 252
CHAPTER 16: Final remarks 261

CHAPTER 1: Introduction: Thermal processes in food industry and their optimization

In food industry, heat transfer and, in general, thermal processes are the main tool for ensuring the preservation of food over time. Temperature plays a key role for the food shelf-life, aimed to guarantee the safety of the final consumer. For this reason, the related technologies can be considered the core of the food conservation.

During food production, temperature is in fact mainly used for two purposes. The first one is to reduce the microbial load present in the raw materials to make the final product commercially sterile or stable under the intended storage conditions for a certain time. In these cases, the use of the temperature is classified under the unit operations commonly called “thermal treatments”, like pasteurization or sterilization.

Sterilization can be considered the extreme form of a thermal treatment, since it is aimed to heat the product, reaching such temperature to be lethal for both

vegetative forms of microorganisms and for spores, and keeping those thermal condition long enough to achieve their destruction. Usually, the temperature involved in sterilization processes are above the 100°C, like 110°C - 121°C or more due to the great thermal-resistance of the spores. Specifically, in the food industry, “commercial sterilization” is defined as the heat treatment aimed at destroying not all microbial forms, but just the ones able of growing up in the food at room temperature under conserving conditions established. A sterilization treatment, if well performed, ensures that the food, stored preventing further contamination, is microbially stable for a long period of time without refrigeration. Commonly, food industry considers foods commercially sterilized when the heat treatment applied ensures 12 logarithmic reductions of spores of *Clostridium botulinum,* since it is the sporal pathogenic form with the highest thermal resistance. In this kind of products, it is essential to ensure that the time-temperature combination, and so the sterilizing effect, of the treatment applied is effective over the entire mass of product treated, in fact if spores are not completely destroyed, vegetative form will grow from them producing pathogenic toxins in case of favorable conditions.

However, it is important to highlight that there are microorganisms more thermal resistant than *Clostridium botulinum* in some food matrix. These microorganisms are non-pathogenic and they do not represent a danger for human health but, due to their thermophilic nature, they start to grow up at temperatures of about 35°C and their growth could cause the deterioration of the

product. This could be the example of sterilized food destined to tropical country, where room temperatures could reach such values. In these cases, the sterilization temperature should be increased in order to destroy also these microbial forms and obtain a stable product.

In contrast, pasteurization is a treatment aimed to reduce the only vegetative forms of microorganisms, reaching within the product lethal temperature for them only. It is clear that spores, after this kind of treatments, will still be present and other strategies have to be applied to prevent their germination. One of these strategies is the maintenance of the cold chain after the heat treatment.

a) b)

Figure 1.1*: a) example of commercially sterilized food. b) example of pateurized food*

In this key, it is easy to understand that the second purpose of the use of temperature in food industry is not only related to heating processes, but it is related to maintenance of the cold chain: keeping temperatures below room temperature (in specific lower than 4°C) also plays an essential role in guaranteeing the shelf-life of the food after production or of the raw materials waiting to be processed. The cold chain is in fact necessary for those products

that have undergone pasteurization treatments, and thus retain the presence of the most heat-resistant microbial forms. In this case, refrigeration temperatures act as a barrier to the development of these microorganisms, making the product safe and guaranteeing the safety of the final consumer.

At this purpose, freezing also is a technique used for keeping the microbial conditions of the product stable over the time, but it is important to remember that these two uses of the temperature have not the effect of microbial reduction and we can consider them as only preservation method. In other words, refrigeration and freezing do not reduce the possible microbial load in the food, but they keep it constant over time, preventing any increase. Moreover, the cooling operation is also fundamental in some production processes, not for safety but for technical reasons. For example, cooling is necessary when the control of the temperature of the product must be maintained in specific ranges in order to promote the growth of some useful microbic forms. Typical cases are fermentation processes, like the lactic one for dairy food or the alcoholic one for oenological industry. In this case microorganisms, commonly yeast, need an optimal temperature for their metabolism for transforming the raw material in the final product and an efficient cooling system is required to achieve this goal.

Until now, when analyzing thermal processes in the food industry, we have only considered the (fundamental) final aim of the safety of the final consumer. However, another object of the thermal processes used in food industry is to develop the nutritional and/or the sensory quality of the product for making it

edible and/or tasteful. In boiling, grilling, toasting, frying and in any other cooking methods, the temperature directly affects the organoleptic features of the product in terms of texture, aromatic compound, and color. Maillard reaction and Strecker reaction could be taken in example for highlighting these phenomena. It is clear that in the cases of the transformation processes above mentioned, these effects are reached in the final product for obtaining a product with specific features and consequently a high-quality product.

Nevertheless, it is equally clear that these effects, since they are related to the exposition of the food to high temperatures, could also occur during the thermal treatment of pasteurization and sterilization, especially if the thermal treatment is oversized, despite they may be unwanted in these occasions. Specially, they are evaluated as a deteriorating effect when a final product, after being processed, should retain most of its characteristics of fresh raw material. At this purpose, taking a commonly pasteurized or sterilized raw material such as milk as an example, it is possible to highlight the main negative effect generated by the treatments:

- Loss of nutritional quality: vitamins are in general very sensitive to heat and an exposition to too high temperature for a too long time has a destructive effect on them. The result is a final product with a lower concentration of vitamins if compared to the raw one.

- Creation of off-flavours: the cook flavour is a typical unwanted aroma generated by Maillard reaction and from the consumer it is usually evaluated as a negative characteristic.
- Modification of the colour: milk, if exposed to too high temperature tends in yellowing and/or browning.

In conclusion, the less severe is the exposure to heat, the better the product quality of such food in which the fresh and row flavours are needed. For this reason, sterilised and UHT products are perceived as poorer in sensory quality respect the pasteurized ones by consumers and consequently they have a lower market image [1].

Once that the role and the impact of temperature during thermal processes in the food industry is clear, it is easy to understand the importance of their optimisation in order to achieve safer and higher quality products. The optimization of the thermal processes in the food industry is a trial that certainly does not disregard the energy aspect. Indeed, food industry, by means the food processes, uses a significant amount of energy transforming the raw material in safety final products: together with the tobacco industry, it reaches the 9.8% of the total energy demand in the manufacturing sector of the European Union [2]. The 75% of this portion of energy is used by heating and refrigeration processes [2].

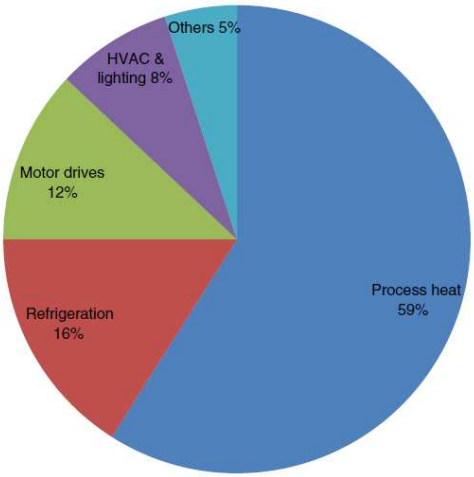

***Figure 1.2**: detail of energy consumption in food sector [4]*

For this reason, the optimization of thermal treatments in this sector should be considered and provided not only for increasing the food safety and quality but also for reducing energy consumption, related costs and reducing the environmental pollution [3].

Despite in the last 2 decades the energy intensity, calculated as the energy used per EUR of output, registered a decrease, the total energy consumption in food sector increased [2]. This testifies that what has been done so far is positive but not sufficient.

Heating and cooling food processes, and so pasteurization, sterilization, refrigeration, and freezing are very energy-intensive operations and their energy saving solution could be classified considering two aspects [4]:

- improvement of energy efficiency for existing unit
- replacement of energy-intensive units with novel units.

The energy efficiency enhancement in food industry, especially in thermal processes, is a very challenging target since it must combine with the maintenance or improvement the effectiveness of such treatment in order to guarantee the safety of the food and the health of the final consumer.

The above cited food industrial operations expect the use of specialized equipment identified in the category of “heat exchanger”. Increasing the efficiency of these existing kind of devices, under the points of view of energetic and microbial load reduction effectiveness, could be translated in increasing their heat transfer rate. Since most pasteurisation and sterilisation heat treatments are carried out on food fluid matrixes, an improvement of an existing unit corresponds to an enhancement in its internal convective heat transfer coefficients.

Related the available techniques to achieve this goal, a large number of papers are available in the scientific literature or textbooks: Webb [5], Bergles [6], Kuppan [7], but passive ones are certainly those that can best meet both the above requirements: obtain an energetic improvements and guarantee their effectiveness. Passive techniques are very attractive in this fields because they do not need an external power source to facilitate the enhancement. An example of such techniques applied to tubular and plate heat exchangers is the modification of heat exchange surfaces area, i.e. the adoption of a fine-scale alteration like coating for promoting the boiling, corrugations on the pipes wall

[8]–[12], displaced enhancement devices [13] and swirl-flow devices [5][7], use of coiled pipe [6].

Passive solutions are also a good possibility for the replacements of energy-intensive units with novel units. For example, in operation like the cooling or the thermal control of a liquid food substrate, the active system generally composed by a pump and a heat exchanger could be replaced by a device based on heat pipe [3] to quickly remove heat from the food and dissipating it in the environment. A heat pipe is a pipe, filled with a working fluid in saturation condition, through which heat passes also if there is a small temperature difference between its two ends. Since a heat pipe uses latent heat for transferring heat from the hot source to the cold one, it represents a highly efficient and totally passive approach. For this reason, a heat pipe can be used to quickly remove heat from a hot medium or transfer heat into a cold medium.

About existing units, another passive approach for achieving the correct thermal sizing of heat exchangers is their thermal characterization by means the inverse problem and parameter estimation approach. These techniques could represent a very interesting tool for designing heat exchangers able to obtain the wanted sterilizing or pasteurizing effect on the food fluid matrix maximizing the energy efficiency of the device [14], [15].

All the above strategies represent an innovation for the heat transfer operations of the food industry and, it is possible to state that it is mainly aimed in increasing the energy efficiency and effectiveness of heat treatments.

In this respect, innovation plays a key role since its efforts are also directed towards the development of totally new techniques for food heat transfer capable of combining high energy efficiency with high effectiveness. In cooling operations, as reported in the review of James et al. [16], several new techniques, like impingement freezing, pressure-assisted freezing, ultrasound-assisted freezing, magnetic resonance-assisted freezing, etc., are being investigated to improve the efficiency of freezing or deep-freezing processes. Also in heating processes new techniques like PEF [17] and Ohmic [18] have been developed and studied in the last decades.

In this thesis, the author is focused on exploiting some of the different approaches above reported for the improvement of both the energy efficiency and the effectiveness of different thermal processes of the food industry.

In specific, in the Part I of the thesis, it was proposed a method for thermal characterization of a triple tube heat exchanger, based on inverse problem approach. This type of heat transfer device represents a promising technology for the always increasing challenge of reducing the consumption of energy and raw materials and their optimal sizing can increase this positive aspect. This method enables a successful and robust estimation of the heat transfer correlation for the product side Nusselt number starting from the temperature measurements at the inlet and outlet sections of the three tubes. The procedure was validated by adopting both synthetic and experimental data acquired from a triple tube heat exchanger for treating highly viscous fluid foods.

In the Part II, the author proposes a study that concerns the design, realization, application and testing of a passive thermal control device for fermentation tank of oenological industry, in order to reduce/delete the energy consumption of this phase and improve the temperature distribution within the fermenting must.

In the Part III, the author proposes an evaluation of the effect of different corrugation on pipes adopted in tubular heat exchanger was evaluated in terms of convective heat flux. Local convective heat coefficient was estimated both by an average point of view and local one. The local measurements were performed using infrared analysis of the external surface of the pipe and the temperature distribution maps obtained were employed as input data for the inverse heat conduction problem in the wall.

References

[1] "Improving the thermal processing of foods," *Improv. Therm. Process. foods*, 2004, doi: 10.1201/9781439823330.

[2] EUROSTAT, "Final energy consumption by industry.," 2013.

[3] L. Wang, "Energy efficiency technologies for sustainable food processing," *Energy Effic.*, vol. 7, no. 5, pp. 791–810, 2014, doi: 10.1007/s12053-014-9256-8.

[4] L. Wang, *Energy efficiency and management in food processing facilities*. CRC press, 2008.

[5] R. L. Webb, *Principles of enhanced heat transfer*. 1994.

[6] D. B. Spalding, *Handbook of heat transfer*, vol. 18, no. 10. 1975.

[7] K. Thulukkanam, *Heat Exchanger Design Handbook*. 2013.

[8] F. Bozzoli, L. Cattani, and S. Rainieri, "Cross-helix corrugation: The optimal geometry for effective food thermal processing," *Int. J. Heat Mass Transf.*, vol. 147, p. 118874, 2020, doi: 10.1016/j.ijheatmasstransfer.2019.118874.

[9] P. Vocale, A. Mocerino, F. Bozzoli, and S. Rainieri, "Numerical analysis of the laminar forced convective heat transfer in coiled tubes with periodic ring-type corrugation," *J. Phys. Conf. Ser.*, vol. 745, no. 3, 2016, doi: 10.1088/1742-6596/745/3/032072.

[10] K. Navickaitė *et al.*, "Enhanced heat transfer in tubes based on vascular heat exchangers in fish: Experimental investigation," *Int. J. Heat Mass Transf.*, vol. 137, pp. 192–203, 2019, doi: 10.1016/j.ijheatmasstransfer.2019.03.067.

[11] F. Bozzoli, L. Cattani, and S. Rainieri, "Effect of wall corrugation on local convective heat transfer in coiled tubes," *Int. J. Heat Mass Transf.*, vol. 101, pp. 76–90, 2016, doi: 10.1016/j.ijheatmasstransfer.2016.04.106.

[12] Z. S. Kareem, M. N. Mohd Jaafar, T. M. Lazim, S. Abdullah, and A. F. Abdulwahid, "Passive heat transfer enhancement review in corrugation," *Exp. Therm. Fluid Sci.*, vol. 68, pp. 22–38, 2015, doi: 10.1016/j.expthermflusci.2015.04.012.

[13] M. Rinaldi, M. Cordioli, M. Alinovi, M. Malavasi, D. Barbanti, and G. Mucchetti, "Development and Validation of CFD Models of Thermal

Treatment on Milk Whey Proteins Dispersion In Batch and Continuous Process Condition," *Int. J. Food Eng.*, vol. 14, no. 9–10, 2018, doi: 10.1515/ijfe-2018-0142.

[14] S. Rainieri, F. Bozzoli, L. Cattani, and P. Vocale, "Parameter estimation applied to the heat transfer characterisation of Scraped Surface Heat Exchangers for food applications," *J. Food Eng.*, vol. 125, no. 1, pp. 147–156, 2014, doi: 10.1016/j.jfoodeng.2013.10.031.

[15] P. Vocale, F. Bozzoli, A. Mocerino, K. Navickaitė, and S. Rainieri, "Application of an improved parameter estimation approach to characterize enhanced heat exchangers," *Int. J. Heat Mass Transf.*, vol. 147, 2020, doi: 10.1016/j.ijheatmasstransfer.2019.118886.

[16] C. James, G. Purnell, and S. J. James, "A Review of Novel and Innovative Food Freezing Technologies," *Food Bioprocess Technol.*, vol. 8, no. 8, pp. 1616–1634, 2015, doi: 10.1007/s11947-015-1542-8.

[17] K. Nowosad, M. Sujka, U. Pankiewicz, and R. Kowalski, "The application of PEF technology in food processing and human nutrition," *J. Food Sci. Technol.*, vol. 58, no. 2, pp. 397–411, 2021, doi: 10.1007/s13197-020-04512-4.

[18] H. S. Ramaswamy, M. Marcotte, S. Sastry, and K. Abdelrahim, *Ohmic heating in food processing*. CRC press, 2014.

PART I: TRIPLE TUBE HEAT EXCHANGER FOR FOOD INDUSTRY

List of figures

Figure 2.1: Schematic section of a double pipe heat exchanger 20

Figure 2.2: 3D view of e tube in tube heat exchanger [2] 20

Figure 2.3: Schematic representation of a shell and tube heat exchanger [3] .. 21

Figure 2.4: Schematic section of different configuration of three tube heat exchangers: a) three thermal communications heat exchangers b) two thermal communications heat exchangers 24

Figure 2.5: parallel flow disposition: a) co-current b) counter current c) countercurrent-cocurrent d) cocurrent-countercurrent 25

Figure 4.1: Schematic representation of the studied THE: (a) axial and b) cross view. 49

Figure 4.2:Finite difference scheme of the investigated heat exchanger 53

Figure 4.3:Sensitivity coefficients versus the Reynolds number 66

Figure 4.4: Sensitivity coefficients versus the Reynolds number 67

Figure 4.5: Coefficients of variation obtained with synthetic data for different noise levels 71

Figure 4.6: Estimation error E_{Q2} as a function of the noise level (a) and comparison between exact and estimated heat power Q_2 for noise level $\zeta = 1$ K (b) 73

Figure 4.7: (a) Sketch of the section of the experimentally tested TTHE. (b) 3D view of TTHE 75

Figure 4.8: Scheme of the experimental setup 76

Figure 4.9: Comparison between experimental and estimated heat power Q2 82

Figure 4.10: Coefficients of variation for different noise levels for the case of 4 parameters estimation 86

Figure 4.11: Estimation error E_{Q2} as a function of the noise level (a) and comparison between exact and estimated heat power Q_2 for noise level $\zeta = 1$ K (b) for the case of 4 parameters estimation 89

Figure 4.12: Coefficients of variation for different noise levels for the case of 6 parameters estimation 89

Figure 4.13: Estimation error E_{Q2} as a function of the noise level (a) and comparison between exact and estimated heat power Q_2 for noise level $\zeta = 1$ K (b) for the case of 6 parameters estimation 91

Figure 4.14: Solution time for the 2, 4 and 6 parameters estimation procedures 93

CHAPTER 2: Thermal aspects of three tube heat exchangers

2.1 Heat exchanger in food industry

When we speak of heat exchangers, we mean devices used to transfer thermal energy between two or more fluids having different temperatures. In most cases, in the food industry, heat exchangers transfer heat between the two fluids indirectly: a separating wall (the heat transfer surface) usually divide the fluids not allowing mixing o leaking. Heat exchangers, in food industry, are very important as they represent the main tool used for carrying out thermal processes on which the safety of the final product depends, such as sterilization, pasteurization and heating and cooling. [1]

Heat exchangers can be classified according to various criteria: construction, flow arrangement, surface compactness, transfer process and phase of the fluids

involved. However, the most useful and commonly used criteria in the food industry can be identified in the first two.

i. Classification according to construction

This is the most complex and articulated classification and there are many different construction configurations that make difficult to have an exhaustive list. However, it is possible to focus on the main heat exchangers used in the food industry: tubular heat exchanger and plate heat exchanger:

- Tubular heat exchanger: these heat exchangers are usually composed by different shape of pipe like circular, elliptical, twisted or corrugated, depending on the final application of the device. To this category belong tube-in-tube exchangers (“double tube” and “triple tube”) and shell-and-tube exchangers. The possibility of varying the length, the internal diameter, the arrangement, the number and the shape of the pipes and the possibility to link them parallelly or in series with different modules, for changing their total length, makes these heat exchangers very flexible and for that reason very appreciate in food industry. [2] The most common variant of *tube-in-tube heat exchangers* is composed by two tubes of material for food contact (AISI 304, 306, 316L, titanium and aluminium), mounted coaxially, usually in a 'U' arrangement (Figure 2.1) to reduce the overall length. One of the fluids flows in

the inner tube, while the other one flows counter currently on the annular section between the two tubes.

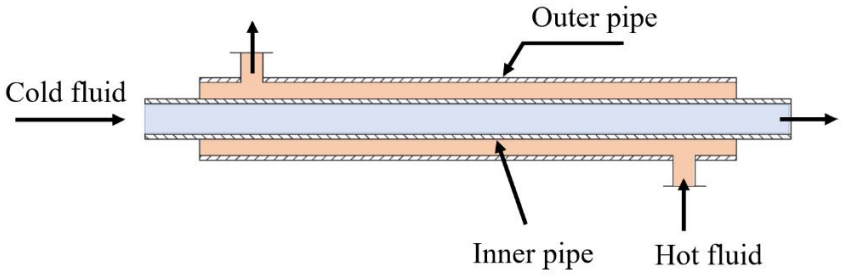

***Figure 2.1**: Schematic section of a double pipe heat exchanger*

This type of heat exchangers is widely used in the food industry for fruit juices with fibres and for relatively water-like foods, fluids of moderate to high viscosity with only small particulates [1] due to the above characteristics which give them a high-cost efficiency.

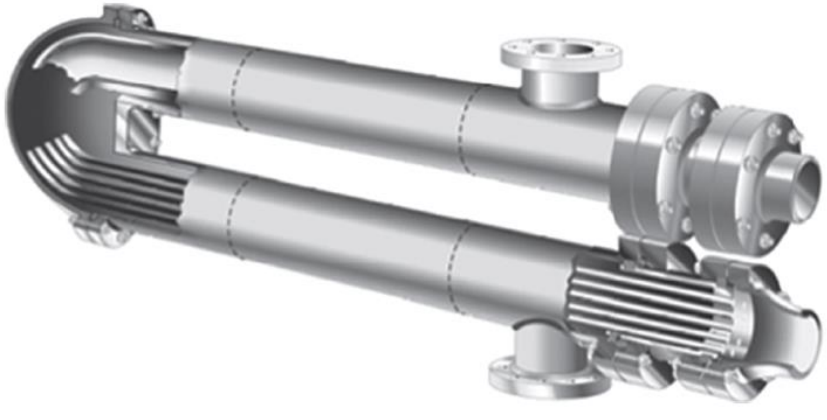

***Figure 2.2**: 3D view of e tube in tube heat exchanger [2]*

A particular case of tube-in-tube exchanger is the triple tube heat exchanger. In general, in this device, compared to the two-pipe

configuration, a third concentric pipe is added allowing the increase of the total heat exchange surface.

Shell-and-tube heat exchangers consist of an external mantle within which there are several tubes. One of the two fluids flows on the shell side, the other one flows on the tube side. Often diaphragms baffles are inserted with the aim of favouring a turbulent flow that allows greater uniformity and efficiency of heat exchange.

The scheme in Figure 2.3 can be considered representative of this type of device.

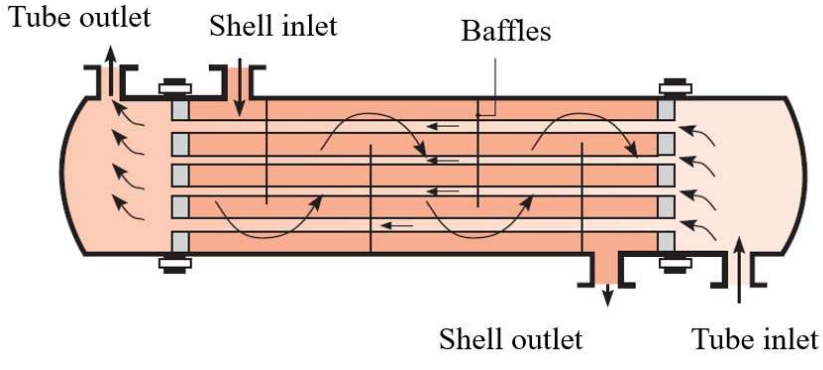

***Figure 2.3**: Schematic representation of a shell and tube heat exchanger* [3]

– Plate heat exchanger (PHE): a PHE essentially consists of several of texturized plates made in stainless steel, in contact. On every plate there are four apertures used for inlet and outlet of the working fluid and the product. Inlet and outlet are sealed in order to create an alternate flow passage of the two fluids [2]. All the plates are clamped together in support that includes. PHEs are less widely

used than tubular heat exchangers but offer certain important advantages and it is possible to consider them as an alternative to tubular heat exchanger for low viscosity fluids like milk and dairy products, and fruit juices. [4] Plate exchangers have the advantage of having smaller footprint due to a more compact layout if compared to tubular exchangers. They are also very flexible as they are easily expandable in case of changing process requirements (just increase the number of plates by inserting more). On the opposite, they have the advantage of being particularly sensitive to dirt on the exchange surfaces and not being easy cleanable.

ii. Classification according to flow directions:

The main configurations are:

- Co-current flows
- Counter-current flows
- Cross-flows

In the co-current configuration, the two flows are parallel and equiverse: the fluids enter at the same end, flow parallelly and leave at the other end. This arrangement, if compared to the other two, has the lowest exchanger effectiveness for the same flow rates and exchange surface area. Nevertheless, they are adopted when high viscous fluids are processed, indeed, the higher difference in temperature at the inlet section provide a faster heating of the food

fluid resulting in a reduced pumping power needed for moving the product inside the pipe. [2]

In the counter-current configuration the flows are parallel, but they proceed in opposite direction. This configuration can be considered the most efficient for single-pass arrangements under the same parameters but, in some type of heat exchanger, it is not appliable due to difficulties associated to the design of the device. [2]

As an alternative to these two configurations, there are cross-flow exchangers in which banks of tubes, internally crossed by a fluid, are hit orthogonally by an external flow. The effectiveness of this kind of arrangement is placed between the other two and it is preferred when great heat exchange surface areas are needed, like in shell-and-tube devices. [2]

2.2 Three-tubes heat exchangers

A three-tubes heat exchanger is a device in which the heat transfer takes place among three fluid streams. Depending on how heat transfer takes place, it is possible to distinguish devices in which only one fluid stream transfers heat to the other two fluid streams, or devices in which all the three fluid streams transfer heat among each other. In the first case it is possible to define the device as a “two thermal communications heat exchangers” while in the second one as “three thermal communications heat exchangers”.

According to this definition, in a three-tubes heat exchanger, the three pipes can be organized as reported in (**Figure 2.4**), with the most common configuration for the food industry that is represented by the "two thermal communications" also called triple concentric tube heat exchanger or more commonly triple tube heat exchanger (TTHE).

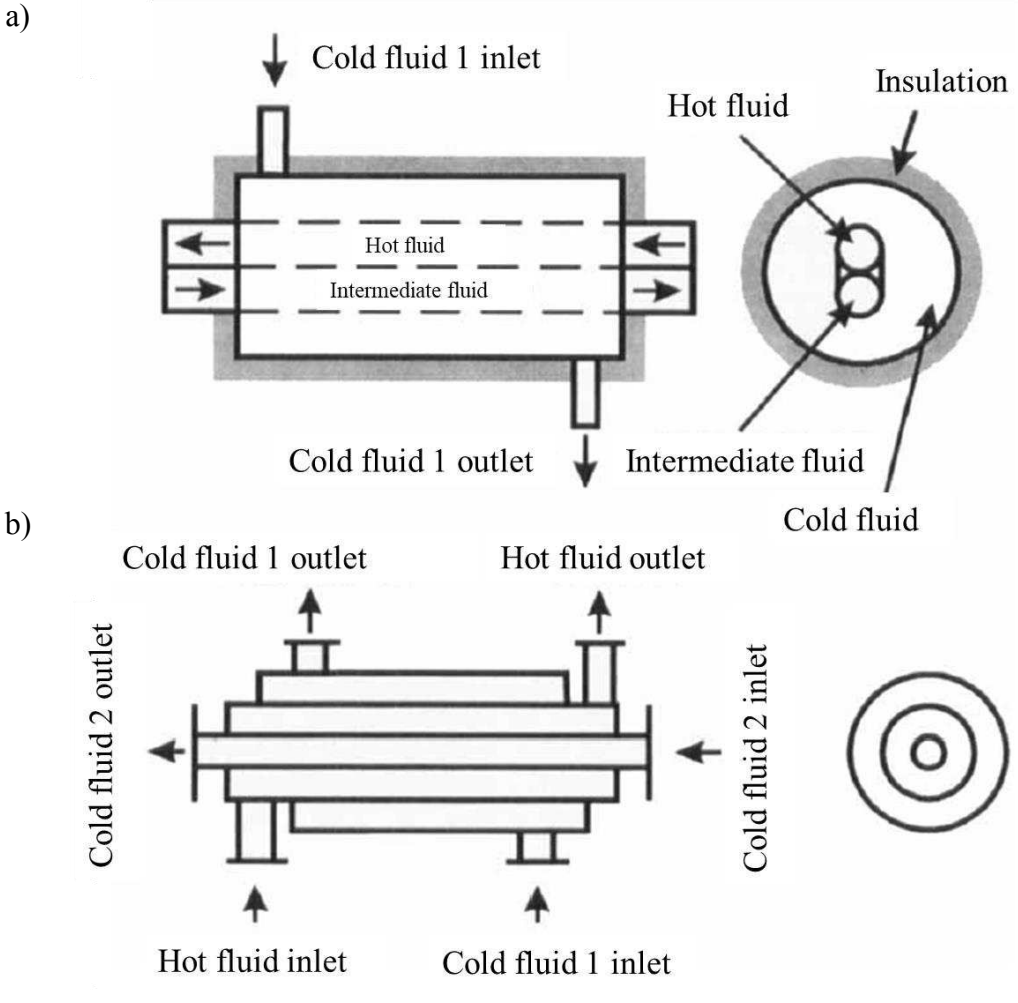

***Figure 2.4**: Schematic section of different configuration of three tube heat exchangers: a) three thermal communications heat exchangers b) two thermal communications heat exchangers*

In TTHE the most common flow arrangement is the parallel one. As reported in Figure 2.5, three different parallel flow arrangement are available for this kind of device: a) cocurrent where the fluids in all the three sections flow in the same direction, b) countercurrent, (c) countercurrent-cocurrent and cocurrent-countercurrent where one of the fluids flows in the opposite direction compared to the other two.

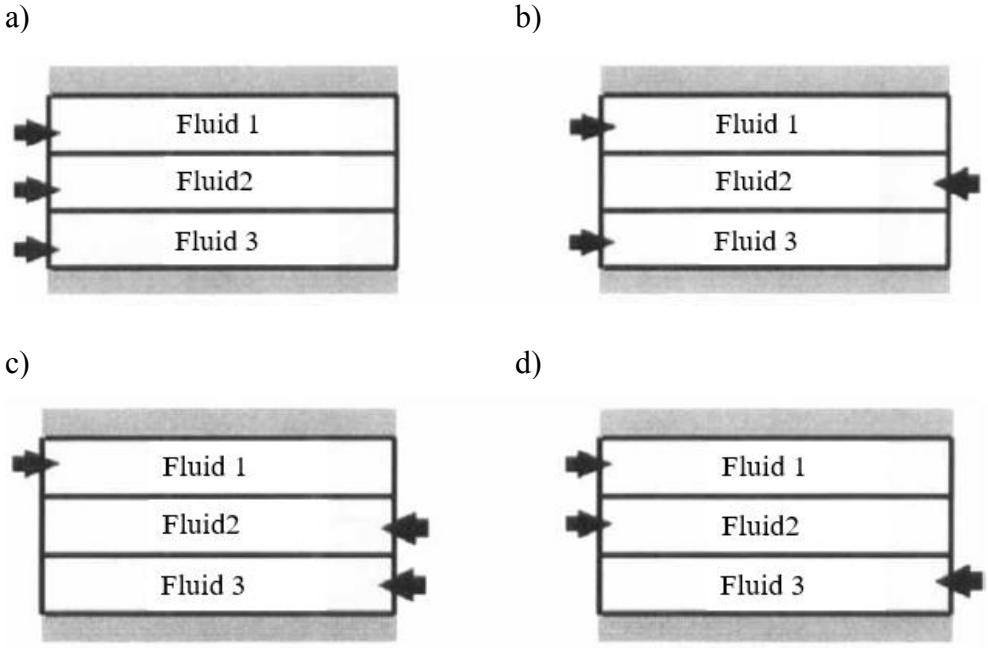

***Figure 2.5**: parallel flow disposition: a) co-current b) counter current c) countercurrent-cocurrent d) cocurrent-countercurrent*

TTHEs are widely used in the food and pharmaceutical industries. In the food industry, this heat exchanger is used for sterilisation, pasteurisation, and cooling

treatments; for instance, liquid products such cream and pulpy orange juice are often pasteurised using TTHE. [5]

Despite the advantages and wide use of TTHEs, especially in cases where the fluid under treatment is highly viscous and exhibits complex rheological behaviour, the scientific literature on this topic contains some gaps, including the thermal design of these apparatuses, as highlighted by Kumar and Hariprasath in their recent review [6].

Moreover, it is difficult to apply the few data available in the literature to TTHEs due to the specificity of each product, thermal treatment, and geometrical configuration, making the thermal design of these apparatuses critical. Therefore, it appears to be more useful to assess the methodology used to derive a proper heat transfer correlation than to assess the form of the heat transfer correlation itself, as the correlation often cannot be transferred to other heat exchangers, even those that belong to the same class. Generally, the experimental investigations reported in the literature [5], [6], [15], [16], [7]–[14] aim to measure the average thermal performance of the device for different conditions (different Reynolds number values in the three sections, heating/cooling conditions, etc…) and different geometric configurations, often adopting the effectiveness-NTU method or the log-mean temperature. Despite the DTHE, in which there are only two fluid flows, the energy of the fluid that flows in the inner annulus is exchanged in two opposite directions in a TTHE (to

the fluids in the inner tube and outer annulus); therefore, the approach based on the evaluation of the logarithmic mean temperature difference is no longer valid. To overcome this problem, Gomaa et al. [7] introduced an average log-mean temperature difference between the three fluids, defined as the arithmetic mean between the log-mean temperature difference between the fluid in the annulus and the one in the external tube and the log-mean temperature difference between the annulus and internal pipe. The same approach was recently adopted by Tiwari et al. [8] Another study, Ünal [9], [10] conducted a theoretical analysis of this type of heat exchanger, deriving closed form expressions for the effectiveness-NTU relations, including both the counter-flow and parallel flow configurations. Batmaz and Sandeep [11] and Radulescu et al.[12] proposed and developed a procedure that included a calculation algorithm that could determine the overall heat transfer and axial temperature distribution in a TTHE. Recently, Moya Rico et al. [13] proposed an alternative tool based on artificial neural networks to accurately predict the heat transfer rate and the pressure drop in a TTHE. By adopting the same approach, Bahiraei et al. [14]–[16] predicted the overall heat transfer coefficient of a TTHE and investigated heat transfer enhancement due to the insertion of nanofluid and crimpled spiral ribs. Even if the experimental data are treated by adopting the dimensional analysis approach due to the specificity of each plant and product treated, it is often difficult to extend the validity of the suggested heat transfer correlations that often hold for

the specific geometry under investigation. Considering the more critical procedure of defining a correlation for heat transfer for TTHEs than the form of correlation itself due to the specificity of any single application case of these devices, this study proposes and validates a data processing procedure intended to characterise TTHEs, which helps in estimating the heat transfer correlation for the product side Nusselt number. One of the simplest methods used to estimate the inside heat transfer coefficient in heat exchangers is the well-known Wilson plot technique [17]. In this technique, a simple linear curve fitting procedure was used to estimate both the sum of the wall and shell side resistances and the constant of the internal side heat transfer correlation. Briggs and Young [18] suggested and validated a procedure for determining three unknowns rather than two, as the exponent expressing the power law dependence of the internal Nusselt number on the Reynolds number was also estimated. A more general approach based on a non-linear regression scheme was presented by Khartabil and Christensen [19]. A unified Wilson plot method based on nonlinear regression was applied by Styrylska and Lechowska [20] . A general review of the Wilson plot method and its modifications to determine convection coefficients in heat exchanger devices was presented by Rose [21] and Fernández Seara et al. [22] . However, the application technique proposed by Wilson to TTHE presents some macroscopic problems due to the impossibility of defining a univocal behaviour of the ‘shell’ side: the two sections in which

flows the service fluid influence each other, making it difficult to determine a unique thermal resistance for the service side. These limitations of the approach used by Wilson could be overcome as proposed by Gomaa et al. [7] and Pătrăşcioiu et al. [23] by adopting an average log-mean temperature, as previously described.

A promising solution to completely bypass the limitations of the Wilson plot technique can be found in the parameter estimation procedure, which represents a powerful tool for many engineering applications [24], [25] . Particularly, the parameter estimation procedure helps to estimate unknown parameters that play an important role in the design and optimisation of heat transfer devices and heat exchangers that are customised for certain specific purposes, as often happens with TTHE. This methodology has recently been adopted to investigate the performance of DTHE based on the assumption that both internal and external convective heat trans- fer coefficients can be expressed as a function of the Reynolds and Prandtl numbers [26] .

CHAPTER 3: Inverse heat transfer problems (IHTPs) and parameter estimation

Frequently, in the engineering field it is necessary to relate the physical parameters characterizing a model, *m*, to a series of collected observations composing a dataset, *d*. Assuming that the fundamental physics of the phenomenon is adequately understood, a function, *G*, may be found and specified to relate *m* and *d*.

$$G(m_1, m_2, \dots) = d \qquad (1)$$

In most cases, *d* is a set of discrete observations obtained experimentally using measuring instruments. Precisely for this reason, the data obtained are affected by a certain level of noise and are characterised by an error with respect to the true value. For this reason, we can imagine the data as generally consisting

of noise-free observations from a "perfect" experiment, d_{true}, added by a noise component η.

$$G(m_{true}) + \eta = d_{true} + \eta \quad (2)$$

When we know *m*, while *d* is unknown, we are in the presence of a so-called "forward problem". In the opposite case, i.e., when *d* is known but we have to estimate *m*, we are in the presence of an "inverse problem".

In applied physics, when studying heat transfer by means inverse problem technique, it is common to talk specifically of inverse heat transfer problems (IHTPs). They can be mathematically classified as *ill-posed* problems. For classifying a mathematical problem as *well-posed,* its solution must satisfy these conditions:

- Existence
- Uniqueness
- Stability under small changes in the input data.

If the existence of a solution for an IHTP may be assured by physical reasons, demonstrate that it is uniqueness is in general very challenging.

Moreover, inverse problems are very sensitive to errors in the measurements used in input dataset, as cited above. For this reason, their solutions are more complicated than the direct one and it requires regularization techniques. It is possible to state that *ill-posed* inverse problems have solution that are based on their approximation to *well-posed* ones by means the regularization.

These regularization techniques are: Tikhonov's regularization technique, Alifanov's iterative regularization technique and Beck's sequential function specification technique, and, thanks them, the interest on the solution of IHTPs was revitalized [27].

IHTPs can be classified based on different criteria. One of the most common classification criteria for IHTP is the nature of the heat transfer process:

- IHTP of conduction
- IHTP of convection (forced or natural)
- IHTP of surface radiation
- IHTP of radiation in participating medium
- IHTP of phase change (melting or solidification)
- IHTP of coupled modes of heat transfer.

Another classification method can be based on the type of causal feature to estimate:

- IHTP of boundary conditions
- IHTP of thermophysical properties
- IHTP of initial condition
- IHTP of source term
- IHTP of geometric characteristics of a heated body.

Moreover, IHTP can be classified as one-dimensional, two-dimensional or three-dimensional, and linear or nonlinear one. Concluding, another common

classification of inverse problems is the distinction between parameter estimation and function estimation. In parameter estimation only a limited number of parameters has to be estimated; they usually refer to a physical property, like thermal conductivity of a material at a particular temperature. In the function estimation the functional form is not known and thus the number of parameters that have to be determined is high.

For explain more practically the basic concepts of an inverse problem, it is possible to use a IHTP in which a function estimation is performed, in specific case reference can be made to the example given by Özisik and Orlande [27]: let's consider a transient linear heat conduction in a plate of thickness L. The temperature distribution of the plate is initially F(x). For times $t > 0$, a heat source of strength $f(t)$ is applied on the boundary $x = 0$ and $x = L$ is kept at constant temperature T_L.

$$\frac{\partial}{\partial x}\left(k\frac{\partial T}{\partial x}\right) = \rho\, c_p\, \frac{\partial T}{\partial t} \qquad in\ 0 < x < L, for\ t > 0 \qquad (3)$$

$$-k\frac{\partial T}{\partial x} = f(t) \qquad at\ x = 0, for\ t > 0 \qquad (4)$$

$$T = T_L \qquad at\ x = L, for\ t > 0 \qquad (5)$$

$$T = F(x) \qquad for\ t = 0, in\ \ 0 < x < L \qquad (6)$$

If we consider the direct problem associated, the heat flow *f(t)*, T_L and the initial condition $F(x)$ are known, consequently, the objective of the direct problem is to determine the transient temperature field *T(x, t)* in the plate. On contrary, if we consider the inverse problem, the time-varying power released by the heat source on the plane *f(t)* is to be considered as unknown. The additional information, ρ, c_p, F(x), and T_L are known.

Moreover, to obtain obtained essential additional information, the temperature $T(x_{meas}, t_i) = Y_i$ is measured measurements taken at a location $x = x_{meas}$, at times t_i, i= 1, 2, …, I, is then used for the estimation of *f(t)*.

At this point, the formulation of the inverse problem can be written as follow:

$$\frac{\partial}{\partial x}\left(k\frac{\partial T}{\partial x}\right) = \rho\, c_p\, \frac{\partial T}{\partial t} \qquad in\ 0 < x < L, for\ 0\ < t\ \leq\ t_f \qquad (7)$$

$$-k\frac{\partial T}{\partial x} = f(t) = ? \qquad at\ x = 0, for\ 0 < t\ \leq\ t_f \qquad (8)$$

$$T = T_L \qquad at\ x = L, for\ 0 < t\ \leq\ t_f \qquad (9)$$

$$T = F(x) \qquad for\ t = 0, in\ \ 0 < x < L \qquad (10)$$

Moreover, the temperature measurements at x_{meas} at time t_i are:

$$T(x_{meas}, t) \equiv Y_i \qquad at\ x =\ x_{meas}\ for\ t = t_i\ (i = 1,2, \dots, I) \qquad (11)$$

Considering the boundary inverse problem considered, we can assume that the unknown function *f(t)* can be represented as follow:

$$f(t) = \sum_{j=1}^{N} P_j \, C_j(t) \qquad (12)$$

where P_j are unknown parameters and $C_j(t)$ are known basis functions, *N* is the total number of parameters, and it is known and has to be smaller than *I*.

As cited above, for solving inverse problems, it is common to consider 2 approaches: if some information is available on the functional form of the unknown quantity, the approach defined as "parameter estimation" since the solution is reduced to the estimation of only a finite number of unknown parameters. In the opposite case, if no prior information on the basis functions is available, the inverse problem can be considered as “function estimation” approach, like in the example reported.

Generally, inverse problems are solved by minimizing an objective function *S* if they satisfy the following condition:

- The errors in measurements are additive
- The errors in measurements have a zero mean
- The errors in measurements have constant variance
- The errors associated with different measurements are uncorrelated
- The measurement errors have a normal (Gaussian) distribution

- The only variables that contain random errors are the measured values
- There is no prior information regarding the quantities to be estimated

In this case, the objective function *S,* that provides minimum variance estimates, is the ordinary least squares norm [24] [28] defined as follow:

$$S = (\boldsymbol{Y} - \boldsymbol{T})^T (\boldsymbol{Y} - \boldsymbol{T}) \qquad (13)$$

where $\boldsymbol{Y}$ and $\boldsymbol{T}$ are the vectors containing the experimentally measured values and estimated temperatures obtained from the solution of the direct problem with estimates for the unknown quantities, respectively, and the superscript *T* means the transpose of the vector.

If we consider a study case that is time dependent, the different measurements Y_i, obtained at times $t_i, i = 1,2,3, \dots I$, of a sensor are used as input values in the IHTP. The transpose vector of the residuals can be written as follows:

$$(\boldsymbol{Y} - \boldsymbol{T})^T = (Y_1 - T_1,\ Y_2 - T_2, Y_3 - T_3, \dots, Y_I - T_I) \qquad (14)$$

and the related objective function could be written as:

$$O_f = (\boldsymbol{Y} - \boldsymbol{T})^T (\boldsymbol{Y} - \boldsymbol{T}) = \sum_{i=1}^{I} (Y_i - T_i)^2 \qquad (15)$$

At the same time, the following expression can be used for a steady study with the different measurements Y_n, taken at the same time but at different positions by different sensors $n = 1,2,3 \dots N$:

$$O_f = (\boldsymbol{Y} - \boldsymbol{T})^T(\boldsymbol{Y} - \boldsymbol{T}) = \sum_{n=1}^{N}(Y_n - T_n)^2 \quad (16)$$

Differently, in a transient analysis executed with multiple sensors, the transpose vector of residuals can be written as follows:

$$(\boldsymbol{Y} - \boldsymbol{T})^T = \left(\vec{Y}_1 - \vec{T}_1, \vec{Y}_2 - \vec{T}_2, \vec{Y}_3 - \vec{T}_3, \dots, \vec{Y}_I - \vec{T}_I\right) \quad (17)$$

where at any time t_i, $\left(\vec{Y}_i - \vec{T}_i\right)$ represent the vector of N element corresponding to the number of sensor:

$$\left(\vec{Y}_i - \vec{T}_i\right) = (Y_{i1} - T_{i1}, Y_{i2} - T_{i2}, Y_{i3} - T_{i3}, \dots, Y_{iN} - T_{iN}) \quad (18)$$

where the *i* subscript refers to time step and the second one refers to the sensor number. In this way, the objective function can be written as follow:

$$O_f = (\boldsymbol{Y} - \boldsymbol{T})^T(\boldsymbol{Y} - \boldsymbol{T}) = \sum_{n=1}^{N}\sum_{i=1}^{I}(Y_{in} - T_{in})^2 \quad (19)$$

If the standard deviation values of the various measurements are not the same, the ordinary least squares method doesn't provide minimum variance estimates.

As suggested by Özisik and Orlande [27] in their classification, a lot of techniques could be used for solving IHTPs and overcome this problem. Among this scenario, only the techniques used in this thesis will be reported below.

The Levenberg-Marquardt Method will be explained since it could be considered powerful tool for nonlinear parameter estimation problems, and it is used in the next paragraphs. However, it is important to remember that other techniques are available, like the conjugate gradient method and conjugate gradient method with adjoint problem.

The solution based on Levenberg-Marquardt Method can be summarized in the following steps:

- The Direct Problem definition
- The Inverse Problem definition
- The Iterative Procedure definition
- The Stopping Criteria definition

i. Direct and inverse problem definition

Let's consider a transient linear transient heat conduction in a plate of dimensionless unitary thickness. The temperature of the plate is zero at the initial moment and insulation is placed at boundaries x = 0 and x = 1. For times $t > 0$, a heat source of strength $g_p(t)$ is applied on the boundary $x = 0.5$.

The mathematical formulation of this heat conduction problem can be written as follow:

$$\frac{\partial^2 T(x,t)}{\partial x^2} + g_p(t)\delta(x-0.5) = \frac{\partial T(x,t)}{\partial t} \quad in\ 0 < x < L, for\ \ t > 0 \qquad (20)$$

$$\frac{\partial T(0,t)}{\partial x} = 0 \qquad at\ x = 0, for\ t > 0 \qquad (21)$$

$$\frac{\partial T(1,t)}{\partial x} = 0 \qquad at\ x = 1, for\ t > 0 \qquad (22)$$

$$T(x,0) = 0 \qquad for\ t = 0, in\ \ 0 < x < 1 \qquad (23)$$

If we consider the direct problem associated, the heat flow $g_p(t)$, is known and, consequently, the objective of the direct problem is to determine the transient temperature field $T(x, t)$ in the plate. On contrary, if we consider the inverse problem, the time-varying power released by the heat source on the plane $g_p(t)$ is to be considered as unknown. The temperature $T(x_{meas}, t_i)$ measured measurements taken at a location $x = x_{meas}$, at times t_i, i= 1, 2, …, I, is then used for its estimation.

At this point, the inverse problem can be summarized as follow:

$$g_p(t) = \sum_{j=1}^{N} P_j\, C_j(t) \qquad (24)$$

where P_j are unknown parameters and $C_j(t)$ are known basis functions, N is the total number of parameters, and it is known and has to be smaller than I.

Its solution can be written as follow:

$$S(\boldsymbol{P}) = \sum_{i=1}^{I} [Y_i - T_i(\boldsymbol{P})]^2 \quad (25)$$

where S is the sum of squares error or objective function, P^T is the unknown parameters vector, $T_i(\mathbf{P})$ is the estimated temperature at instant t_i, Y_i is the measured temperature at instant t_i, *N* is total number of unknown parameters and *I* is total number of measurements.

In matrix form it could be rewritten as follow:

$$S(\boldsymbol{P}) = [\boldsymbol{Y} - \boldsymbol{T}(\boldsymbol{P})]^T [\boldsymbol{Y} - \boldsymbol{T}(\boldsymbol{P})] \quad (26)$$

The minimization of the least squares norm above expressed passes through the equalization to zero of the derivatives of S(**P**) with respect to each of the unknown parameters P:

$$\frac{\partial S(\boldsymbol{P})}{\partial P_1} = \frac{\partial S(\boldsymbol{P})}{\partial P_2} = \cdots = \frac{\partial S(\boldsymbol{P})}{\partial P_N} = 0 \quad (27)$$

that in matrix notation can be written as follow:

$$\nabla S(\boldsymbol{P}) = 2\left[-\frac{\partial T^T(\boldsymbol{P})}{\partial \boldsymbol{P}}\right][\boldsymbol{Y} - \boldsymbol{T}(\boldsymbol{P})] = 0 \quad (28)$$

where,

$$\frac{\partial T^T(\boldsymbol{P})}{\partial \boldsymbol{P}} = \begin{bmatrix} \frac{\partial}{\partial P_1} \\ \frac{\partial}{\partial P_1} \\ \vdots \\ \frac{\partial}{\partial P_N} \end{bmatrix} [T_1\ T_2\ \cdots\ T_I] \qquad (29)$$

The sensitivity matrix J(**P**) is than defined its transpose:

$$J(\boldsymbol{P}) = \left[\frac{\partial T^T(\boldsymbol{P})}{\partial \boldsymbol{P}}\right]^T = \begin{bmatrix} \frac{\partial T_1}{\partial P_1} & \frac{\partial T_1}{\partial P_2} & \cdots & \frac{\partial T_1}{\partial P_N} \\ \frac{\partial T_2}{\partial P_1} & \frac{\partial T_2}{\partial P_2} & \cdots & \frac{\partial T_2}{\partial P_N} \\ \vdots & \vdots & \ddots & \vdots \\ \frac{\partial T_I}{\partial P_1} & \frac{\partial T_I}{\partial P_1} & \cdots & \frac{\partial T_I}{\partial P_N} \end{bmatrix} \qquad (30)$$

Where *N* is the total number of unknown parameters and *I* is the total number of measurements.

The sensitivity matrix is composed by the so called "sensitivity coefficients". The sensitivity coefficient J_{ij} can be defned as the first derivative of the estimated temperature at time T_i with respect to the unknown parameter P_j:

$$J_{ij} = \frac{\partial T_i}{\partial P_j} \qquad (31)$$

The sensitivity coefficient J_{ij}, measures the change in the estimated temperature T_i with respect to a variation in the parameter P_j. A small value of the magnitude of J_{ij} means that large changes in P_j yield small changes in T_i and,

in this case the estimation of P_j parameter is very difficult in such cases. For this reason, it is desirable to have sensitivity coefficients linearly independent and with great values, in order to have and inverse problem low sensitive to measurement errors and very accurate in the estimation of the parameters.

Several methods could be use for the calculation of the sensitivity coefficients:

- Direct Analytic Solution
- The Boundary Value Problem
- Finite difference approximation

Only the finite difference approximation method will discuss in this section since it is the one used in the next paragraphs.

The first derivative of the definition of the sensitivity coefficient can be calculated using finite differences, as follow:

$$J_{ij} = \frac{T_i\left(P_1, P_2, \dots, P_j + \varepsilon P_j, \dots, P_N\right) - T_i(P_1, P_2, \dots, P_j, \dots, P_N)}{\varepsilon P_j} \qquad (32)$$

It is possible to observe that N experimental result of the direct problem are needed for the calculation of the sensitivity coefficients and their accuracy is dependent on the increment ε. For this reason, it is recommended to use several values of ε, comparing the sensitivity coefficients in order to avoid numerical mistakes. Common value used for ε are 10^{-5} or 10^{-6}.

ii. Iterative procedure

The Eq. 22, using the definition reported in Eq. 24 becomes:

$$-2\boldsymbol{J}^{T}\,(\boldsymbol{P})[\boldsymbol{Y}-\boldsymbol{T}(\boldsymbol{P})]=0 \qquad (33)$$

Since in nonlinear inverse problem, the sensitivity matrix has dependence on the vector of unknown **P**, the solution of Eq. 27 needs iterative procedure. This procedure can be obtained with the linearization of **T**(**P**) with a Taylor series expansion around the solution $\mathbf{P^k}$ at iteration k:

$$\boldsymbol{T}(\boldsymbol{P})=\boldsymbol{T}\left(\boldsymbol{P^k}\right)+\boldsymbol{J^k}(P-\boldsymbol{P^k}) \qquad (34)$$

Where $\boldsymbol{T}\left(\boldsymbol{P^k}\right)$ and $\boldsymbol{J^k}$ are the estimated temperature and the sensitivity matrix at k^{th} iteration, respectively. Substituting Eq. 28 in Eq. 27 the iterative procedure becomes:

$$\boldsymbol{P^{k+1}}=\boldsymbol{P^k}+\left[(\boldsymbol{J^k})^{\boldsymbol{T}}\boldsymbol{J^k}\right]^{-1}\left(\boldsymbol{J^k}\right)^{\boldsymbol{T}}\left[\boldsymbol{Y}-\boldsymbol{T}(\boldsymbol{P^k})\right] \qquad (35)$$

However, it is important to remember that the matrix $\mathbf{J^TJ}\approx 0$ in ill-conditioned problems and the Levenberg-Marquardt Method bypasses the difficulty using an iterative procedure in the following form:

$$\boldsymbol{P^{k+1}}=\boldsymbol{P^k}+\left[(\boldsymbol{J^k})^{\boldsymbol{T}}\boldsymbol{J^k}+\boldsymbol{\mu^k\Omega^k}\right]^{-1}\left(\boldsymbol{J^k}\right)^{\boldsymbol{T}}\left[\boldsymbol{Y}-\boldsymbol{T}(\boldsymbol{P^k})\right] \qquad (36)$$

where μ^k is a positive scalar (damping parameter) and Ω^k is a diagonal matrix. These terms have the aim to damp the oscillation caused by the ill-conditioned nature of the problem.

iii. Stopping Criteria definition

Dennis and Schnabel [29] propose criteria for stopping the iterative procedure of Levenberg-Marquardt Method:

$$S(P^{k+1}) < \varepsilon_1 \quad (37)$$

$$\|(J^k)^T[Y - T(P^k)]\| < \varepsilon_2 \quad (38)$$

$$\|P^{k+1} - P^k\| < \varepsilon_3 \quad (39)$$

where ε_1, ε_2, and ε_3 are user defined tolerance.

A second approach that allows to solve the problem of solution instability, used in the Part II of this thesis for a case of function estimation, is the *Tikhonov's regularization* method that add a regularization term to the least square solution. Considering the case of a estimation of a transient function *f(t)* at time t_i, $i = 1,2,3, \ldots I$, it is possible to write the objective function as follow:

$$O_f[f(t)] = \sum_{i=1}^{I} (Y_i - T_i)^2 + \lambda^* \sum_{i=1}^{I-d} (\boldsymbol{L_d} f_i)^2 \quad (40)$$

where $\lambda^* (> 0)$ is the regularization parameter and $\boldsymbol{L_d}$ is the derivative operator of *d* order of derivation.

When the regularization order is zero and the whole domain procedure is considered, the objective function can be written as follows:

$$O_f[f(t)] = \sum_{i=1}^{I}(Y_i - T_i)^2 + \lambda^* \sum_{i=1}^{I} {f_i}^2 \quad (41)$$

If $\lambda^* \to 0$ means that exact matching between measured and estimated temperatures is obtained. It is then important remember that the sum of the ${f_i}^2$ terms increases for small time steps while if λ^* is very large, the magnitude of the f_i terms decreases with the limit being $f_i = 0$. It means that the effect of $\lambda^* \neq 0$ is to reduce the magnitude of the f_i values.

Considering the whole domain first-order regularization procedure the objective function becomes:

$$O_f[f(t)] = \sum_{i=1}^{I}(Y_i - T_i)^2 + \lambda^* \sum_{i=1}^{I-1}(f_{i+1} - f_i)^2 \quad (42)$$

Another time if $\lambda^* \to 0$, exact matching is reached generating instability in the inverse problem. Large λ^* absolute values promote f_i to be constant. For this reason the magnitude of the f_i is not affected and for the values of $\lambda^* \neq 0$ the differences in the f_i terms decreases.

Finally, in the second-order regularization procedure of the entire domain, the objective function can be written as follow:

$$O_f[f(t)] = \sum_{i=1}^{I} (Y_i - T_i)^2 + \lambda^* \sum_{i=1}^{I-2} (f_{i+2} - 2\, f_{i+1} + f_i)^2 \qquad (43)$$

Again if $\lambda^* \to 0$, the exact matching of the temperatures is obtained whereas high λ^* values cause f_i to be a straight line. Therefore moderate values of λ^* reduce the rate of change of $f_i(t)$.

Resuming, the zeroth order reduces the magnitude of f_i, the first order reduces the magnitude of changes in the f_i and the second order regularization term tends to reduce rapid oscillations in the f_i.

The choice of the regularization parameter strongly affects the stability of the solution: if it is too small, a good fitting between the measured and the estimated temperatures will be verified but the solutions could present instabilities; large regularisation parameter negatively influences the fitting of the data and the ability to obtain a great residual. For this reason, the correct selection of the regularization parameter is fundamental in solving IHTPs.

Finally, also the *filtering technique* can be used for obtaining the smoothest approximated solution consistent with available data, handling the ill-posed nature of the IHCPs overcoming the instability of the solutions with respect to random errors or noise in the input data. Filtering allows to suppress the frequency components of the signal. This technique, in specific, is used in the Part III of this thesis for assessing a parameter estimation. Errors in measurements are distributed as Gaussian noise on the raw data and they are

uniformly distributed on them over the entire domain of frequencies, while important information are usually limited and concentrated in the low frequency range of the spectrum. When applying filtering techniques, it is important to define how many frequencies delete for solving the ill-posed nature of the inverse problem, but maintaining the more possible information in the spectrum for not losing important data.

Among the available techniques, low pass filter and Gaussian filter are the most adopted for this purpose.

It is important to observe that for successfully apply a filtering technique to IHTPs, a high resolution (spatially and/or temporally) temperature maps is required, otherwise they are not appliable.

However, their very low computational cost, makes them very attractive for these kinds of applications.

CHAPTER 4: Thermal characterization of Triple Tube Heat Exchangers by parameter estimation approach

4.1 Heat exchanger model

In this study, a TTHE operating in a parallel counter current arrangement was considered, where the process fluid to be heated (e.g. sterilisation of a food fluid) flows into Section 2 (Figure 4.1), and the hot service fluid flows both in Sections 1 and 3. The parallel counter current configuration was chosen for this analysis because it is the most commonly adopted in industrial applications, since it provides the best performance. The three fluids that passed through the system are assumed to be single phase, incompressible with constant thermal properties.

The inlet temperatures of the three fluids are assumed to be known, and so are the three mass flow rates (Figure 4.1).

a)

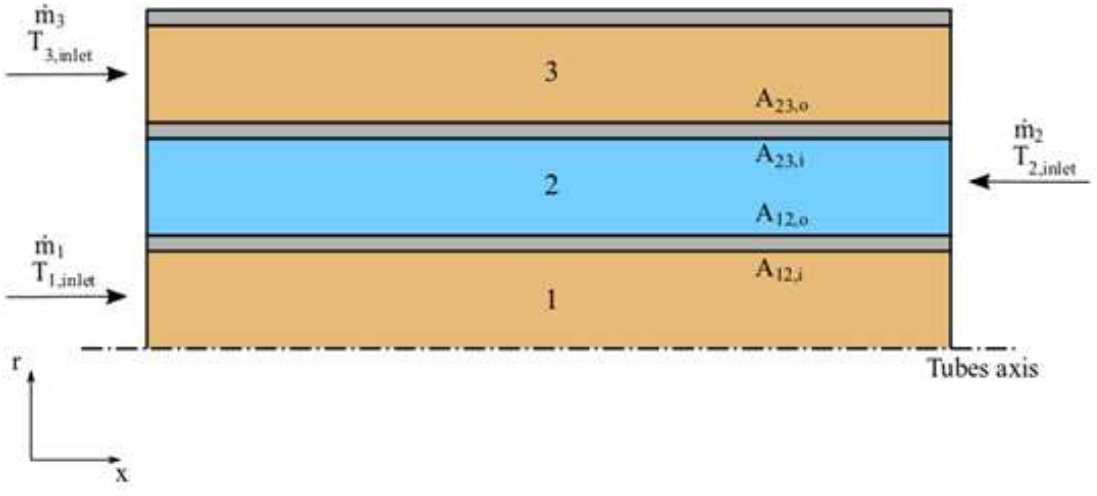

b)

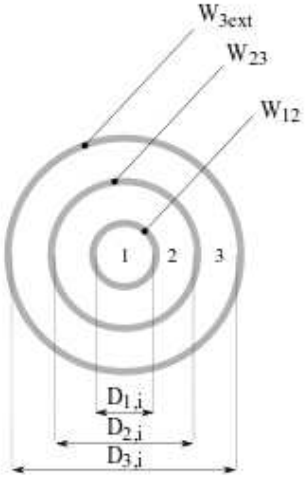

***Figure 4.1**: Schematic representation of the studied THE: (a) axial and b) cross view.*

The heat exchanger is assumed to be in a steady state regime and thermally insulated. Therefore, the heat transfer rates exchanged is obtained from the energy balance that for an infinitesimal fluid element is as follows:

$$dQ_1 = -\dot{m}_1 c_{p1} dT_1 \quad (44)$$

$$dQ_2 = -\dot{m}_2 c_{p2} dT_2 \quad (45)$$

$$dQ_3 = -\dot{m}_3 c_{p3} dT_3 \quad (46)$$

where $\dot{m}$ is the mass flow rate, c_p is the fluid specific heat at a constant pressure and T is the fluid bulk temperature. The subscripts $_{1,2,3}$ indicate the fluids flowing in the sections 1, 2 and 3 (Figure 4.1), respectively.

The negative sign in the energy equations is due to the x axis direction (Eq. (35)) and to the counter-current flows configuration (Eqs. (34,36)). Being the heat exchanger thermally insulated, energy balance equation for the section 2 (product side) could be evaluated also by:

$$dQ_2 = dQ_1 + dQ_3 \quad (47)$$

By introducing the overall heat transfer coefficients U_{12} between the product and the hot fluid that flows in section 1 and U_{23} between the product and the hot fluid that flows in section 3, Eqs. (34) and (36) can be rewritten as follows:

$$dQ_1 = U_{12} \Delta T_{12} dA_{12} \quad (48)$$

$$dQ_3 = U_{23} \Delta T_{23} dA_{23} \quad (49)$$

where:

- ΔT_{12} and ΔT_{23} are the temperature difference between the product and the hot fluid that flows in section1 and between the product and

the hot fluid that flows in section 3 for each axial coordinate, respectively:

$$\Delta T_{12} = T_1 - T_2 \quad (50)$$

$$\Delta T_{23} = T_3 - T_2 \quad (51)$$

– dA_{12} and dA_{23} are the heat transfer area between section1 and section 2 and between section 2 and section 3, respectively. They can be expressed in terms of the perimeter of the pipes, i.e. $dA = Pdx$.

Therefore, Eqs. (38) and (39) can be rewritten as follows:

$$dQ_1 = U_{12}P_{12}\Delta T_{12}dx \quad (52)$$

$$dQ_3 = U_{23}P_{23}\Delta T_{23}dx \quad (53)$$

By substituting Eqs. (42) and (43) in Eq. (44):

$$dQ_2 = U_{12}P_{12}\Delta T_{12}dx + U_{23}P_{23}\Delta T_{23}dx \quad (54)$$

Therefore, the complete set of energy equations (34-36) becomes:

$$\dot{m}_2 c_{p2} dT_2 = -U_{12}P_{12}\Delta T_{12}dx - U_{23}P_{23}\Delta T_{23}dx \quad (55)$$

$$\dot{m}_1 c_{p1} dT_1 = -U_{12}P_{12}\Delta T_{12}dx \quad (56)$$

$$\dot{m}_3 c_{p3} dT_3 = -U_{23}P_{23}\Delta T_{23}dx \quad (57)$$

Energy equations are solved by applying the finite difference method. Referring to Figure 2 Eqs. (45-47) can be formulated as follow:

$$\dot{m}_2 c_{p2}\left(T_{2\,(k-1)} - T_{2\,(k)}\right) = U_{12}P_{12}(T_1 - T_2)_{(k)}\Delta x + U_{23}P_{23}(T_3 - T_2)_{(k)}\Delta x \quad (58)$$

$$\dot{m}_1 c_{p1}\left(T_{1\,(k)} - T_{1\,(k-1)}\right) = -U_{12}P_{12}(T_1 - T_2)_{(k-1)}\Delta x \quad (59)$$

$$\dot{m}_3 c_{p3}\left(T_{3\,(k)} - T_{3\,(k-1)}\right) = -U_{23}P_{23}(T_3 - T_2)_{(k-1)}\Delta x \quad (60)$$

where $k=1,\ldots,K$ corresponds to the different axial coordinates at which the equations are solved and Δx is the space step. Equations (48-51) are solved by considering the following boundary conditions:

$$T_{2\,(K)} = T_{2,inlet} \quad (61)$$

$$T_{1\,(1)} = T_{1,inlet} \quad (62)$$

$$T_{3\,(1)} = T_{3,inlet} \quad (63)$$

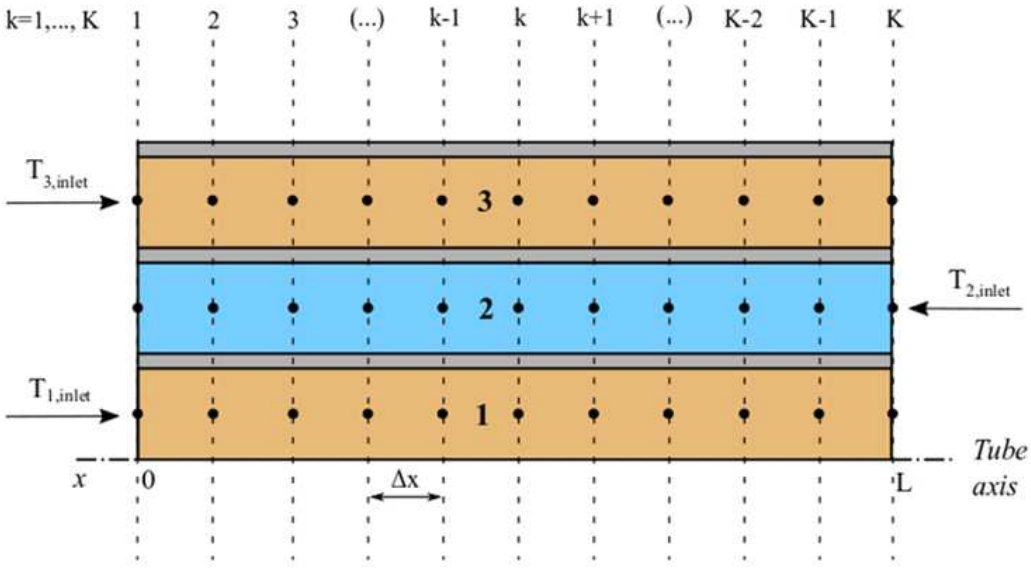

***Figure 4.2**:Finite difference scheme of the investigated heat exchanger*

Therefore, the temperatures at the different k axial coordinates can be evaluated as follows:

$$T_{2\,(k-1)} = T_{2\,(k)} + \frac{\Delta x}{\dot{m}_2 c_{p2}}\left[U_{21}P_{21}\left(T_{1\,(k)} - T_{2\,(k)}\right) + U_{23}P_{23}\left(T_{3\,(k)} - T_{2\,(k)}\right)\right] \quad (64)$$

$$T_{1\,(k)} = T_{1\,(k-1)} - \frac{U_{21}P_{21}\left(T_{1\,(k-1)} - T_{2\,(k-1)}\right)\Delta x}{\dot{m}_1 c_{p1}} \quad (65)$$

$$T_{3\,(k)} = T_{3\,(k-1)} - \frac{U_{23}P_{23}\left(T_{3\,(k-1)} - T_{2\,(k-1)}\right)\Delta x}{\dot{m}_3 c_{p3}} \quad (66)$$

The overall heat transfer coefficients U can be computed as [13]:

$$\frac{1}{U_{12}A_{12i}} = \frac{1}{h_1 A_{12i}} + R_{w12} + \frac{1}{h_2 A_{12o}} \quad (67)$$

$$\frac{1}{U_{23i}A_{23i}} = \frac{1}{h_2 A_{23i}} + R_{w23} + \frac{1}{h_3 A_{23o}} \quad (68)$$

where A_{12i} and A_{12o} (figure 1) are the internal and external heat transfer area of the section 1 respectively, while A_{23i} and A_{23o} (figure 1) are the internal and external heat transfer area of the section 2, respectively; U_{12i} is the internal overall heat transfer coefficient between section 1 and 2; h_{12i} and h_{12o} are the internal and external convective heat transfer coefficients between section 1 and 2, respectively; U_{23i} is the internal overall heat transfer coefficient between section 2 and 3; h_{23i} and h_{23o} are the internal and external convective heat transfer coefficients between section 2 and 3, respectively. R_{w12} and R_{w23} are the wall thermal resistances, which can be computed as [3]:

$$R_{w12} = \frac{ln[(D_{1o})/D_{1i}]}{2\pi\lambda_w L} \quad (69)$$

$$R_{w23} = \frac{ln[(D_{2o})/D_{2i}]}{2\pi\lambda_w L} \quad (70)$$

where D_{1i} and D_{1o} are the internal and external diameter of section 1, while D_{2i} and D_{2o} are the internal and external diameter of section 2 (see Figure 1), respectively; λ_w, and L are the wall thermal conductivity, and pipe length, respectively.

The convective heat transfer coefficients can be evaluated by the Nusselt numbers, which were expressed by the following equations:

$$Nu_1 = \frac{h_1 D_{1i}}{\lambda_1} \quad (71)$$

$$Nu_2 = \frac{h_2 D_{2h}}{\lambda_2} \quad (72)$$

$$Nu_3 = \frac{h_3 D_{3h}}{\lambda_3} \quad (73)$$

where D_{2h} and D_{3h} are the hydraulic diameter of the sections 2 and 3, respectively. The value of the Nusselt number can be computed if any correlation is already available in literature or can be determined conducting a set of experimental results as it is proposed in the present paper.

The Nusselt number in the fully developed region can be generally expressed as a function of Reynolds and Prandtl numbers [3]:

$$Nu_1 = C_1 Re^{\alpha_1} Pr^{\beta_1} \quad (74\,a)$$

$$Nu_2 = C_2 Re^{\alpha_2} Pr^{\beta_2} \quad (34\,b)$$

$$Nu_3 = C_3 Re^{\alpha_3} Pr^{\beta_3} \quad (34\,c)$$

where C, α, β are a set of characteristic coefficients of each of the three sections of the heat exchanger under test. In sight of this, substituting in Eqs. (54-56) the definitions of U_{12i} and U_{23i} (Eqs. (57, 58)), where R_{w12} and R_{w23} are

defined by Eqs. (59, 60), h_1, h_2, $h3$ are obtained from Eqs. (61-63) adopting the Nusselt numbers formulations given by Eqs. (64a-64c), it is possible to obtain:

$$T_{2\,(k-1)} = T_{2\,(k)} + \frac{\Delta x}{\dot{m}_2 c_{p2}}\left[\frac{1}{A_{12i}}\left(\frac{D_{1i}}{C_1 Re^{\alpha_1} Pr^{\beta_1}\lambda_1 A_{12i}} + R_{w12} + \frac{D_{2h}}{C_2 Re^{\alpha_2} Pr^{\beta_2}\lambda_2 A_{12o}}\right)^{-1} P_{21}\left(T_{1\,(k)} - T_{2\,(k)}\right) + \frac{1}{A_{23i}}\left(\frac{D_{2h}}{C_2 Re^{\alpha_2} Pr^{\beta_2}\lambda_2 A_{23i}} + R_{w23} + \frac{D_{3h}}{C_3 Re^{\alpha_3} Pr^{\beta_3}\lambda_3 A_{23o}}\right)^{-1} \cdot P_{23}\left(T_{3\,(k)} - T_{2\,(k)}\right)\right] \quad (75)$$

$$T_{1\,(k)} = T_{1\,(k-1)} - \frac{\frac{1}{A_{12i}}\left(\frac{D_{1i}}{C_1 Re^{\alpha_1} Pr^{\beta_1}\lambda_1 A_{12i}} + R_{w12} + \frac{D_{2h}}{C_2 Re^{\alpha_2} Pr^{\beta_2}\lambda_2 A_{12o}}\right)^{-1} P_{21}\left(T_{1\,(k-1)} - T_{2\,(k-1)}\right)\Delta x}{\dot{m}_1 c_{p1}} \quad (76)$$

$$T_{3\,(k)} = T_{3\,(k-1)} - \frac{\frac{1}{A_{23i}}\left(\frac{D_{2h}}{C_2 Re^{\alpha_2} Pr^{\beta_2}\lambda_2 A_{23i}} + R_{w23} + \frac{D_{3h}}{C_3 Re^{\alpha_3} Pr^{\beta_3}\lambda_3 A_{23o}}\right)^{-1} P_{23}\left(T_{3\,(k-1)} - T_{2\,(k-1)}\right)\Delta x}{\dot{m}_3 c_{p3}} \quad (77)$$

Eqs (32-34) represent the direct formulation of the problem under study that is concerned with the determination of the outlet temperatures of the three sections when all the coefficients C, α, β are known. In the inverse formulation, the coefficients C, α, β are instead regarded as being unknown, whereas the outlet temperatures of the three sections are measured.

4.2 Parameter estimation and sensitivity analysis for the characterisation of TTHE behaviour

The parameter estimation procedure is embedded in the inverse solution of the problem expressed by Eqs (65-67). The outlet temperatures of the three sections T_1, T_2, and T_3 can be easily computed by imposing trial values of the coefficients C, α, β. In the inverse formulation, the computed values of the outlet temperatures are forced to match the experimental temperature values, by tuning the coefficients C, α, β. The matching of the two temperature distributions (the computed and the experimentally acquired) could be easily performed under a least square approach. Therefore, the coefficients C, α, β could be estimated by minimizing the following functional:

$$S(\boldsymbol{P}) = \sum_{n=1}^{N} \left[\boldsymbol{T}_{exp,n} - \boldsymbol{T}_{calc,n} \right]^2 \qquad (78)$$

where $\boldsymbol{P}$ is the vector of the parameters that we want to estimate, $\boldsymbol{T}_{exp}$ and $\boldsymbol{T}_{calc}$ are the experimental and predicted variables, respectively, and N is the total number of measurements.

In a TTHE heat exchanger the coefficients C, α, β must be estimated for all the three sections in which are flowing the fluids: in this way the number of unknowns ($\boldsymbol{P}$ vector) that must be found are 9. In the parameter estimation procedure here adopted these 9 parameters are forced to vary by means of a non-

linear fit algorithm that is based on the iterative reweighted least squares method [20] in order to minimize the objective function expressed in Eq. (68). Being a nonlinear regression, it requires a significant computational cost and an elevated number of measurements to proper estimate all the unknowns. For this reason, when talking about parameter estimation procedures and inverse problems in general it is fundamental to do all the simplifications that can be reasonably performed. In the present case we can made the following simplifications:

- The β coefficients that characterize the dependency of the Nusselt number from the Prandtl number can be considered 0.4 in heating processes and 0.3 in cooling processes. This choice is very common, also when double tube heat exchangers are considered, because β coefficients have a limited impact on the accuracy of the Nusselt correlation.
- C and α for the section 1 could be find from one of the correlations available in literature for straight smooth wall tube. This geometric configuration has been widely studied in the past and considering that moreover mostly of the times the fluid flowing in section 1 is in turbulent regime it is a reasonable approximation to consider them a priori known.

– The same argumentation for section 1 could be done also for section 3: in this case we are talking about annular section that has been deeply investigated in literature too.

After these considerations the number of unknowns is decreased to two: C and α for section 2, that we are going to call in the following C_2 and α_2.

To endorse the assumptions above explained, it must be said that, also from the practical point of view, these two parameters are the crucial ones in the design process in the great majority of applications of TTHE because these heat exchangers are especially adopted for highly viscous fluids and, consequently, the thermal resistance of the product side is the dominant in the overall heat exchange performance.

Finally, the function that should be minimized using the usual least squares approach can be written as follows:

$$S(C_2, \alpha_2) = \sum_{i=1}^{M} \left[\boldsymbol{T}_{exp,i} - \boldsymbol{T}_{calc,i} \right]^2 \qquad (79)$$

where $\boldsymbol{T}_{exp}$ is the measurements vector composed as follows:

$$\boldsymbol{T}_{exp} = [T_{1,outlet}, T_{2,outlet}, T_{3,outlet}] \qquad (80)$$

$T_{1,outlet}$, $T_{2,outlet}$, $T_{3,outlet}$ are the outlet temperatures of the three sections measured for the N tests. Consequently, the vector $\boldsymbol{T}_{exp}$ has dimensions 1 x M where $M = 3 \cdot N$. Analogously it works for the vector $\boldsymbol{T}_{calc}$ that is obtained by

solving the direct problem described by Eqs (32-34) by imposing the values of the coefficients C, α, β.

Then, the parameter estimation procedure applied to the heat transfer characterization of TTHE results in the minimization of the objective function S given by Eq. (36) by assuming Re and Pr as the independent variables, C_2 and α_2 as the unknown variables, and all the other properties and geometrical quantities as known.

The practical possibility of concurrently estimating all the unknown parameters (C_2 and α_2) is feasible only if the parameter sensitivity coefficients for the output variable T with respect to each parameter are linearly independent over the range of interest [24]. In practice, the sensitivity coefficients quantify the extent to which variations of the parameters of interest affect the answer output of the system. The coefficients are then defined with respect to the generic parameter P_i as follows:

$$J_i = \frac{\partial \boldsymbol{T}}{\partial P_i} P_i \qquad (81)$$

where P_i stands for the unknown variables, i.e., C_2 and α_2 and $\boldsymbol{T}$ is the outlet temperature vector (Eq.69).

Although the sensitivity analysis is a useful tool to theoretically verifying the possibility of concurrently estimating several unknown variables, it does not

provide any quantitative information about the uncertainty associated with each estimated value [21]. A well-known method used to address this issue involves the computation of confidence intervals for the parameter estimates by asymptotic theory [30] [31]. Following this approach, once the optimal curve-fit parameters P_{fit} are determined, the parameter standard errors σ_P are given by:

$$\boldsymbol{\sigma}_P = \sqrt{\sigma_T^2 \cdot diag([\boldsymbol{J}^T \cdot \boldsymbol{J}]^{-1})} \quad (82)$$

where $\boldsymbol{J}$ is the Jacobian matrix of the target variable, i.e., the function $\boldsymbol{T}_{calc}$

$$\boldsymbol{J} = \left[\frac{\partial \boldsymbol{T}_{calc}(\boldsymbol{P}_{fit})}{\partial \boldsymbol{P}}\right] \quad (83)$$

and σ^2_T is the residual variance:

$$\sigma_T^2 = \frac{1}{M - z}\sum_{i=1}^{M}\left[\boldsymbol{T}_{exp,i} - \boldsymbol{T}_{calc,i}(P_{fit})\right] \quad (84)$$

where M is the number of measurements and z is the number of parameters to be fitted.

To express the reliability of the parameter estimates and to compare the relative precision of different parameter estimates the 95% confidence interval, $CI^{95\%}$, and the coefficient of variation, CV, are generally used [30]. Regarding the parameter P_i, they are defined as follows:

$$CI_{P_i}^{95\%} = (P_i - 1.96\sigma_{P_i}, P_i + 1.96\sigma_{P_i}) \quad (85)$$

$$CV_{P_i} = \frac{\sigma_{P_i}}{P_i} \quad (86)$$

4.3 Application of the parameter estimation procedure to synthetic data

Before the experimental measurements were used, the parameter estimation procedure was validated by means of synthetic data. The geometrical and thermal characteristics of the triple tube heat exchanger are summarized in Table 1. These geometrical characteristics were chosen because the proposed method was validated against the experimental data obtained using this type of heat exchanger. It must be pointed out that these properties, coupled with the proper Nusselt number correlations both for the pipe and the shell sides, allow the evaluation of the heat transfer mechanism.

Dimension	Value
D_{1i} (mm)	40.9
D_{1o} (mm)	48.3
D_{2i} (mm)	66.9
D_{2o} (mm)	73.0
D_{3i} (mm)	83.8
D_{3o} (mm)	88.9
L (mm)	1010
λ (W/m·K)	15

Table 4.1*:Geometrical characteristics of TTHE*

Synthetic data for the outlet temperatures of the three sections were obtained by solving the direct problem described by Eqs (65-67) by imposing the values of the coefficients C, α, β.

It was considered a possible application in food industry: water is assumed as service heating fluid that flow in sections 1 and 3 while a highly viscous product flows (i.e., fruit purees or concentrated juices) in section 2 in a counter current configuration. Constant physical properties are considered: ρ_S= 1000 Kg·m^{-3}, μ_S= 10^{-3} Pa·s and λ_S= 0.6 W·m^{-1}·K^{-1} for the water while the product is characterized by ρ_P= 1054 kg·m^{-3}, μ_P= 2.6·10^{-1} Pa·s and λ_P= 5.9 ·10^{-1} W·m^{-1}·K^{-1}, calculated considering a 16°Bx juice at 50°C [32].

The fluids flowing in sections 1 and 3 were considered flowing in turbulent regime: Re_1 and Re_3 were kept fixed at 2.1·10^5, while the product was considered in a laminar condition with Re_2 varying in the range of 5 – 500, generating a set of 100 tests. Synthetic noiseless data are obtained with Eqs. (65-67) assuming $C_1 = C_2 = C_3 = 0.023$, $\alpha_1 = \alpha_2 = \alpha_3 = 0.8$, $\beta_1 = \beta_3 = 0.3$ and $\beta_2 = 0.4$.

To simulate the presence of experimental noise, the synthetic data obtained from the solution of the direct problem (Eqs (65-67)) assuming the data above reported, were deliberately spoiled by random noise. A Gaussian white noise was introduced. For the T synthetic data were generated according to the following:

$$
\begin{aligned}
T_{1,outlet} &= T_{1,outlet,noiseless} + \zeta\epsilon \\
T_{2,outlet} &= T_{2,outlet,noiseless} + \zeta\epsilon \\
T_{3,outlet} &= T_{3,outlet,noiseless} + \zeta\epsilon \\
T_{1,inlet} &= T_{1,inlet,noiseless} + \zeta\epsilon \\
T_{2,inlet} &= T_{2,inlet,noiseless} + \zeta\epsilon \\
T_{3,inlet} &= T_{3,inlet,noiseless} + \zeta\epsilon
\end{aligned}
\qquad (87)
$$

where ζ is the temperature noise level and ϵ is a random Gaussian variable with zero mean and unit variance. Five different noisy datasets were generated using five levels of noise, specifically: ζ = 0.01 K, ζ = 0.05 K, ζ= 0.1 K, ζ = 0.5 K, and ζ = 1 K. Finally, the noisy datasets were elaborated with the inverse estimation procedure based on the minimization of the squared errors of the prediction with respect to the experimentally measured outlet temperatures values (Eq. (69)).

The objective of this procedure is to find a correlation for the Nusselt number that can describe the heat transfer behaviour of section 2 of the heat exchanger. To reach this goal and referring to Eq. (64) it is necessary to estimate, as it is highlighted in paragraph 3, the coefficients C and α for section 2.

To verify the practical possibility of concurrently estimating the two parameters (C_2 and α_2), it is important to analyse the behaviour and the relative magnitude of their sensitivity coefficients versus the independent variables, i.e., the Reynolds number in section 2. The sensitivity coefficients calculated respect

to the vector composed by the outlet temperatures of the three sections (Eq (70)) of the heat exchanger were computed and reported in Figure 4.3

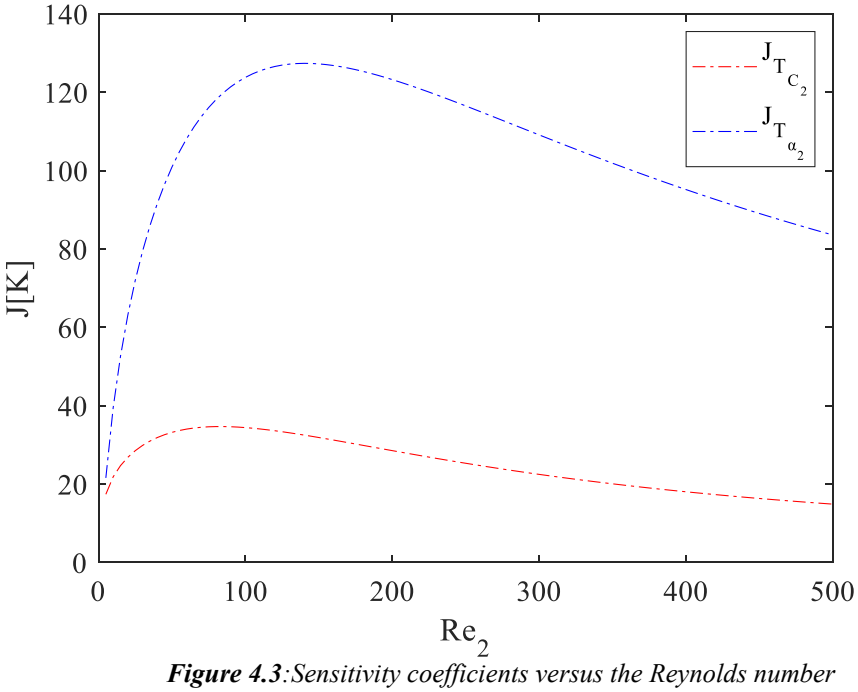

***Figure 4.3**:Sensitivity coefficients versus the Reynolds number*

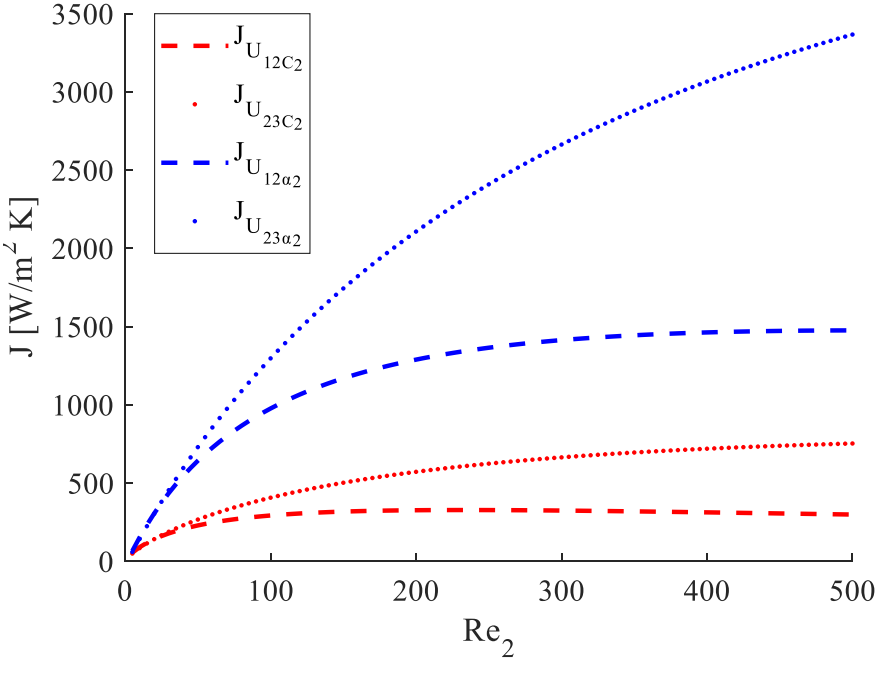

***Figure 4.4**: Sensitivity coefficients versus the Reynolds number*

Figure 4.3 shows that, $J_{T_{c_2}}$ displays a linear independence from $J_{T_{\alpha_2}}$ for Re_2 lower than 400 while for higher values they are not completely linearly independent. The highest values of sensitivity coefficients are obtained in the range $50 < Re_2 < 300$ for $J_{T_{c_2}}$ and in the range $100 < Re_2 < 350$ for $J_{T_{\alpha_2}}$. These two evidences mean that, the optimal estimation of both C_2 and α_2 can be obtained for product Reynolds number values between 100 and 300 and that their concurrent estimation in the same Reynolds number range is feasible since they are linearly independent. The fact that the highest sensitivity coefficients can be found for Re_2 lower than 300 is related to the elevated values that the thermal

resistance of the product side assumes when the mass product flow is low: being the flow in sections 1 and 3 turbulent the greatest contribution to overall thermal resistance of the heat exchanger is due to the one related to section 2 permitting to have a high sensitivity in the estimation of the coefficients that describe the thermal behaviour of that section. Another important element is related to the fact that the sensitivity coefficient for α_2 presents significantly higher values than that for C_2 highlighting that its estimation can be performed with higher accuracy.

To better investigate this point, the influence of the estimated parameters on the overall heat transfer coefficients was evaluated. In Figure 4.4 the sensitivity coefficients for U_{12} and U_{23} as a function of the Reynolds number of the product are presented. The sensitivity coefficient for α_2 presented significantly higher values than that for C_2, confirming that the estimation of α_2 could be performed with higher accuracy, as highlighted above by the sensitivity coefficient for the outlet temperatures. The uncertainty associated with each estimated parameter value was assessed using the parameter covariance matrix by asymptotic theory [30], [31]. Both the 95% confidence intervals and the coefficients of variation are calculated according to Eqs. (75, 76).

Table 4.2 reports the results of the minimization for each level of noise and in Figure 4.5 there are graphically shown the trend of the coefficients of variation

as a function of noise level. It is possible to observe that the adopted estimation procedure allows to obtain a great estimation of the unknown coefficients.

Noise level (ζ)	Unknow parameter	Exact value	Estimated value	CI 95%	CV (%)
0.01	C_2	0.023	0.023	(0.023, 0.023)	0.04%
	α_2	0.800	0.800	(0.800, 0.800)	0.01%
0.05	C_2	0.023	0.023	(0.023, 0.023)	0.23%
	α_2	0.800	0.800	(0.799, 0.801)	0.06%
0.1	C_2	0.023	0.023	(0.023, 0.023)	0.45%
	α_2	0.800	0.800	(0.796, 0.801)	0.12%
0.5	C_2	0.023	0.023	(0.022, 0.024)	2.03%
	α_2	0.800	0.803	(0.794, 0.811)	0.52%
1	C_2	0.023	0.023	(0.021, 0.025)	4.2%
	α_2	0.800	0.802	(0.785, 0.819)	1.07%

***Table 4.2**: Results of parameter estimation with synthetic data*

Even in the case with the highest noise level (ζ = 1 K), the confidence intervals and the CVs, for both C_2 and α_2, are very small confirming the efficacy of the estimation procedure. In the worst conditions the highest value of CV is 4.2% underlying the very good results achieved. Moreover, the higher values of CV for C_2 with respect to the ones of α_2, confirm what can be seen from the sensitivity coefficients reported in Fig.3 where, $J_{T_{C_2}}$ displays lower values than $J_{T_{\alpha_2}}$ revealing a, even if slightly, major difficulty in the estimation of C_2.

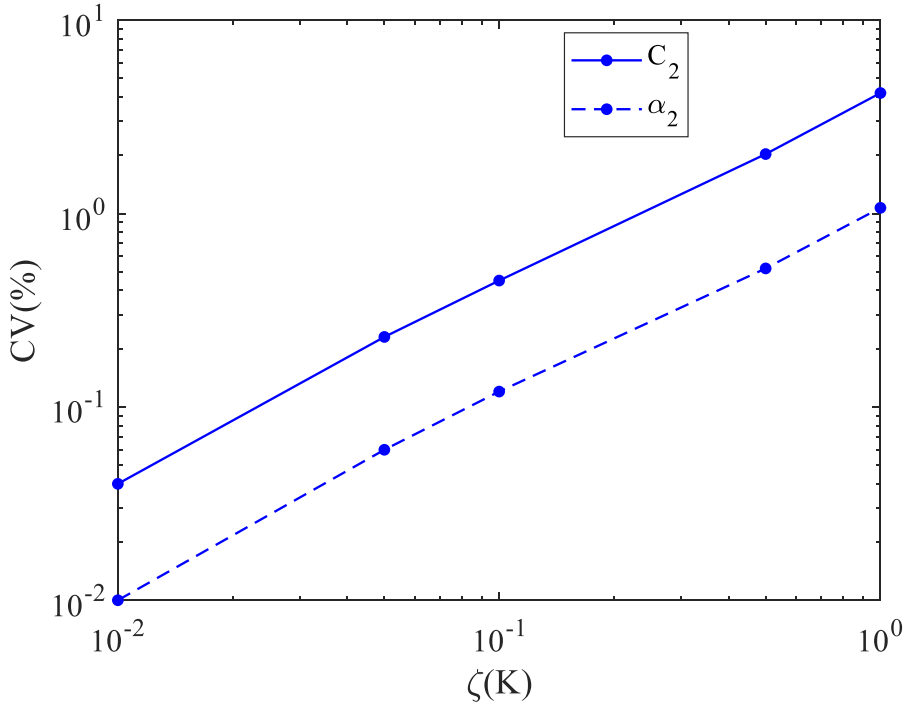

Figure 4.5: Coefficients of variation obtained with synthetic data for different noise levels

To give additional insight in the evaluation of the effectiveness of the proposed estimation approach at different noise level values a residual analysis

was performed by computing the relative estimation error on the heat power exchanged by the product Q_2, defined as follows:

$$E_{Q_2} = \frac{\|(\boldsymbol{Q_2})_{restored} - (\boldsymbol{Q_2})_{exact}\|_2}{\|(\boldsymbol{Q_2})_{exact}\|_2} \quad (88)$$

where $(\boldsymbol{Q_2})_{restored}$ and $(\boldsymbol{Q_2})_{exact}$ are the vectors composed by the restored and exact heat power values of the 100 considered tests. This estimation error is calculated on the heat power exchanged by the product since it is the quantity of major interest in heat exchangers: the final goal is that the product receives or dissipates the prescribed heat power. The E_{Q_2} distribution as a function of noise is reported in Figure 4.6a while in Figure 4.6b it is shown the deviation of the computed values of Q_2, obtained using the estimated parameters, respect to the exact values for the case of the highest noise level (ζ = 1 K).

a)

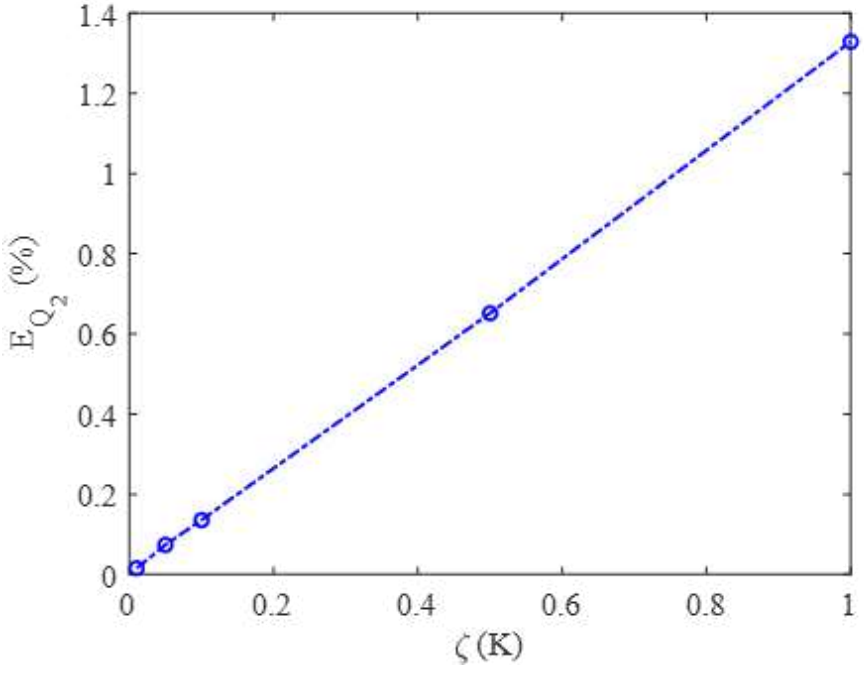

b)

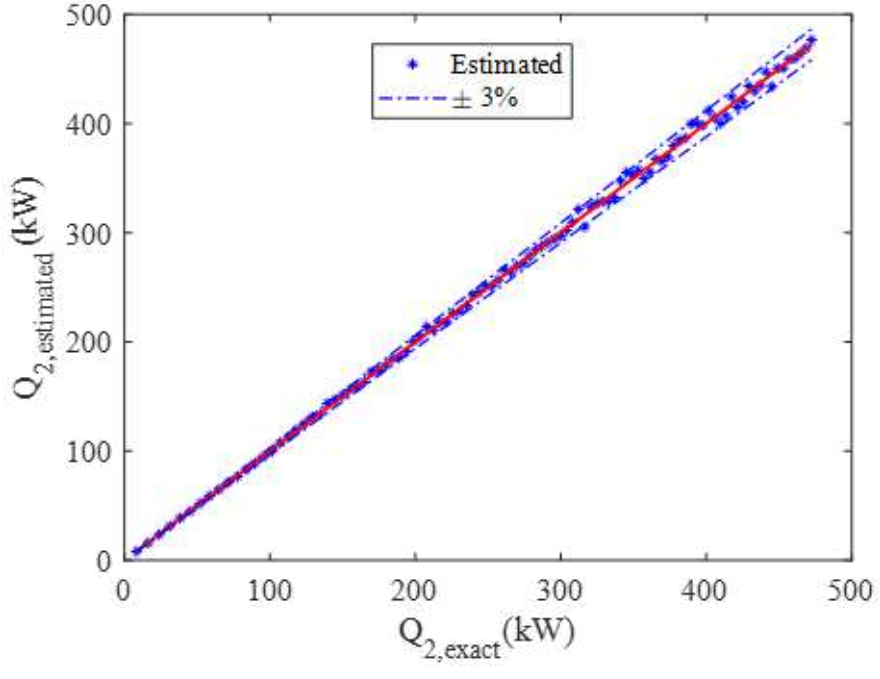

***Figure 4.6**: Estimation error E_{Q2} as a function of the noise level (a) and comparison between exact and estimated heat power Q_2 for noise level ζ = 1 K (b)*

The estimation error (Figure 4.6a) on the exchanged heat power underlines the high efficacy of the present procedure showing very low values with a maximum of 1.4%. Moreover, the random distribution of the estimated heat power values respect to the exact ones put additional emphasis on the high assessment ability of the proposed method: all the values (Figure 4.6b) are within a ±3% band.

4.4 Application of the parameter estimation approach to experimental data

i. Experimental facility

The estimation methodology described above is assessed in a TTHE located in the pilot plant of the company JBT-FoodTech (Parma- Italy). The heat exchanger, made of AISI 304 and characterized by the geometrical features reported in Table 4.1, is schematically represented in section in Figure 4.7 Figure 2.1(a) and in 3D view in Figure 4.7 (b).

The scheme of the experimental setup where the tested TTHE is inserted is shown in Figure 4.8. It essentially consists of a hydraulic circuit coupled with a data acquisition system. The hydraulic circuit moves the treated fluid (tomato double concentrate), which is heated through the TTHE, then passes to a short thermal rest section, and finally is cooled so that it can be used again under the same initial conditions.

The product is loaded into a feed tank with a capacity of about 0.5 m^3 and supported by a single screw volumetric feed pump that sends the product into a piston pump controlled by a frequency variator.

a)

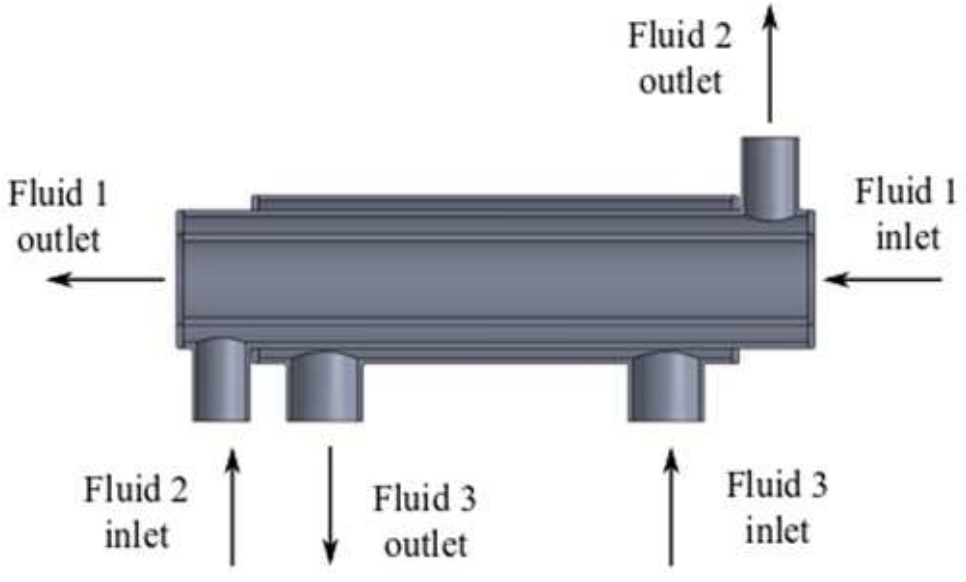

b)

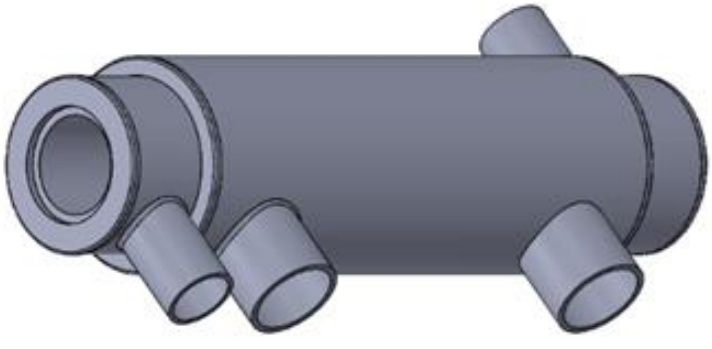

Figure 4.7*: (a) Sketch of the section of the experimentally tested TTHE. (b) 3D view of TTHE*

The service fluid used to heat the product is hot water that is heated by means of a tube-in-tube heat exchanger, in which steam, produced by an external boiler, circulates. The steam flow rate is controlled in feedback from the product outlet temperature of the TTHE, through a modulating valve. For the cooling of the product, a series of dimpled tube exchangers are used in which cold water circulates. The flow rate of cold water is controlled in feedback from the outlet temperature of the product in the cooling section. Finally, to prevent heat transfer with the external environment, the heat exchanger was thermally insulated all length long of its transfer area.

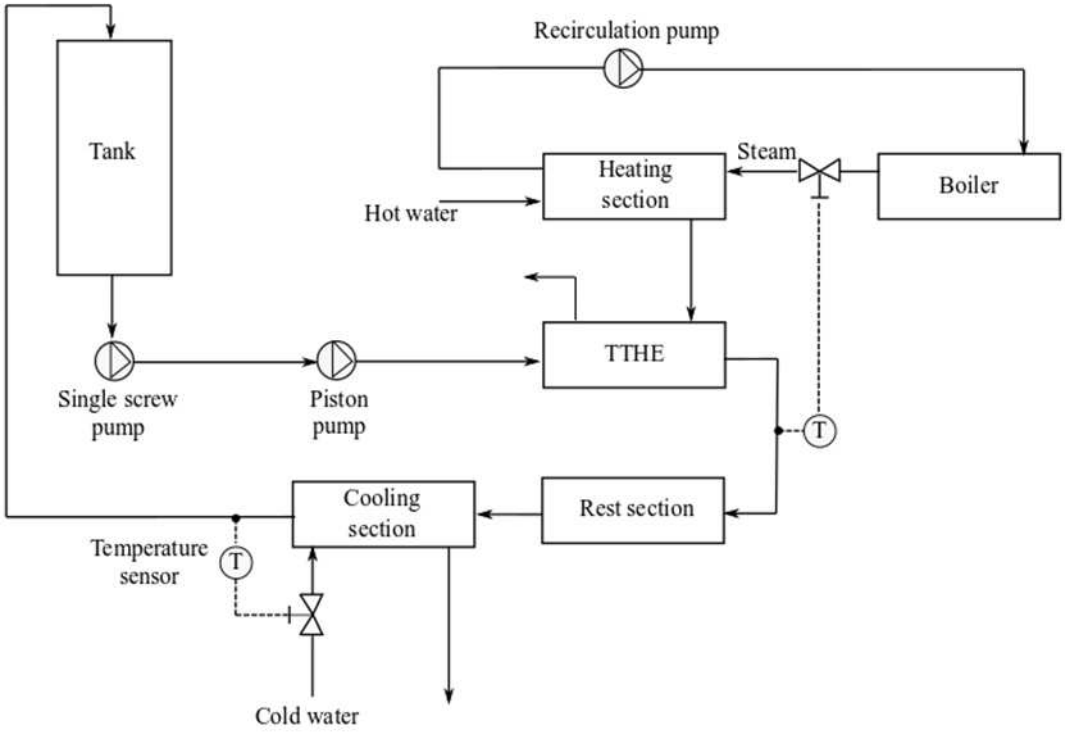

***Figure 4.8**: Scheme of the experimental setup*

The product flow rate is measured using a Rosemount electromagnetic flowmeter placed between the piston pump and the TTHE. The hot water flow rate is measured using a Siemens electromagnetic flowmeter positioned before the heating section. The measurement of the product inlet temperature in section 2 is done by Pt 100 thermo-resistances placed inside the feed tank. The product outlet temperature is measured with another thermo-resistance placed at the end of section 2. For the hot water that flows in sections 1 and 3, four thermo-resistances measure the temperature at the inlet and at the outlet of both section 1 and section 3.

In the data reduction the average bulk temperature between the inlet and outlet sections is used for evaluating all fluids properties. For the fluids' properties there are used the tabulated values reported by [3]. However, the tested product is tomato double concentrate, and the definition of its properties can be quite tricky; in particular the determination of viscosity is critical due to its non-Newtonian behaviour.

The viscosity μ_P of the double tomato concentrate for each test is determined according to the Ostwald-de Waele model [32]:

$$\mu_P = \frac{\tau_P}{\dot{\gamma}} = -\frac{K \cdot \dot{\gamma}^n}{\dot{\gamma}} = -K(\dot{\gamma})^{n-1} \quad (89)$$

where, K is the consistency index, $\dot{\gamma}$ is the shear rate and n is the flow behaviour index.

A Brookfield R/S+ rheometer equipped with the coaxial cylinders probe CC25 in "Searle system" configuration is used to measure the shear stress (τ_b) of the tomato concentrate by varying the share rate in the range of 0,13 - 1290 s-1 at four different temperatures: 20°C, 30°C, 40°C and 50°C. Values of *K* and *n* are determined as follow:

$$n = \frac{d(ln\,\tau_P)}{d(ln\,V_r)} \tag{90}$$

$$K = \frac{exp\ i}{(\frac{\pi}{15\,n} \cdot \frac{1}{1-(\frac{R_b}{R_c})^{2/n}})^n} \tag{91}$$

where V_r, R_b and R_c are the rotation velocity of the internal cylinder, the radius of the cylinder and the internal radius of the external cylinder respectively. According with Trifirò et al. [33], an exponential dependence on temperature for *K* value and a linear one for *n* value is assumed and a regression is performed using these two models:

$$K = K_0 \cdot K_T^{(\frac{1000}{T})} \tag{92}$$

$$n = n_0 + n_T \cdot 1000/T \tag{93}$$

where K_0, K_T, n_0 and n_T are the parameters to determine to calculate the values of *n* and *K* for any value of temperature of interest in the range considered for the tests using Eq. (46).

The generalised Reynolds number values were then calculated adopting the equation given by Kozicki et al. [34] valid for non-Newtonian fluids flowing in an annular section:

$$Re_g = \frac{\rho\, \tilde{u}^{2-n} D_h^n}{8^{n-1} K (b + \frac{a}{n})^n} \qquad (94)$$

where D_h is the hydraulic diameter and a and b are geometrical parameters considered equal to 0.499 and 0.999, respectively.

ii. Results

To consider the typical operating conditions of TTHEs in the food industry, which generally handle highly viscous fluids, tomato double concentrate is used as the working fluid and water is used as the service fluid.

the experimental conditions of the test runs. In the data processing and in the definition of the dimensionless parameters, the properties of the working fluid (tomato double concentrate) are evaluated at the average bulk temperature between the inlet and outlet sections.

Test	$\dot{m}_2$	$T_{1,inlet}$	$T_{1,outlet}$	$T_{2,inlet}$	$T_{2,outlet}$	$T_{3,inlet}$	$T_{3,outlet}$	Re_1	Pr_1	Re_{g2}	Pr_{g2}	Re_3	Pr_3
1	5.70	56.5	53.5	21.9	50.1	56.5	55.4	$4.5 \cdot 10^3$	3.2	4.3	$6.2 \cdot 10^3$	$7.3 \cdot 10^4$	3.2
2	5.71	58.1	54.5	21.8	50.2	58.1	56.7	$4.0 \cdot 10^3$	3.1	5.7	$5.4 \cdot 10^3$	$7.8 \cdot 10^4$	3.1
3	5.71	59.2	55.3	22.2	50.3	59.2	57.6	$3.9 \cdot 10^3$	3.0	7.0	$5.0 \cdot 10^3$	$8.0 \cdot 10^4$	3.0
4	5.71	60.8	56.3	22.0	50.4	60.8	59	$4.2 \cdot 10^3$	3.0	8.7	$4.5 \cdot 10^3$	$8.1 \cdot 10^4$	3.0
5	5.71	60.9	55.9	21.8	50.2	60.9	58.8	$4.7 \cdot 10^3$	3.0	10.8	$4.1 \cdot 10^3$	$7.8 \cdot 10^4$	3.0
6	5.71	60.6	55.4	21.7	50.2	60.6	58.4	$4.6 \cdot 10^3$	3.0	12.6	$3.8 \cdot 10^3$	$7.9 \cdot 10^4$	3.0
7	5.70	60.2	54.7	21.7	50.2	60.2	57.8	$4.4 \cdot 10^3$	3.0	14.6	$3.6 \cdot 10^3$	$7.8 \cdot 10^4$	3.0
8	5.70	60.6	55	21.7	50.3	60.6	58.2	$5.0 \cdot 10^3$	3.0	15.7	$3.5 \cdot 10^3$	$7.6 \cdot 10^4$	3.0
9	5.71	61.2	55.3	21.7	50.2	61.2	58.6	$4.9 \cdot 10^3$	3.0	18.1	$3.3 \cdot 10^3$	$7.8 \cdot 10^4$	3.0
10	5.72	62.2	55.9	21.7	50.3	62.2	59.4	$4.6 \cdot 10^3$	3.0	20.4	$3.1 \cdot 10^3$	$8.0 \cdot 10^4$	3.0
11	5.71	61.9	55.5	22.3	50.2	61.9	59.0	$4.6 \cdot 10^3$	3.0	23.0	$3.0 \cdot 10^3$	$8.0 \cdot 10^4$	3.0
12	5.66	121.3	106.9	49.3	99.0	121.3	114.1	$8.7 \cdot 10^3$	1.5	51.1	$1.6 \cdot 10^3$	$16 \cdot 10^4$	1.5
13	5.66	120.9	107.0	48.2	98.3	120.9	114.1	$8.8 \cdot 10^3$	1.5	41.5	$1.7 \cdot 10^3$	$15 \cdot 10^4$	1.5
14	5.66	121.0	108.6	48.9	98.8	121.0	114.9	$8.5 \cdot 10^3$	1.5	33.1	$1.9 \cdot 10^3$	$16 \cdot 10^4$	1.5
15	5.67	115.0	104.8	49.5	98.5	115.0	110.1	$8.1 \cdot 10^3$	1.5	24.1	$2.2 \cdot 10^3$	$15 \cdot 10^4$	1.5
16	5.67	113.1	104.1	50.6	98.6	113.1	108.8	$8.1 \cdot 10^3$	1.6	19.2	$2.4 \cdot 10^3$	$15 \cdot 10^4$	1.6
17	5.67	113.1	104.6	49.5	98.4	113.1	109.1	$6.6 \cdot 10^3$	1.6	15.7	$2.6 \cdot 10^3$	$15 \cdot 10^4$	1.6
18	5.67	111.8	104.7	49.6	98.5	111.8	108.5	$6.6 \cdot 10^3$	1.6	9.7	$3.2 \cdot 10^3$	$15 \cdot 10^4$	1.6
19	5.67	105.6	101.0	49.1	98.4	105.6	103.7	$4.4 \cdot 10^3$	1.7	5.0	$4.3 \cdot 10^3$	$15 \cdot 10^4$	1.7

***Table 4.3**: Experimental conditions*

The measured and calculated values of the outlet temperatures of the three sections of the TTHE are forced to match by minimising the functional given by Eq. (69) as described in the previous paragraph.

The estimated values of C_2 and α_2 for the product side are reported in Table 4 together with the confidence intervals and the coefficient of variation.

Unknow parameter	**Estimated value**	**CI$^{95\%}$**		**CV**
C_2	0.313	0.273	0.354	6.55%
α_2	0.707	0.662	0.751	3.20%

***Table 4.4**: Estimates values for the experimental data set*

As predicted by the application of the estimation procedure to the synthetic data, the highest uncertainty is associated with the estimation of the multiplicative constant C_2 (coefficient of variation of approximately 6.5%), while the Reynolds number exponent α_2 is determined with a coefficient of variation of approximately 3%. Anyway, both the parameters have been estimated with a very small coefficient of variation and limited confidence intervals demonstrating the goodness of the parameter estimation approach here presented.

The experimental values of heat power exchanged by the product Q_2 are compared in Figure 4.9 to the values obtained by using the optimal correlation found for section 2:

$$Nu_2 = 0.313\, Re^{0.707} Pr^{0.4} \qquad (95)$$

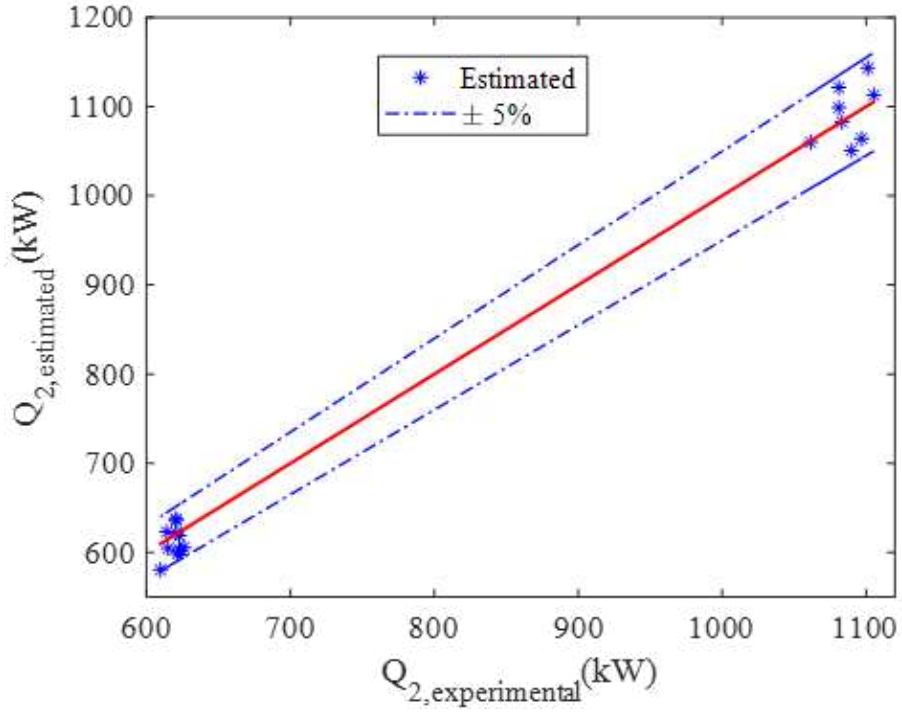

***Figure 4.9**: Comparison between experimental and estimated heat power Q2*

The results show that the correspondence between experimental and estimated heat power Q_2 is very good proving that the correlation for the product Nusselt number is adequate: all the results are within a band of uncertainty of ± 5%. Moreover, the estimation error computed with Eq. (78) corresponds to 2.7%.

It is not surprising that the global estimation error related to the correlation in Eq. (52) is smaller than the maximum uncertainty of the various coefficients and exponents (Table 4.4) because these terms are related to each other, and the simple propagation of error approach cannot be employed [35]. Finally, for the

considered case, as far as the correspondence between experimental and estimated heat power is already excel- lent from an engineering viewpoint, the implementation of a more complicated model is not recommended because it would require a more extensive experimental campaign, giving negligible beneficial results.

4.5 Parameter estimation extension: 4 and 6 parameters

To further study the possibilities given by the described estimation method two variants of the procedure defined in paragraph 4 are considered: estimation of 4 parameters (C_2, α_2, C_3, α_3) and estimation of 6 parameters (C_1, α_1, C_2, α_2, C_3, α_3). Then the functional to minimize (Eq. (69)) becomes:

$$S(C_2, \alpha_2, C_3, \alpha_3) = \sum_{i=1}^{M} \left[\boldsymbol{T}_{exp,i} - \boldsymbol{T}_{calc,i} \right]^2 \qquad (96\text{ a})$$

$$S(C_1, \alpha_1, C_2, \alpha_2, C_3, \alpha_3) = \sum_{i=1}^{M} \left[\boldsymbol{T}_{exp,i} - \boldsymbol{T}_{calc,i} \right]^2 \qquad (96\text{ b})$$

In the case of 4 parameters estimation the choice of considering as known the coefficients of section 1 and not those of section 3 is due to the fact that section 1 is constituted by a straight smooth wall tube: this geometric configuration is the mostly investigated in the available literature and thus it will be easier to find the correlation that perfectly fit the conditions of the studied case respect to

section 3 which is an annular section, that is also deeply investigated geometry, but surely less than smooth straight tube.

Respect to the case of 2 parameters, Re_3 is not kept fixed but is assumed to vary in the range $10^4 < Re_3 < 1.9 \cdot 10^4$ with the number of tests that is increased to 200.

In table 4.5 there are reported the results of the minimization together with 95% confidence intervals and the coefficients of variation for the case of 4 parameter estimation. In Figure 4.10, to help the visualisation of the results, there are graphically shown the trend of the coefficients of variation as a function of noise level.

Noise level (ζ)	Unknown parameter	exact value	estimated value	CI $^{95\%}$	CV (%)
0.01	C_2	0.023	0.023	(0.023, 0.023)	0.02%
	α_2	0.800	0.800	(0.800, 0.800)	0.01%
	C_3	0.023	0.023	(0.022, 0.024)	2.57%
	α_3	0.800	0.801	(0.796, 0.807)	0.33%
0.05	C_2	0.023	0.023	(0.023, 0.023)	0.11%
	α_2	0.800	0.800	(0.800, 0.801)	0.03%
	C_3	0.023	0.024	(0.018, 0.030)	13.63%
	α_3	0.800	0.796	(0.768, 0.824)	1.79%
0.1	C_2	0.023	0.023	(0.023, 0.023)	0.22%
	α_2	0.800	0.798	(0.800, 0.802)	0.06%
	C_3	0.023	0.028	(0.013, 0.043)	27.37%
	α_3	0.800	0.781	(0.725, 0.837)	3.65%
0.5	C_2	0.023	0.022	(0.022, 0.023)	1.08%
	α_2	0.800	0.808	(0.795, 0.804)	0.31%
	C_3	0.023	0.030	(-0.055, 0.116)	144.70%
	α_3	0.800	0.781	(0.485, 1.076)	19.32%
1	C_2	0.023	0.024	(0.022, 0.024)	2.17%
	α_2	0.800	0.790	(0.795, 0.814)	0.62%
	C_3	0.023	0.048	(-0.196, 0.292)	257.68%
	α_3	0.800	0.719	(0.193, 1.245)	37.32%

***Table 4.5**: Results of parameter estimation on synthetic data (4 parameter case)*

From

and Figure 4.10 it is possible to notice that the adopted procedure permits to obtain a very good estimation of all the unknown parameters until a noise level of 0.1 K even if the confidence intervals of C_3 become larger and the coefficient of variation reach a maximum values of 27%.

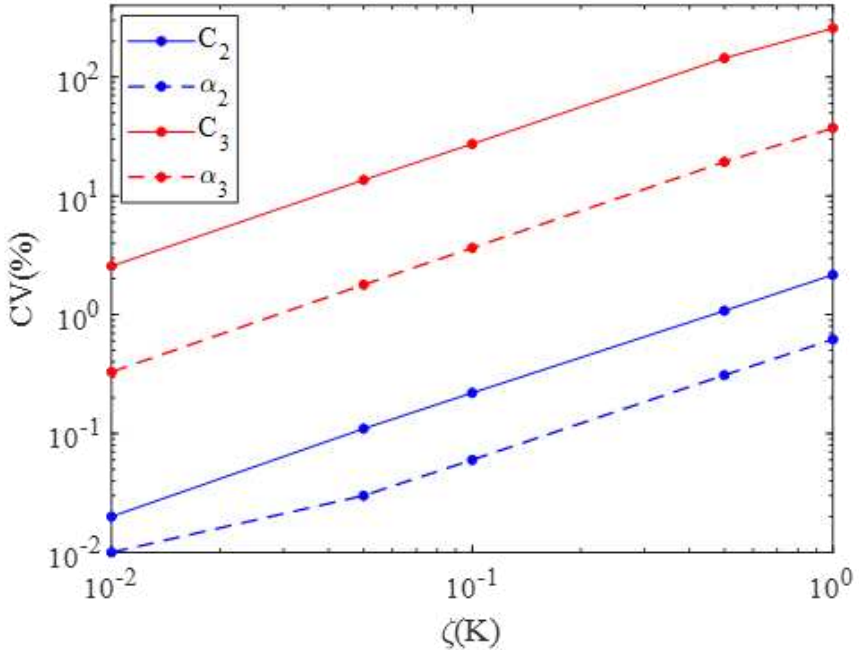

***Figure 4.10**: Coefficients of variation for different noise levels for the case of 4 parameters estimation*

For noise levels of 0.5 and 1 K, the parameters restoration is still satisfying for all the unknowns but the confidence of variance of C_3 rise pointedly and the one of α_3 increase to 19% and 37%, respectively. At the same time the confidence intervals greatly widen. Nevertheless, the estimation of C_2 and α_2, is

still optimal for all the noise levels: CV values and confidence intervals of the product side coefficients are comparable to the ones obtained for the 2 parameters estimation. This behaviour is ascribable to the fact that for the usual TTHE working conditions the most part of the thermal resistance is due to the contribute of the product side: consequently, it is obvious that it is easier to estimate the coefficients that describes the behaviour of section 2 respect to the ones of section 3 whose variation don't affect significantly the overall thermal resistance.

In addition, in Figure 4.11a it is reported the estimation error on the heat power exchanged by the product (Eq. (78)) while in Figure 4.11b it is shown the comparison between the computed values of Q_2 and the exact ones for the case of the highest noise level ($\zeta = 1$ K). As in 2-parameters estimation, the estimation error (Figure 4.11a) on the exchanged heat power Q_2 is characterised by very small values with a maximum of 1.5%. Analogously, the distribution of the calculated heat power values respect to the exact ones presents a random trend with all the values (Figure 4.11b) within a ±5% band. The same conduct can be observed for the results obtained with the 6 parameters estimation procedure that are reported in Table 6. Respect to the case of 4 parameters, Re_1 is not kept fixed but is assumed to vary in the range $1.9 \cdot 10^4 < Re_1 < 2.1 \cdot 10^4$ with the number of tests that is increased to 300.

In Figure 4.12 the coefficients of variation are graphically shown as a function of noise level.

a)

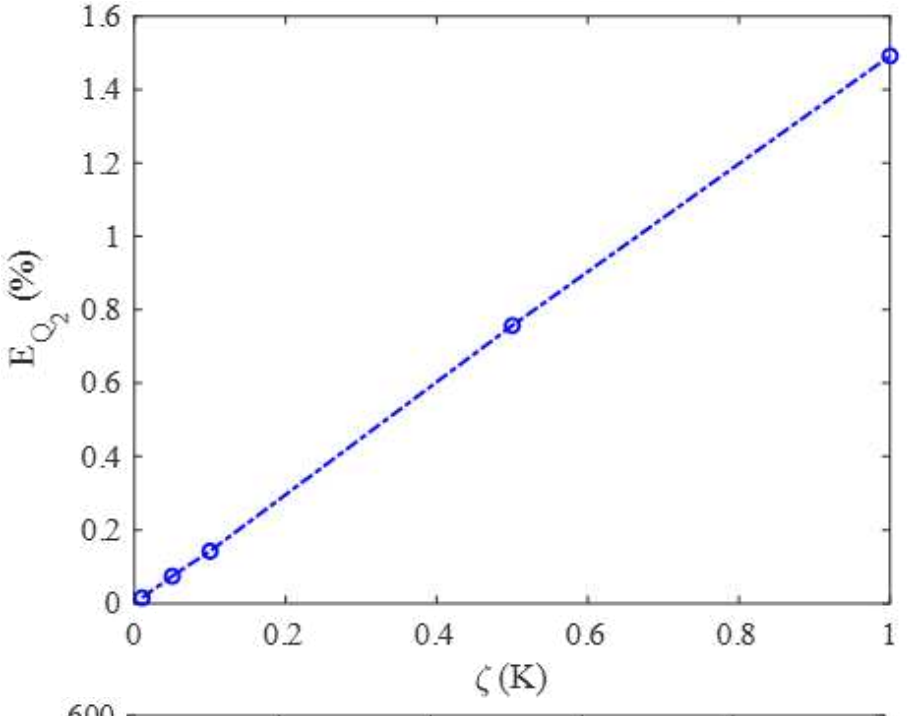

b)

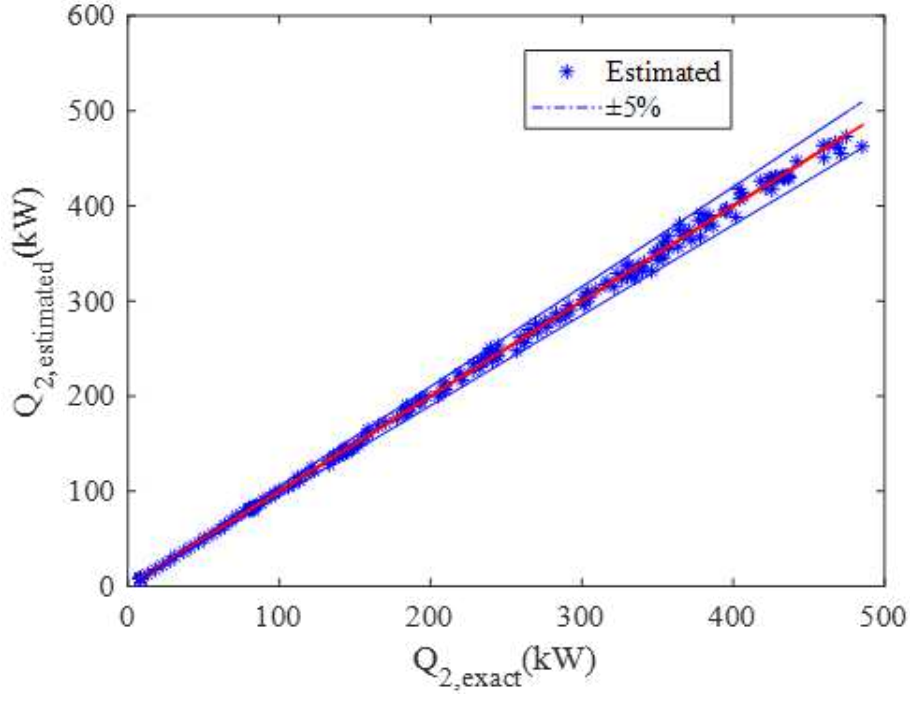

***Figure 4.11**: Estimation error E_{Q2} as a function of the noise level (a) and comparison between exact and estimated heat power Q_2 for noise level ζ = 1 K (b) for the case of 4 parameters estimation*

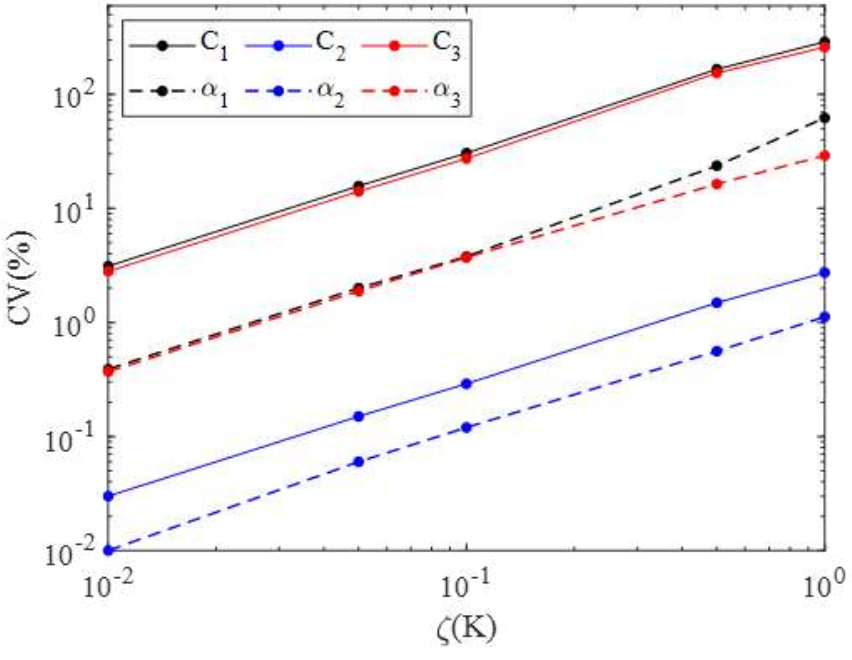

***Figure 4.12**: Coefficients of variation for different noise levels for the case of 6 parameters estimation*

The estimation of C_2 and α_2 is again excellent for all the noise levels and CV values and confidence intervals are like the ones obtained for the 2 and 4 parameters estimation procedures. C_1, α_1, C_3, α_3 are estimated with success until the noise value of 0.1 K even if CV for C_1 and C_3 reach values of 30%. For higher noise values, CI intervals become significantly larger, and CV greatly increase, highlighting the unfeasibility of the estimation of the coefficients of the service fluid sides.

Noise level (ζ)	Unknow parameter	exact value	estimated value	CI $^{95\%}$	CV (%)
0.01	C_1	0.023	0.023	(0.022, 0.025)	3.12
	α_1	0.800	0.798	(0.792, 0.805)	0.39
	C_2	0.023	0.023	(0.023, 0.023)	0.03
	α_2	0.800	0.800	(0.800, 0.800)	0.01
	C_3	0.023	0.023	(0.022, 0.024)	2.81
	α_3	0.800	0.800	(0.794, 0.806)	0.37
0.05	C_1	0.023	0.025	(0.017, 0.032)	15.71
	α_1	0.800	0.793	(0.762, 0.824)	2.00
	C_2	0.023	0.023	(0.023, 0.023)	0.15
	α_2	0.800	0.800	(0.800, 0.801)	0.06
	C_3	0.023	0.025	(0.018, 0.033)	14.11
	α_3	0.800	0.789	(0.760, 0.818)	1.88
0.1	C_1	0.023	0.020	(0.008, 0.031)	30.55
	α_1	0.800	0.816	(0.755, 0.876)	3.79
	C_2	0.023	0.023	(0.023, 0.023)	0.29
	α_2	0.800	0.802	(0.800, 0.804)	0.12
	C_3	0.023	0.029	(0.013, 0.045)	27.40
	α_3	0.800	0.775	(0.718, 0.831)	3.72
0.5	C_1	0.023	0.019	(0.007, 0.131)	166.49
	α_1	0.800	0.811	(0.510, 1.263)	23.69
	C_2	0.023	0.023	(0.022, 0.023)	1.49
	α_2	0.800	0.803	(0.788, 0.805)	0.56
	C_3	0.023	0.027	(-0.05, 0.113)	154.01
	α_3	0.800	0.769	(0.512, 1.006)	16.39
1	C_1	0.023	0.608	(-2.838, 4.054)	289.13
	α_1	0.800	0.469	(-0.103, 1.042)	62.27
	C_2	0.023	0.023	(0.021, 0.024)	2.74
	α_2	0.800	0.804	(0.787, 0.822)	1.12
	C_3	0.023	0.006	(-0.023, 0.035)	259.54
	α_3	0.800	0.944	(0.406, 1.482)	29.06

Table 4.6: Results of parameter estimation on synthetic data (6 parameter case)

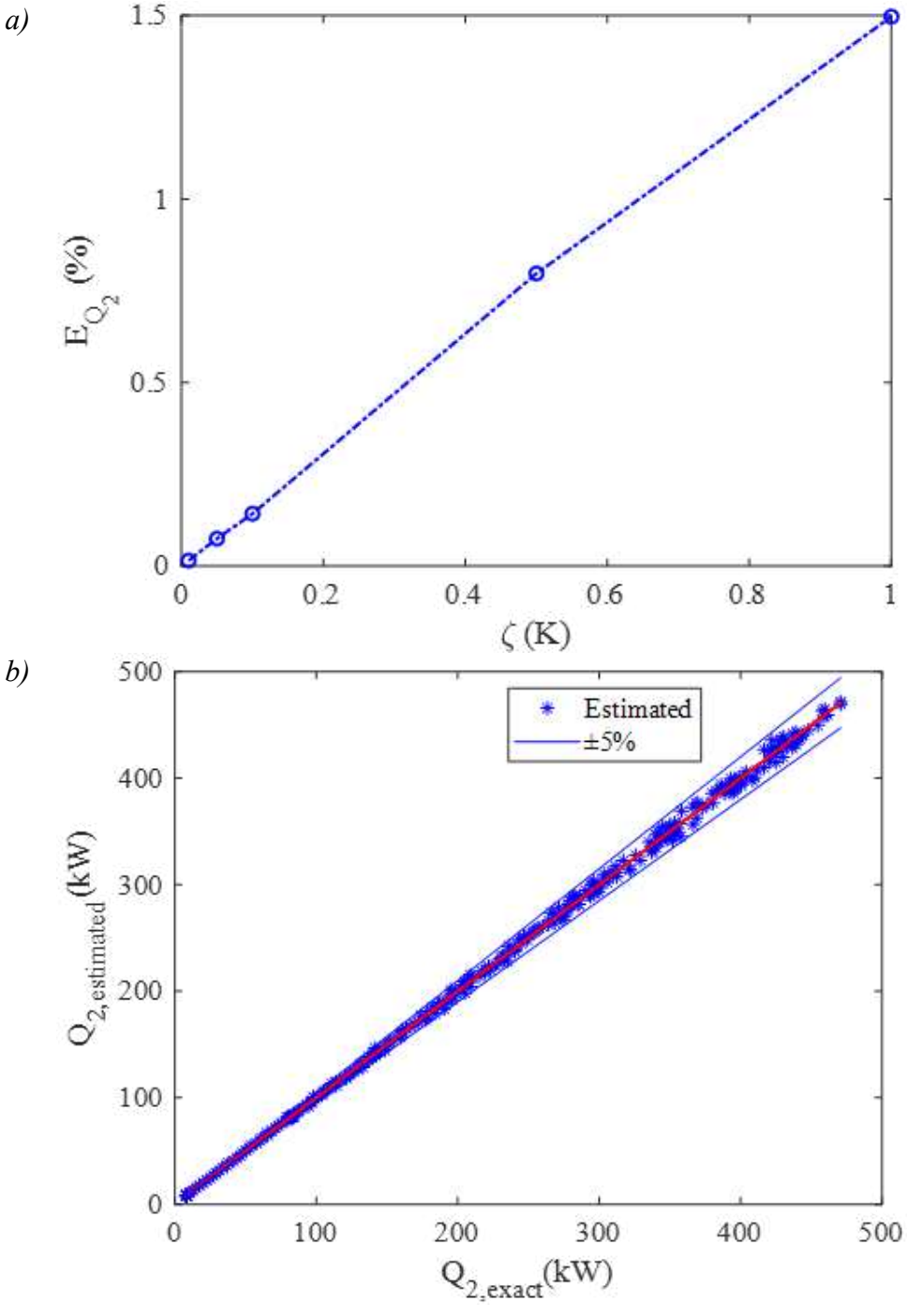

***Figure 4.13**: Estimation error E_{Q2} as a function of the noise level (a) and comparison between exact and estimated heat power Q_2 for noise level ζ = 1 K (b) for the case of 6 parameters estimation*

Even for the case of 6 parameters estimation, in Figure 4.13a it is reported the estimation error (Eq. (78)) while in Figure 4.13b it is shown the comparison between the computed values of Q_2 and exact ones for the case of the highest noise level (ζ = 1 K).

To conclude, also for the 6 parameters approach, the estimation error (Figure 4.13a) on the exchanged heat power Q_2 is lower than 1.5%. Moreover, the distribution of the values of calculated heat power of the central annulus respect to the exact ones (Figure 4.13b) has a random spread and it is included in band of ±5%.

To compare the computational cost of the 2, 4 and 6 parameters estimation procedures in Figure 4.14 it is reported the time necessary to find the wanted unknowns for the representative case of ζ = 0.1 K for the three different cases. The adopted calculator is an Intel® Core ™ i3-2120 CPU 3.3GHz with 8GB of RAM memory.

It can be seen that the calculation time increases as the number of parameters to be estimated rises. In particular, when going from 2 to 4 parameters, the calculation time increases by about 38 times (from 41 min. to 26 h), while going from 4 to 6 it increases by 3.6 times (from 26h to ca. 4 days). In this case, it means that tripling the number of parameters to be estimated causes an increase of 2 orders of magnitude in the computational time.

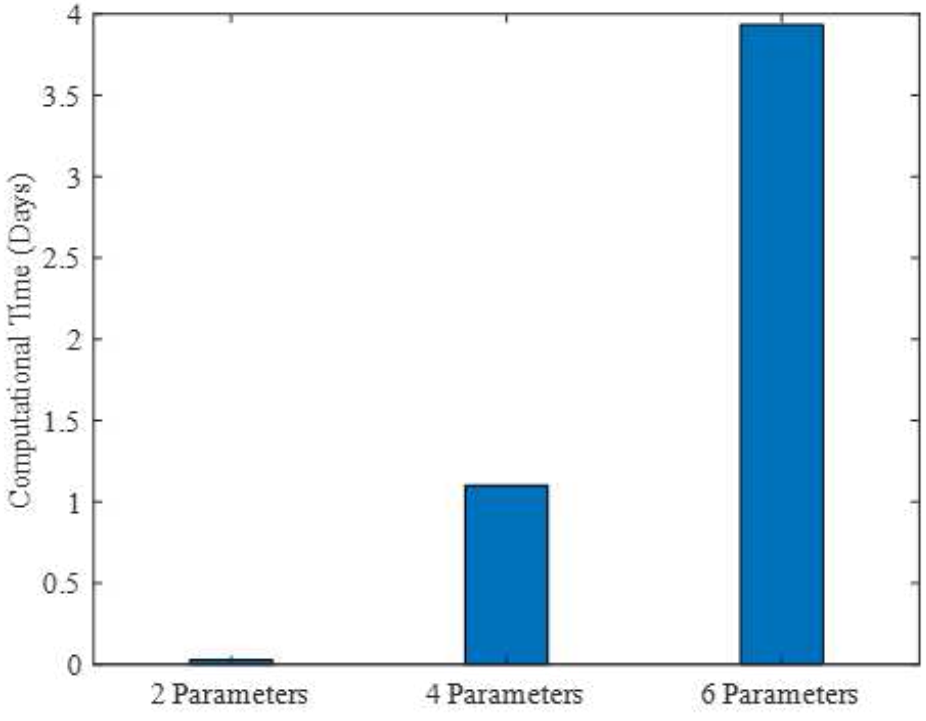

***Figure 4.14**: Solution time for the 2, 4 and 6 parameters estimation procedures*

Resuming, the assessment of the multiplicative constant C_2 and the Reynolds number exponent α_2 for the product side is obtained with optimal results with all the 3 approaches tested for the proposed estimation procedure. Even in the case with the highest noise level ($\zeta = 1$), the confidence intervals and CV are very limited upholding the effectiveness of the estimation methodology for these parameters.

Furthermore, the 4 and 6 parameters estimation procedures present the advantage of assessing the C and α for the service fluid sides without the necessity of doing a priori assumptions.

However, in the case study considered, the estimation of the parameters of the services (C_1 , α_1 , C_3 , α_3) was found to be feasible only with low noise values ($\zeta \leq 0.1$), while for high noise values ($\zeta \geq 0.5$), 4 and 6-parameter estimation procedures showed an increase in confidence intervals and *CV* s of the estimated coefficients. As mentioned earlier, this weakness for estimating service sides' coefficients at high noise levels is ascribable to the typical food application case studied in this work, in which most of the thermal resistance of the device is due to the contribution of the product side; consequently, it is easier to estimate the coefficients that describe the behaviour of this section than those of the service ones, whose variation does not affect significantly the overall thermal resistance. Moreover, the estimation procedure for 4 and 6 parameters requires more tests than for 2 parameters, increasing the time required for executing the experimental activities. Also, the computational cost of the estimation procedure critically increases with more parameters. This confirms what has been said in paragraph 3 that when talking about parameter estimation procedures, doing all the simplifications that can be reasonably performed can significantly improve the results and reduce the required time and computational costs. Hence, it is possible to affirm that the 2-parameter estimation procedure is the best one to adopt in most of the working conditions of TTHE, i.e. strictly laminar flow of highly viscous fluid in section 2 and turbulent flow in Sections 1 and 3, while only when the thermal resistances of the three sections assume comparable values can the 4 and 6-parameter estimation procedure be suggested.

CHAPTER 5: Closure

This study reports the application of an innovative procedure based on parameter estimation methodology to characterise TTHEs. This investigation is intended to enable the robust estimation of the heat transfer correlation for the product side Nusselt number. The parameter estimation procedure was validated through its application to both synthetic and experimental data acquired from TTHE for treating highly viscous fluid food. The validation yielded the following results: the application of the procedure to synthetic data helped in obtaining an accurate estimation of the unknown coefficients in the product side Nusselt number correlation. Even for the highest noise level considered in this study (ζ= 1 K), the highest value of the coefficient of variation was 4.2%, underlying the very good results achieved. The application of the procedure to the experimental data demonstrated that for the product side, the power law dependence of the internal fluid Nusselt number on the Reynolds number can be successfully estimated together with the multiplicative constant. The uncertainty associated with

estimating the multiplicative constant C2 (coefficient of variation of approximately 6.5%) is very low, and the Reynolds number exponent α2 is determined with a coefficient of variation of approximately 3%. the application of the two variants of the procedure (i.e. 4 parameters and 6 parameters) on synthetic data highlighted that, by increasing the number of parameters to be estimated, the coefficients of the product side are still well assessed. However, when most of the thermal resistance of the device is located on the product side, the coefficients of the service sides are well estimated until a low level of noise, while at a high level, their assessment becomes unachievable, making the 2-parameter procedure preferable. The application of the two variants of the procedure to synthetic data highlighted that the two variants of the procedure involve an important increase in the time required for executing the experimental activities and an increase in the computational costs, making them the best solution only when the service side thermal resistance is comparable to the product side. In conclusion, considering the limited effort for the experimental measurements required to apply this estimation procedure (i.e. moderate number of experimental measurements and relatively small computational cost and time), the proposed methodology of characterising TTHEs could also represent an effective tool for the producers of this type of device, permitting them to estimate the unknown parameters that are crucial for the design and optimisation of this equipment, which often must be customised to enable specific thermal processes.

References

[1] "Improving the thermal processing of foods," *Improv. Therm. Process. foods*, 2004, doi: 10.1201/9781439823330.

[2] K. Thulukkanam, *Heat Exchanger Design Handbook*. 2013.

[3] TheodoremL. Bergman Adrienne S. Lavine, *Fundamentals of heat and mass transfer*, vol. 7, no. 1. 2015.

[4] R. K. Shah and D. P. Sekuli, *Selection of Heat Exchangers and Their Components*. 2007.

[5] O. García-Valladares, "Numerical simulation of triple concentric-tube heat exchangers," *Int. J. Therm. Sci.*, vol. 43, no. 10, pp. 979–991, 2004, doi: 10.1016/j.ijthermalsci.2004.02.006.

[6] P. C. Mukesh Kumar and V. Hariprasath, "A review on triple tube heat exchangers," *Mater. Today Proc.*, vol. 21, pp. 584–587, 2020, doi: 10.1016/j.matpr.2019.06.719.

[7] A. Gomaa, M. A. Halim, and A. M. Elsaid, "Experimental and numerical investigations of a triple concentric-tube heat exchanger," *Appl. Therm. Eng.*, vol. 99, pp. 1303–1315, 2016, doi: 10.1016/j.applthermaleng.2015.12.053.

[8] A. K. Tiwari, S. Javed, H. F. Oztop, Z. Said, and N. S. Pandya, "Experimental and numerical investigation on the thermal performance

of triple tube heat exchanger equipped with different inserts with WO3/water nanofluid under turbulent condition," *Int. J. Therm. Sci.*, vol. 164, no. August 2020, p. 106861, 2021, doi: 10.1016/j.ijthermalsci.2021.106861.

[9] A. Ünal, "Theoritical analysis of triple concentric-tube heat exchangers - Part 2: Case Studies," *Int. Commun. Heat Mass Transf.*, vol. 28, no. 2, pp. 243–256, 2001, doi: 10.1016/S0735-1933(01)00231-7.

[10] A. Ünal, "Effectiveness-NTU relations for triple concentric-tube heat exchangers," *Int. Commun. Heat Mass Transf.*, vol. 30, no. 2, pp. 261–272, 2003, doi: 10.1016/S0735-1933(03)00037-X.

[11] E. Batmaz and K. P. Sandeep, "Overall heat transfer coefficients and axial temperature distribution in a triple tube heat exchanger," *J. Food Process Eng.*, vol. 31, no. 2, pp. 260–279, 2008, doi: 10.1111/j.1745-4530.2007.00154.x.

[12] S. Radulescu, I. L. Negoita, and I. O. N. Onutu, "Heat Transfer Coefficient Solver for a Triple Concentric-tube Heat Exchanger in Transition Regime," *Rev. Chim.*, vol. 63, no. 11, pp. 1143–1147, 2012.

[13] J. D. Moya-Rico, A. E. Molina, J. F. Belmonte, J. I. Córcoles Tendero, and J. A. Almendros-Ibáñez, "Characterization of a triple concentric-tube heat exchanger with corrugated tubes using Artificial Neural Networks (ANN)," *Appl. Therm. Eng.*, vol. 147, no. October 2018, pp. 1036–1046, 2019, doi: 10.1016/j.applthermaleng.2018.10.136.

[14] M. Bahiraei, N. Mazaheri, and M. Hanooni, “Performance enhancement of a triple-tube heat exchanger through heat transfer intensification using novel crimped-spiral ribs and nanofluid: A two-phase analysis,” *Chem. Eng. Process. - Process Intensif.*, vol. 160, no. December 2020, p. 108289, 2021, doi: 10.1016/j.cep.2020.108289.

[15] M. Bahiraei, L. Kok Foong, S. Hosseini, and N. Mazaheri, “Neural network combined with nature-inspired algorithms to estimate overall heat transfer coefficient of a ribbed triple-tube heat exchanger operating with a hybrid nanofluid,” *Meas. J. Int. Meas. Confed.*, vol. 174, no. December 2020, p. 108967, 2021, doi: 10.1016/j.measurement.2021.108967.

[16] M. Bahiraei, L. K. Foong, S. Hosseini, and N. Mazaheri, “Predicting heat transfer rate of a ribbed triple-tube heat exchanger working with nanofluid using neural network enhanced by advanced optimization algorithms,” *Powder Technol.*, vol. 381, pp. 459–476, 2021, doi: 10.1016/j.powtec.2020.12.003.

[17] E. E. Wilson, “A basis for rational design of heat transfer apparatus,” *J. Am. Soc. Mech. Engrs.*, vol. 37, pp. 546–551, 1915.

[18] D. E. Briggs and E. H. Young, “Modified Wilson plot techniques for obtaining heat transfer correlations for shell and tube heat exchangers,” in *Chemical Engineering Progress Symposium Series*, 1969, vol. 65, no. 92, pp. 35–45.

[19] H. F. Khartabil and R. N. Christensen, “An improved scheme for determining heat transfer correlations from heat exchanger regression models with three unknowns,” *Exp. Therm. Fluid Sci.*, vol. 5, no. 6, pp. 808–819, 1992, doi: 10.1016/0894-1777(92)90125-O.

[20] T. B. Styrylska and A. A. Lechowska, “Unified Wilson plot method for determining heat transfer correlations for heat exchangers,” 2003.

[21] J. W. Rose, “Heat-transfer coefficients, Wilson plots and accuracy of thermal measurements,” *Exp. Therm. Fluid Sci.*, vol. 28, no. 2–3, pp. 77–86, 2004, doi: 10.1016/S0894-1777(03)00025-6.

[22] J. Fernández-Seara, F. J. Uhía, J. Sieres, and A. Campo, “A general review of the Wilson plot method and its modifications to determine convection coefficients in heat exchange devices,” *Appl. Therm. Eng.*, vol. 27, no. 17–18, pp. 2745–2757, 2007, doi: 10.1016/j.applthermaleng.2007.04.004.

[23] C. Pătrăşcioiu and S. Rădulescu, “Prediction of the outlet temperatures in triple concentric—tube heat exchangers in laminar flow regime: case study,” *Heat Mass Transf. und Stoffuebertragung*, vol. 51, no. 1, pp. 59–66, 2015, doi: 10.1007/s00231-014-1385-2.

[24] J. V Beck, K. J. Arnold, and J. Wiley, *Parameter estimation in engineering and science*. 1977.

[25] H. R. B. Orlande, O. Fudym, D. Maillet, and R. M. Cotta, *Thermal measurements and Inverse Techniques*. 2011.

[26] P. Vocale, F. Bozzoli, A. Mocerino, K. Navickaitė, and S. Rainieri, "Application of an improved parameter estimation approach to characterize enhanced heat exchangers," *Int. J. Heat Mass Transf.*, vol. 147, 2020, doi: 10.1016/j.ijheatmasstransfer.2019.118886.

[27] M. N. Ozisik and H. R. B. Orlande, *Inverse Heat Transfer*, vol. 7, no. 1. 2015.

[28] Y. Bard, "Nonlinear parameter estimation," 1974.

[29] B. H. Dennis and G. S. Dulikravich, "Simultaneous determination of temperatures, heat fluxes, deformations, and tractions on inaccessible boundaries," *J. Heat Transfer*, vol. 121, no. 3, pp. 537–545, 1999, doi: 10.1115/1.2826014.

[30] B. Blackwell and J. V. Beck, "A technique for uncertainty analysis for inverse heat conduction problems," *Int. J. Heat Mass Transf.*, vol. 53, no. 4, pp. 753–759, 2010, doi: 10.1016/j.ijheatmasstransfer.2009.10.014.

[31] H. T. Banks, K. Holm, and D. Robbins, "Standard error computations for uncertainty quantification in inverse problems: Asymptotic theory vs. bootstrapping," *Math. Comput. Model.*, vol. 52, no. 9–10, pp. 1610–1625, 2010, doi: 10.1016/j.mcm.2010.06.026.

[32] S. Peacock, "Predicting physical properties of factory juices and syrups," *Int. Sugar J.*, vol. 97, no. 1162, pp. 571–577, 1995.

[33] A. Trifirò, A. Bassi, D. Castaldo, D. Bigliardi, and S. Gherardi, "'Effetti della composizione e della temperatura sulla reologia della purea di

albicocca',” *Ind. e Conserv.*, vol. 61, pp. 246–251, 1986.

[34] W. Kozicki, C. H. Chou, and C. Tiu, “Non-Newtonian flow in ducts of arbitrary cross-sectional shape,” *Chem. Eng. Sci.*, vol. 21, no. 8, pp. 665–679, 1966, doi: 10.1016/0009-2509(66)80016-7.

[35] J. R. Taylor, “Error analysis,” *Univ. Sci. Books, Sausalito, Calif.*, vol. 20, 1997.

PART II: FERMENTER FOR OENOLOGICAL INDUSTRY

List of figures

Figure 6.1: Schematic flowsheet of the alcoholic fermentation [2]..... 109

Figure 6.2: Example of modern fermenter for oenological industry realized in stainless steel..... 115

Figure 6.3: schematic representation of the working principle of a thermosyphon heat pipe in vertical position [19] 119

Figure 7.1: (a) Schematic section of the fermenter and the flow of the cooling fluid inside the jacket; (b) schematic section of the ideal heat pipe installed in the tank and (c) a picture of the tank with the ideal heat pipe. 125

Figure 7.2: Schematic representation of the ideal heat pipe: a) external view b) internal view c) top view 128

Figure 7.3: Scheme of the disposition of the thermocouples inside the fermenter tank, b) thermal resistance inside the tank..... 131

Figure 7.4: detail of the mixing system applied to the tank..... 133

Figure 7.5: Temperature distribution of the 3 thermocouple levels for tests with 100 W input power without product mixing a) with cooling jacket; b) with ideal heat pipe..... 135

Figure 7.6: Temperature space distribution: a) Jacket cooling system at 3 h; b) Ideal heat pipe system at 3 h; c) Jacket cooling system at 5.5 h; d) Ideal heat pipe system at 5.5 h. 137

Figure 7.7: Temperature distribution of the thermocouple levels for tests with 100W input power applying mixing of the product a) with the jacket cooling system; b) with the ideal heat pipe as cooling system 139

Figure 8.1: a) Schematic representation of the HP b) Schematic layout of filling system of HP 143

Figure 8.2:a) Detail of the wire thermal resistance and thermocouples on the HP; b) HP with cooling jacket installed on the condenser..... 148

Figure 8.3:Equivalent resistance of the HP in function of the power input at the evaporator 150

Figure 8.4:Temperature distribution of the thermocouple levels for the test of HP (FR= 20%) inside the tank..... 152

Figure 9.1:Rectangular sections (in red) of the 12 circular crowns with their respective thermocouples..... 157

Figure 9.2: Complete resistor network..... 163

Figure 9.3: inside picture of the fermentation tank used for simulating the fermentation for the validation of the model 168

Figure 9.4:average temperature of the product inside the fermenter tank 169

Figure 10.1: comparison between the real input power and the estimated one for the case: a) 100 W-1 h; b) 100 W-2 h; c) 140 W-h; d) 140 W-2 h. 182

Figure 10.2: comparison between the average experimental temperature of the product inside the tank and the estimated temperature obtained by solving the direct problem using the estimated input power for the case: a) 100 W – 1 h; b) 100 W – 2 h; c) 140 W – 1 h; d) 184

CHAPTER 6: Thermal aspects in oenological production

6.1 Alcoholic fermentation in winemaking process

Fermentation is the metabolic process carried out by single-cell organisms, like yeasts and bacteria, in anaerobiosis conditions for extracting energy from organic molecules; in an oxygen-free environment, cells cannot carry out cellular respiration, in this case some microorganisms carry out fermentation to produce energy starting from carbon sources like hexose sugars. In the oenological productions, the fermentation, specifically the alcoholic one, is the central metabolic process involved in the transformation of the grape juice into the final product: wine [1]. The terms “alcoholic” refers to the biochemical conversion of carbon sources, such as the hexose sugars present in the must, into ethanol. Yeasts, in particular those belonging to the species *Saccharomyces cerevisiae*

are the most efficient in this kind of transformation and for this reason they are the most used as starters.

The degradation of the sugars by yeasts starts with the Embden-Meyerhof pathway (also known as glycolysis) for both the fermentation processes and cellular respiration: this first pathway involves 10 reactions and leads to the formation of pyruvic acid: in the first 5 reactions, energy in form of adenosine triphosphate (ATP) is invested to give rise first to the glucose-6-phosfate and then to the fructose-1,6-biphosphate which is successively cleaved to generate 2 moles of triose phosphate. From this point, the energy generation phase of the glycolysis starts with the sequential generation of two compounds: firstly 1,3-bisphosphoglycerate and then phosphoenolpyruvate. Both these 2 compounds transfer a high-energy phosphate group to adenosine diphosphate (ADP), generating 2 ATP each, which are partially transformed by the cells in other form of energy for the growth. In this way pyruvate is obtained as output of the glycolysis process. Moreover, also the step of conversion of glyceraldehyde-3-phosphate in to 1,3-bisphosphoglycerate produces energy: this oxidation reaction is catalysed by the enzyme glyceraldehyde-3-phosphate dehydrogenase that requires the coenzyme nicotinamide-adenine dinucleotide (NAD+) for accepting the electrons from the substrate being oxidized. Therefore, this coenzyme is reduced to NADH, a very high source of energy for cells (about 2.5 ATP). After the glycolysis, the pyruvic acid is firstly decarboxylated to acetaldehyde by the enzyme pyruvate decarboxylase and then, the acetaldehyde is reduced to ethanol

thanks to the enzyme alcohol dehydrogenase in a reaction involving oxidation of NADH to NAD+.

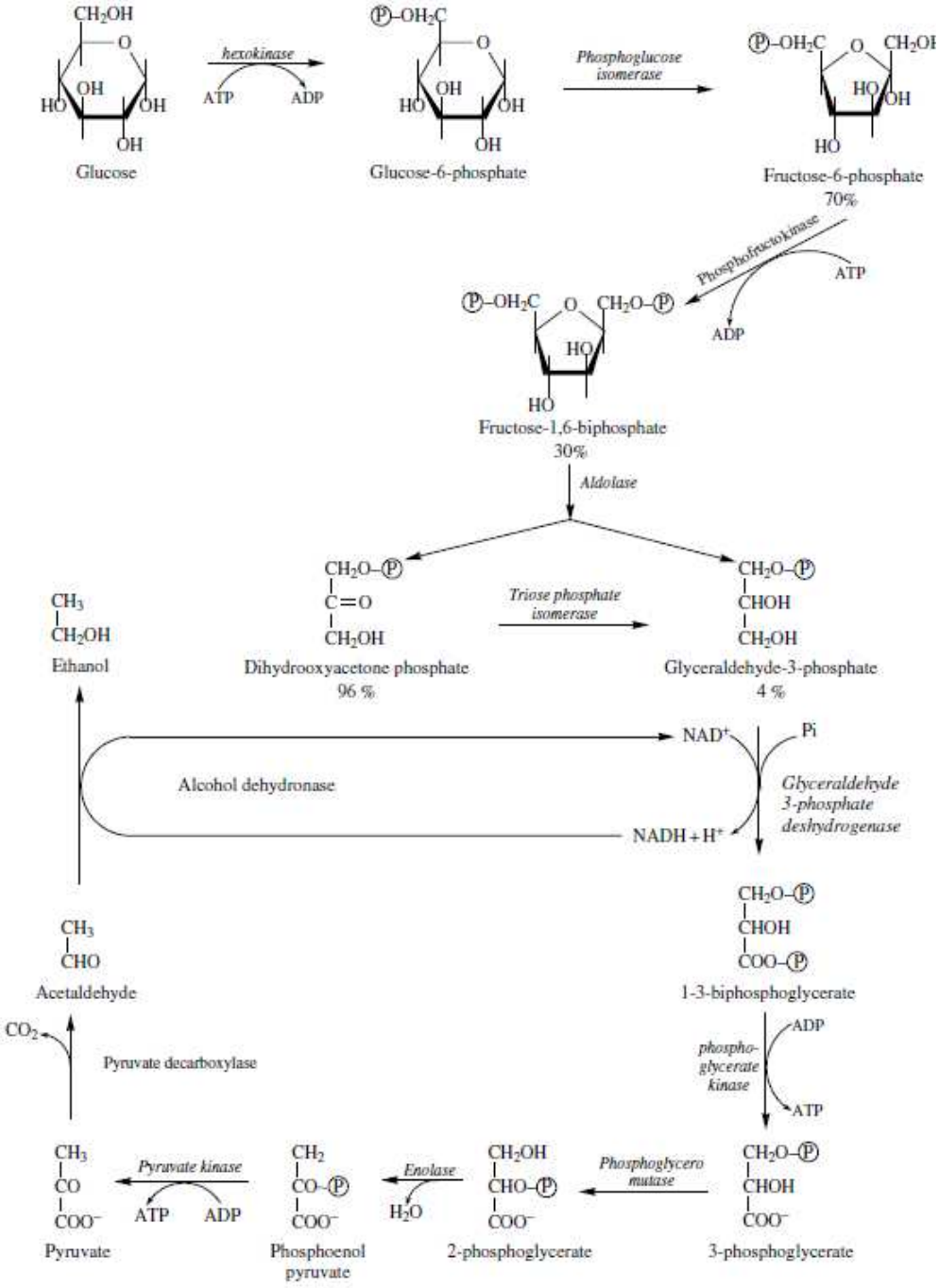

Figure 6.1: *Schematic flowsheet of the alcoholic fermentation* [2]

Moreover, glycolysis and alcoholic fermentation contribute directly and indirectly to the formation of a great variety of metabolites recognised as “secondary metabolites” like the aromatic molecules, that are produced in very small quantity if compared to the ethanol one, but very important because recognisable by the taste and the smell of the final consumer. These “secondary metabolites” are principally aromatic and volatile molecular compounds, like fatty acids, volatile phenols, higher alcohols and esters, responsible of the organoleptic features of the wine. Their presence and concentration are essentially dependent on the yeast’s metabolism during fermentation and consequently on the conditions under which fermentation takes place [1]. Various factors could influence the production of these compounds in the must, such as the presence of nitrogen compounds [3] [4] [5] [6] [7] [8] and especially the temperature [9]. It is easy to understand that the fermentation is therefore a crucial phase in determining the organoleptic features of the final product, in which the qualities of the raw material can be enhanced or, on the opposite, eliminated. For this reason, the control of the parameters that can regulate it, are to be managed with high precision.

To get an overview of the entire fermentation process, it is possible to summarize it in different sequential time steps: after insertion in the grape must, it takes some hours for the yeasts to start the alcoholic fermentation. After that period, the alcoholic fermentation and the formation of the aromatic compounds takes place and usually lasts from a minimum of about 7 days up to even 10 days, depending on the type of wine to be produced. In the first 2-3 days of alcoholic

fermentation, the yeasts kinetics is at the maximum level and the most part (80-90 %) of the glucose is converted in ethanol, this phase, due to the high activity of the yeasts involved, is commonly called “tumultuous”. The result of the process is the pure wine, ready for the stabilization, refinement, maturation and ageing before it can be appreciated by the final consumer.

6.2 Thermal control of the fermentation phase in wine industry

Among the chemical-physical parameters affecting the fermentation, temperature is the most important since it directly determines the growth and the progression of the transformation of sugars in ethanol [10]. In addition, also the formation of aromatic compounds, due to the metabolism of the yeasts involved in this process, is affected by thermal conditions: firstly, the temperature during the fermentation phase can regulate their formation, and secondly, since they consist mostly of highly volatile molecules, a too high temperature during the fermentation could cause their evaporation and loss. On the contrary, a too low temperature during fermentation could cause stuck fermentation, preventing the complete sugar transformation and leaving the fermentation process unfinished. In addition, a too low temperature increases the risk of growth of undesirable microbial forms at the beginning of fermentation. Finally, in red vinification, temperature influences the extraction of the phenolic compounds, pigments responsible for the colour of the wine, that are contained in the grape skins: a higher fermentation temperature corresponds to a greater colour extraction.

Saccharomyces cerevisiae is the most used yeast as starter for fermentation in wine making processes as it is recognised as a "good fermenter", due to its capability to start up and complete the entire transformation of sugars in ethanol and secondary compounds [11]. It has an optimal temperature of growth around 25°C, consequently it can easily adapt its metabolism in a wide range of thermal conditions, also reaching temperature of about 10°C to a maximum of 40°C. However, it does not mean that the fermentation carried out by this yeast occurs with the same results at any temperature within the above-mentioned range. Indeed, a temperature close to the upper limit, could cause a very high velocity in transforming the sugars in ethanol and secondary compounds, but it could stop in early, before the sugar matrix is completely exhausted since higher temperature increase the toxicity effect of the ethanol on the microbial cells. On the contrary, a temperature close to the lower limit, could allow the complete transformation of the sugars but with a very high latency time in the initial start-up that could cause the growth of unwanted microbial forms inside the grape must.

For these reasons, in modern vinification processes, the perfect control of the temperature is an essential element for obtaining wine of high quality and with a desired organoleptic feature. Usually, for generic fermentation processes, the 3 heat sources to be removed come from: the sterilisation processes, mechanical agitation, and the exothermic nature of the alcoholic fermentation process. However, in wine production, the only heat source to be considered for removal is the last one. In fact, the first heat source can be neglected, as there is no

sterilisation of the fermentation media, while, regarding mechanical stirring, it does not have a great impact since it is carried out by not continuous pumping over the must, which makes this type of heat generation negligible [12]. In other words, what makes difficulty the task of the thermal control of the grape must during transformation, is the exothermic feature of the alcoholic fermentation. From a thermodynamic point of view, it is possible to state that a single cycle of alcoholic fermentation liberates about 167 kJ/mol of free energy. Part of this energy, in specific about 30.5 kJ/mol, is used by yeasts to ensure their multiplication and growth and for forming 4 ATP molecules. The remaining free energy, about 106.5 kJ/mol, is dissipated in form of heat, causing an increase of the temperature of the grape must under fermentation [2] [11]. The entity of temperature increases in fermenters depend on several factors:

- The grape must sugar concentration: it determines the amount of heat liberated.
- The initial must temperature.
- The fermentation speed, which depends on must composition and yeast inoculation conditions. Operations such as aeration will increase the speed of fermentation, limiting the dissipation of heat outside the tank, increasing the temperature of the must.
- Geometry of the tank: the heat exchange area volume ratio is to be considered.

- Tank material: the thermal conductivity of the material of the tank for fermentation plays a fundamental role in the determination of the global thermic exchange coefficient between the fermenter and the environment.
- Aeration and cellar temperature: the ventilation of the winery increase the convective heat exchange coefficient, and consequently the heat exchange global coefficient, limiting the raising of the temperature in the tank.

However, in most cases, although all these aspects are thoroughly considered, a cooling system is required to maintain the correct temperature of the wort during fermentation. In this regard, to properly design a fermenter, one aspect of fundamental importance to be considered is the heat dissipation system.

Modern fermenters consist of a mostly cylindrical tank with a self-draining conical bottom, made of stainless steel. These features are dictated by the increasingly stringent hygiene requirements to be met by equipment in the food sector. The most popular cooling techniques for modern fermenters, are represented by a circulating flow of a service fluid, usually water, in the external shell of the metallic tank that is activated when the temperature of the grape must exceed the set limit wanted by the producer [2].

***Figure 6.2**: Example of modern fermenter for oenological industry realized in stainless steel*

Nevertheless, this cooling method presents several problems, such as the possible thermal stratification of must temperatures inside the fermenter and a continuous fluctuation in temperature generated by the on/off activity of the cooling jacket that are dangerous for a correct fermentation since every drastic change in temperature is perceived as a stress by the yeast cells [9]. Moreover, during its activation, a high energy demand and service fluid consumption are required due to the need to circulate it in large quantities.

This case confirms the general trend of food industry, where the heat transfer processes require a high quantity of energy and their optimization could be fundamental in increasing the sector's energy efficiency, since these processes, such as pasteurization, sterilization, and cooling, represent nearly 60% of all energetic consumes in the food industry. In particular, refrigeration applications represent 15% of the overall energy spent in the world [13]. Energy-saving opportunities for this kind of food process operation could be represented by the replacement of energy-intensive units with innovative processing techniques, passive ones [14] [15], that guarantee lower consumes [13]. However, it is important to remember that it is essential to not prejudice the efficacy of thermal treatments, since these are the most widely employed processes to ensure food safety and stability over time [16]. A crucial factor to take into account in designing a thermal treatment is represented by the uniformity of the temperature distribution inside the food product; it has a strong influence both on the process effectiveness and on its energy efficacy [17]. Nevertheless, the demand to achieve huge fabrication quantities frequently imposes the implementation of inadequately monitored treatment conditions, which prevent the presence of uniform temperature distribution within the product during processes and negatively influence the above-mentioned aspects.

In the present work, with the aim to solve the above cited problems and to optimise the thermal control process of the fermentation phase in the oenology field, an innovative temperature monitoring system based on heat pipe

technology was considered as alternative to the classical cooling jacket of a fermenter. The new device is supposed to allow a more uniform product temperature and to reduce the energy consumption during production process.

6.3 Heat pipes

Heat pipes are passive heat transfer devices with a high efficiency that use two-phase cycles of fluids as the operating principle. Through them it is possible to exchange large thermal powers without any contribution of external mechanical energy to the system, even by means of a very small temperature difference between one heat source and the other one. A classic heat pipes is composed by an evacuated tube filled with a certain amount of a working fluid in saturation condition. On its surface it is possible to identify 3 different sections, according to their function:

Evaporator section

Adiabatic section

Condenser section.

During operation, the evaporator is in contact with the item to be cooled down, and from it receives heat. Inside the evaporator, the thermal input is transmitted to the pool of the working fluid, which starts to vaporise. When it becomes a gas, the vapour pressure increases significantly, as it decreases its density by several orders of magnitude. The pressure head resulting from the density difference between the evaporator and condenser moves the vapor to the condenser section, passing by the inner core of the pipe. In the most common case

of a device placed vertically, in normal force of gravity conditions, with the evaporator at the bottom, the fluid then proceeds towards the condenser, placed at the top. Once the vapor of the working fluid reaches the condenser region, it starts to condensate, releasing latent heat to the could source. As it condenses, the density of the fluid comes back much greater and, therefore, tends to flow downwards along the walls by gravity. Once back in the evaporator, the fluid is ready to resume the cycle [18]. If exploiting gravity, for particular applications, is not possible, some solutions are adopted: the most common one involves the use of porous structures (wick structures) placed on the inner side of the walls which, by capillary action, cause the condensate to flow downwards towards the evaporator, bypassing the gravity action. When the wick structure is not present, and so the device needs to be vertically placed to work properly, it is called thermosyphon, otherwise, in presence of wick structure, it is called heat pipe.

From the description of the working principle of a heat pipe, it is easy to understand that many characteristics should be considered in designing such devices, since they can influence their performances and correct operation. For this reason, they have to be deeply evaluated when a heat pipe is designed for specific applications. Firstly, the selected working fluid must have a melting and a critical point temperatures below and above the operating temperature of the heat pipe, respectively [20].

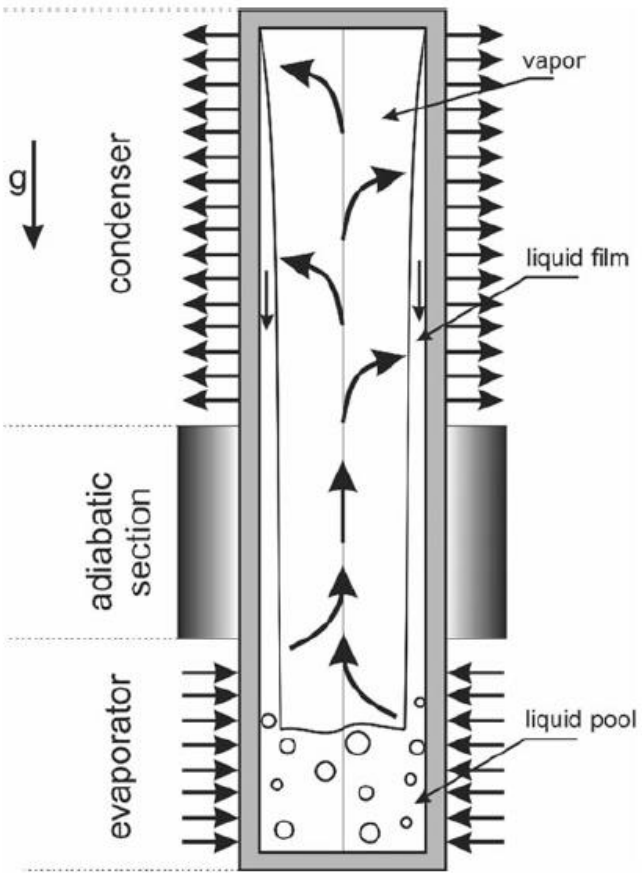

***Figure 6.3**: schematic representation of the working principle of a thermosyphon heat pipe in vertical position [19]*

Consequently, the choice of materials (pipe and working fluid) always strongly depends on the intended use, and they have to avoid non-compatibility between the two elements, thus reducing the risk of corrosion or damage to the device that would compromise its structural strength and safety. Finally, the filling ratio, defined as the ratio between the volume occupied by the fluid and the total volume of the device, given in percent, should be between 20 % and 60 %, Experimental tests in available literature shows that, for devices such as

thermosyphons and heat pipes, the ideal range of filling ratio is the one cited above [21]–[24].

The above-mentioned characteristics are linked in the definition of the parameters influencing the operation of a heat pipe and define the so-called “heat transfer limits”. These parameters can be summarised as follows:

- Viscous limit: when the viscous forces over the vapor are larger than the pressure gradient caused by the temperature difference between evaporator and condenser, the vapor could stop and compromise the operation of the device.
- Sonic limit: this limitation occurs when the working fluid reaches the sonic velocity inside the heat pipe in its flow from the evaporator to the condenser. In this situation, the vapour flow and therefore the heat flow cannot be increased and, as the evaporator input power is increased, the temperature gradient between evaporator and condenser increases.
- Capillary limit: in heat pipes with a capillary or wick structure, the head generated by these structures must be greater than the sum of all the pressure drops within the pipe. the opposite would generate a malfunction of the device due to inefficient transport of the condensate to the evaporator area.
- Entrainment limit: when the shear stress generated by the flow of vapour, migrating towards the condenser, is greater than the surface tension forces that hold the liquid adhering to the wall of the heat pipe or

inside the porous structure, a few drops of condensate could be detached from the wall by the flowing vapour. These droplets are consequently transported by the vapour and their return to the evaporator is prevented. All this causes a backflow of liquid to the condenser, preventing recharge of the evaporator and worsening the performance of the device.

- Boiling limit: the excessive increase in heat flow to the evaporator can cause the so-called dry out phenomenon, i.e. drying of the evaporator itself. In this scenario, all the liquid in the evaporator, is vaporised, as the excessive increase in thermal flux prevents the liquid from being replenished either through the backflow at the wall or through the capillary structure, causing the latter to evaporate before it can reach the lower end of the evaporator in a liquid state.

Up to now, exclusively thermosyphons and heat pipes in their classic versions were considered. However, for the sake of completeness, it is necessary to mention also other types of heat pipes, designed and realized for specific applications. To simplify, some of the most common types will be listed here, classifying them according to their operational mode.

- Vapor chamber: They are flat heat exchangers, consisting of two plates separated by a coil (which, since there is usually an internal vacuum, prevents the structure from collapsing). They are very efficient exchangers, exchanging great thermal power (even 600 W/cm2), have no

orientation problems, and require very low gradients. The only obstacle to their diffusion is the cost of production since they are rather complex devices to manufacture.

- Rotating heat pipe: In contrast to more traditional heat pipes, in this case these devices are dynamic, as they possess an axial or radial axis of rotation. The rotation allows a centrifugal force to be generated on the condensate (which, being of higher density, will tend to move outwards). In both radial and axial configurations, a taper is inserted into the duct to allow or facilitate the separation of vapour from liquid. Examples of applications can be found in electric motors, gears or bearings.
- Pulsating heat pipe (PHP): they are a particular type of heat pipe, in which there is the coexistence of alternating liquid and vapour parts, where transport takes place through pressure differences that make the system pulsate, creating flow. Also, in this case the system is totally passive since the drive of the motion is solely due to the intrinsic construction of the device. These devices are still widely studied because they have internal instabilities that make them more difficult to design with great reliability. However, they have the advantage, for example, to be not affected by orientation in space.

Heat pipes in general have demonstrated a great potential in terms of heat transfer and achievable energy consumption reduction in many industrial fields,

including the food one [25]. Jouhara et al. [26] implemented an innovative design of open display cabinet's shelves, based on flat heat pipe technology achieving a better temperature uniformity and an average energy saving of 12% respect to the original food cabinet. Panyoyai et al. [27] implemented a rice drying chamber heated by thermosyphon heat pipes obtaining a significant reduction of the treatment time in comparison to the classic drying system. Ketteringham and James [28] applied thermosyphon heat pipes for the cooling of canned food showing a reduction of the time of about 29% in comparison to the standard methodology. Heat pipes have been demonstrated to be effective also in direct contact with food during the cooking phase. James et al. [29] applied heat pipes inside meat joints during the cooking phase and obtained a substantial reduction of up to 50% in cooking and up to 25% in cooling times respect the classical cooking procedure, concluding that the use of heat pipes would also result in a significant energy saving.

The objective of this study is to evaluate the feasibility of applying a thermosyphon heat pipe for the implementation of a passive temperature control system in a fermentation tank for winemaking process, comparing it with the standard temperature control methodology. For this reason, a fermenter was designed and realized to simulate grape fermentation; in this device it was possible to use both the new fermentation temperature control system with heat pipes and the standard one based on water flow in the jacket. [reference di questo pezzo=quelle paper fermentatore].

CHAPTER 7: Application of a thermosiphon heat pipe to a wine fermenter: feasibility study

Among the available literature, the authors are not aware of any case of application of a thermosiphon heat pipe for temperature management inside a fermentation tank for wine production. For this reason, as a first step, it seemed essential to understand if this type of device could be suitable for this task and, secondly, to compare its performance with the classical cooling system used in the wine industry. To perform this experimental proof of concept, it was employed a device that was comparable to a thermosyphon heat pipe operating with the best possible conditions: a thermosyphon heat pipe with the maximum theoretical performances.

7.1 Experimental setup: the fermenter tank

A tank for fermentation in stainless steel AISI 316L with an internal maximum volume of 130 l was realized as reported in Figure 7.1 with a height H of 0.9 m and an external diameter of 0.55 m. Every wall of the tank is characterized by a thickness of 1.5 mm. The fermenter was equipped with a classical cooling system composed by an external cooling jacket (see figure 1a) with an external diameter of 0.61 m, where water circulates from the bottom to the upper side.

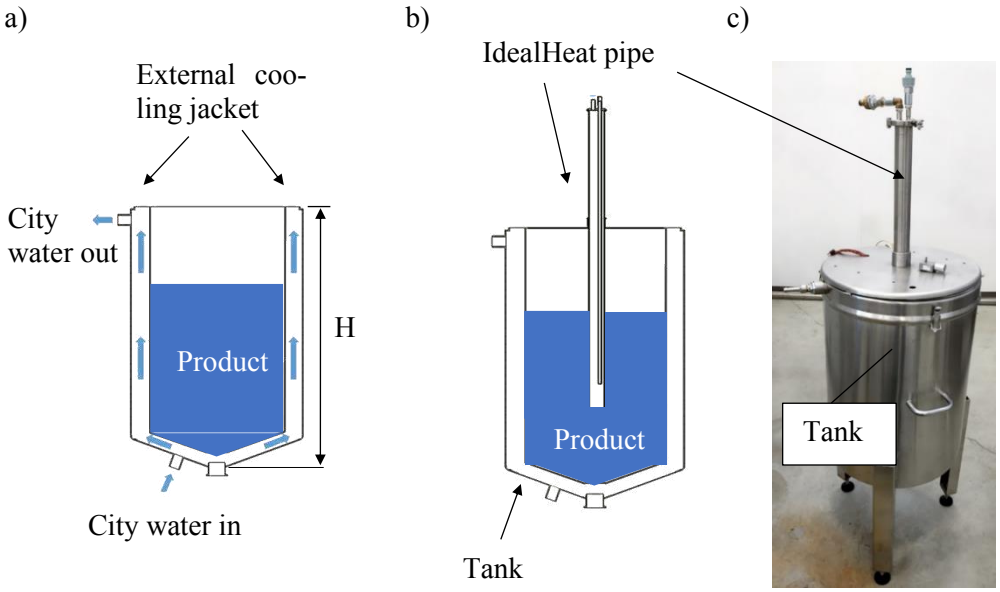

***Figure 7.1**: (a) Schematic section of the fermenter and the flow of the cooling fluid inside the jacket; (b) schematic section of the ideal heat pipe installed in the tank and (c) a picture of the tank with the ideal heat pipe.*

In the jacket, a spiral insert is placed to impose to increase turbulence and to enhance the heat exchange. Finally, a stainless steel AISI 316L cap was made with a central hole with a diameter of approximately 0.052 m with a raised collar

of approximately 0.05 m. It keeps the heat pipe in a perfect vertical position with its bottom part (≈ 45 cm) immersed in the product contained in the tank (Figure 7.1b). Thanks to this set-up, it was possible to test the two different cooling systems on the same fermenter (i.e., cooling jacket and heat pipe cooling) allowing a fair and robust comparison between the two technologies. Others smaller holes were made on the cap for the insertion of the thermocouples in the fluid.

7.2 Experimental setup: the ideal thermosyphon heat pipe (ITHP)

It was developed a device that was comparable to a thermosyphon heat pipe with the maximum theoretical performances. The heat transport is realized by means of evaporating a liquid in the heat input region (called the evaporator) and subsequently condensing the vapor in a heat rejection region (called the condenser).

One of the most used parameters to evaluate the thermal performances of this type of devices is the equivalent thermal resistance (R_{eq}) [25] [24], calculated as follows:

$$R_{eq} = \frac{T_{eva} - T_{cond}}{Q} \qquad (1)$$

where T_{eva} (°C) is the evaporator temperature, T_{cond} (°C) is the condenser temperature and Q (W) is the power input at the evaporator.

Referring to equation (1), it is possible to define a thermosyphon heat pipe with ideal thermal performances as the device characterised by an R_{eq} close to

zero. It means that all the heat that is absorbed at the evaporator to cool down the product is transmitted without any resistance to the condenser where it is dissipated. In practise, it means that the difference between the temperature at the evaporator and the one at the condenser is null . This device, that we are going to call as “ideal thermosyphon heat pipe (ITHP)” is made by pipe made of stainless steel (AISI 316L) with a total length of 1 m, an internal diameter of 0.05 m and a wall thickness of 0.0015 m was realised. At 0.36 m from the top of the pipe, an external sleeve of 0.03 m of thickness was welded for fixing the pipe on the cap of the fermenter and keeping it in the correct position during the tests.

The solution adopted to simulate the ideal condition of $R_{eq} \approx 0$ consists in making a high velocity water flow circulating inside the pipe. The water entered in correspondence of the heat pipe top through a tube with a diameter of 0.0085 m, which almost entirely crossed the heat pipe length, conveying the water to the lower part of the device (Figure 7.2). The water then exits from another hole with the same diameter placed on the top of the heat pipe. Providing a sufficient volumetric flow rate of cooling water, the ideal heat pipe presented a uniform temperature on its entire surface: it means that the thermal resistance between the bottom (evaporator) and the top (condenser), as defined in equation (1) was close to be null.

To provide to the device the required flow rate and the constant required temperature of the water, a chiller (Haake Kryo thermal 140) was used in recirculation mode.

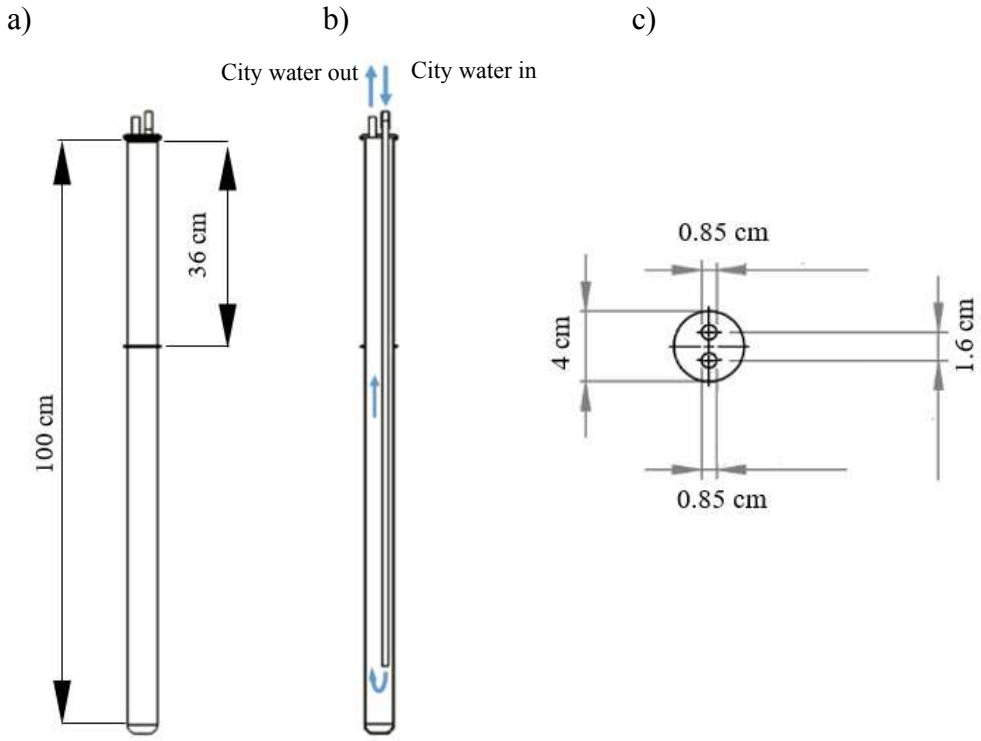

***Figure 7.2**: Schematic representation of the ideal heat pipe: a) external view b) internal view c) top view*

To simulate an ideal behaviour of the device water was circulating with a mass flowrate of 0.1 l/s and temperature equal to 18°C. This value has been chosen because it is a representative value of environmental temperature that is possible to find in a wine cave and therefore the temperature that we would have in case of a real heat pipe that at the condenser exchanges heat with environmental air.

The flowrate 0.1 l/s has been selected to avoid differences of temperature between the inlet and outlet sections. The maximum temperature difference was found to be 0.2 °C: in this way it was possible to consider the temperature at the evaporator and at the condenser equal and therefore the thermal resistance as

almost null, as it was supposed for an ideal heat pipe operating between the hot product and the cold water.

7.3 Experimentally setup: test conditions

The aim of the project was to investigate the behaviour of an innovative cooling system based on the heat pipes technology and understand if it is effective to maintain cold the product temperature during the fermentation process.

Due to the high variability generated by the variety of raw materials (grapes), climatic and terroir conditions and, also, by the producer's preferences in terms of organoleptic customisation of the final product, it is not possible to define a universal optimum temperature, or range of temperatures, for alcoholic fermentation in the oenological production.

However, it is possible to identify a representative temperature range and temperature set point to be considered for the comparison between the two cooling systems. In particular, the system was used to maintain the temperature of the product inside the tank in the range 22-25°C, considering as optimal temperature the mean value of 23.5°C: they can be reasonably considered as well representative for a wine must under fermentation process [2].

Water was used as surrogate of the fermentation substrate: since grape must is mainly composed by water, the thermodynamic behaviour of the surrogated can be quite representative of the real one. From a stoichiometric point of view, it is possible to summarize the alcoholic fermentation process in this way:

$$C_6H_{12}O_6 \rightarrow 2\ CH_3CH_2OH + 2\ CO_2 + 106.3\ kJ \quad (2)$$

During a typical alcoholic fermentation process, each mole of fermented glucose ($C_6H_{12}O_6$) releases about 106.3 kJ [6]. For the experimental tests, it was simulated the fermentation of 100 l of grape must. This amount contains about 300 g/l of glucose, corresponding to a total of 166.6 moles, which means that about $18 \cdot 10^6$ J are generated from their fermentation. Fermentation process normally lasts about 1 week but the fermentation kinetics is principally concentrated in the first 2 days and consequently great part of the heat is released in 48 hours (~80-90%) [30]. Considering that, the thermal power generated in this first interval of time could be approximated to 100 W for 100 litters of fermenting wort. The main challenging condition for the testing of the performance of the cooling system is the one with the higher power generated. For this reason, the first part of fermentation process (i.e., first 48 hours), has been simulated to perform the feasibility study. To provide the power, simulating the heat generated by fermentation, an immersion wire thermoelectric resistance was uniformly disposed inside the tank thanks to a supporting framework.

During the tests, the temperature of the product was acquired in 12 different positions (Figure 7.3) inside the tank by means of T-type thermocouples, at 4 radial distances for 3 axial coordinates.

a b

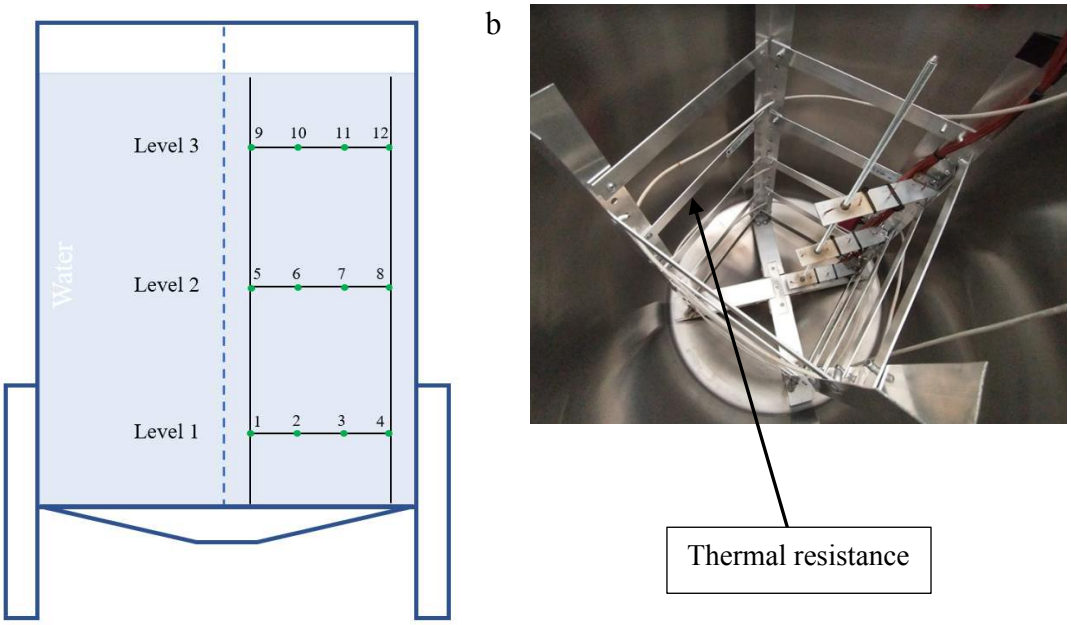

Figure 7.3: *Scheme of the disposition of the thermocouples inside the fermenter tank, b) thermal resistance inside the tank*

The three height levels were spaced 15 cm one from the other with the first level about 15 cm from the bottom of the tank. For each level, the thermocouples were located at the radial distances of 6 cm (i.e., TCs 1, 5 and 9), 11.5 cm (i.e., TCs 2, 6 and 10), 17 cm (i.e., TCs 3, 7 and 11), and 22.5 cm (i.e., TCs 4, 8 and 12) from the central axis, respectively. Temperature signals were measured by a data acquisition system (National Instrument NI CDAQ chassis + 3 NI 9213 C Series modules) connected to an ice point reference, type KAYE K170-274 50C.

The usual temperature control systems in fermentation tanks for wine making process adopted are represented by an external cooling jacket in which cold water flows. The first aim of this work is proposing an alternative solution based

on heat pipe technology and compare its performances with the ones of the usual systems.

Regarding the tests where the cooling jacket is adopted as refrigeration system, water was used as service fluid. Thanks to a chiller (Haake Kryo thermal 140) water is always provided at 13°C: this value has been chosen since it is in the typical range of temperatures at which city water is provided and therefore adopted in the traditional system with the jacket.

In every test for both the tested cooling systems, the product starting temperature was about 22°C. During fermentation, depending on the type of grape vinified, the pumping over of the must to obtain an optimal mixing of the product can be applied or not: to cover the whole case scenario and to compare the two systems under any conditions, tests were executed under two different conditions, i.e., with and without the mixing of the product inside the tank.

The pumping over of the grape was simulated trough the mixing action produced by a stirring system composed by a stirring body and a gear motor. The stirring body is made from an aluminum shaft approximately 1 m long to which 8 profiled fins are attached. The shaft is vertically immersed in the product in a position diametrically opposite the thermocouples.

Figure 7.4: *detail of the mixing system applied to the tank*

7.4 Results

It has to highlighted that, in the classical refrigeration systems, the cooling water does not flow continuously in the jacket, but the system is activated every time that the product temperature overcomes the fermentation upper limit. The activation logic is simply governed by usually one single temperature sensor, generally a thermistor that is placed as much as possible in a central position inside the tank. To simulate this condition, in the present investigation, the fluid circulation in the jacket is activated once the average temperature of the fluid in the tank exceeds 25°C, and it is switched off when the temperature drops down to 22°C.

Results without product mixing:

During the tests it was possible to notice a significant axial stratification of the temperatures inside the product that makes distinguishable the three level of thermocouples fixed inside the fermentation tank for both the experimental configurations and for the entire duration of all the tests. In Figure 7.5, the mean value of temperature for each level of thermocouples is reported as a function of time, for the cooling jacket system and the heat pipe cooling system in the tests without product mixing. It is possible to notice that the above-mentioned thermal stratification appears slightly amplified in the case of the cooling jacket. From Figure 7.5a, it is clear that, during the test interval, the cooling system has been activated three times (at 2.5 h, 5.5 h and at 8.5 h) as a consequence of the reaching of the upper temperature limit. It permits to maintain the average temperature of the product within the set limits (22-25 °C). Nevertheless, the temperature range limit has not been respected for the other thermocouples: the first level is cooled too much reaching about 20 °C, while the third level reached excessive temperatures of about 25.5 °C.

In the case of ideal heat pipe, both the second and the third level were kept in the range limits, while only the first level was cooled too much reaching the temperature of about 20.5°C. Thanks to this first analysis it is possible to note that with the ideal heat pipe device, the whole mass of the product is subjected to a smaller temperature variation (about 4.1°C) respect the jacket cooling system (about 5.5°C). Indeed, taking into consideration the maximum and minimum

temperature values reached by the product during the whole tests, it is possible to note that, for the tests carried out with the cooling jacket, they correspond to 25.7 °C and 20.2 °C, while for the tests with the ideal heat pipe, they correspond to 24.5 °C and 20.4°C, respectively.

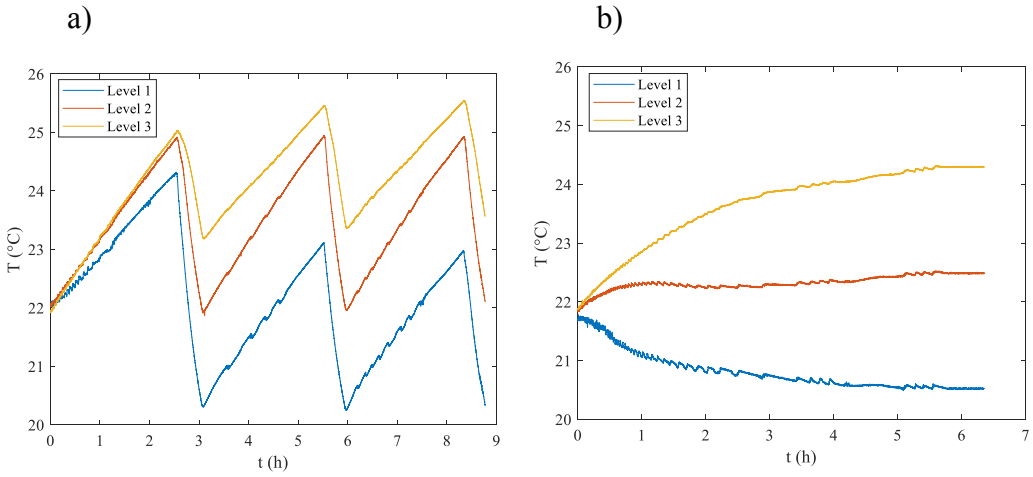

***Figure 7.5**: Temperature distribution of the 3 thermocouple levels for tests with 100 W input power without product mixing a) with cooling jacket; b) with ideal heat pipe*

Instead, considering the radial coordinates, no substantial difference of temperature can be noticed. This behavior is observable in Figure 7.6, that reports the instantaneously temperature distributions in reported only half axial section of the whole space domain occupied by the product in the tank (it is reasonable to consider an axial symmetry) in 2 different time: 3 h (at the end of the second activation of the cooling jacket) and at the time of 5.5 h (just before the third activation of the jacket). For both cases, at the two instants considered, no radial stratification of the temperature can be observed.

To deeper describe the effectiveness and the efficacy of the two cooling systems during tests, the grape must temperature uniformity (σ) was considered, and it was calculated in this way:

$$\sigma = \sqrt{\frac{\sum_{i=1}^{N}(T_i - \bar{T})^2}{N}} \quad (3)$$

where, N is the total number of temperature acquisitions during the whole test, T_i (°C) is the i^{th} measured temperature and $\bar{T}$(°C) is the mean temperature inside the product during the whole test. This parameter describes the capability of the system to maintain a homogeneous temperature inside the product during its activation and its operation. In Table 7.1 the values of the temperature uniformity σ referred to all the N measurements for the test condition without product mixing are reported. It is possible to observe that for the tests with the cooling jacket and the ideal heat pipe it is almost the same, about ± 1.24°C and ± 1.23°C, respectively. It suggests that, under the simulated fermenting conditions here tested, the ideal heat pipe can get a similar dispersion of the temperatures around the mean value compared to the jacket system but limiting the variation of the temperature of the entire mass of the product during the entire time of the process, as confirmed by Figure 7.5 and Figure 7.6.

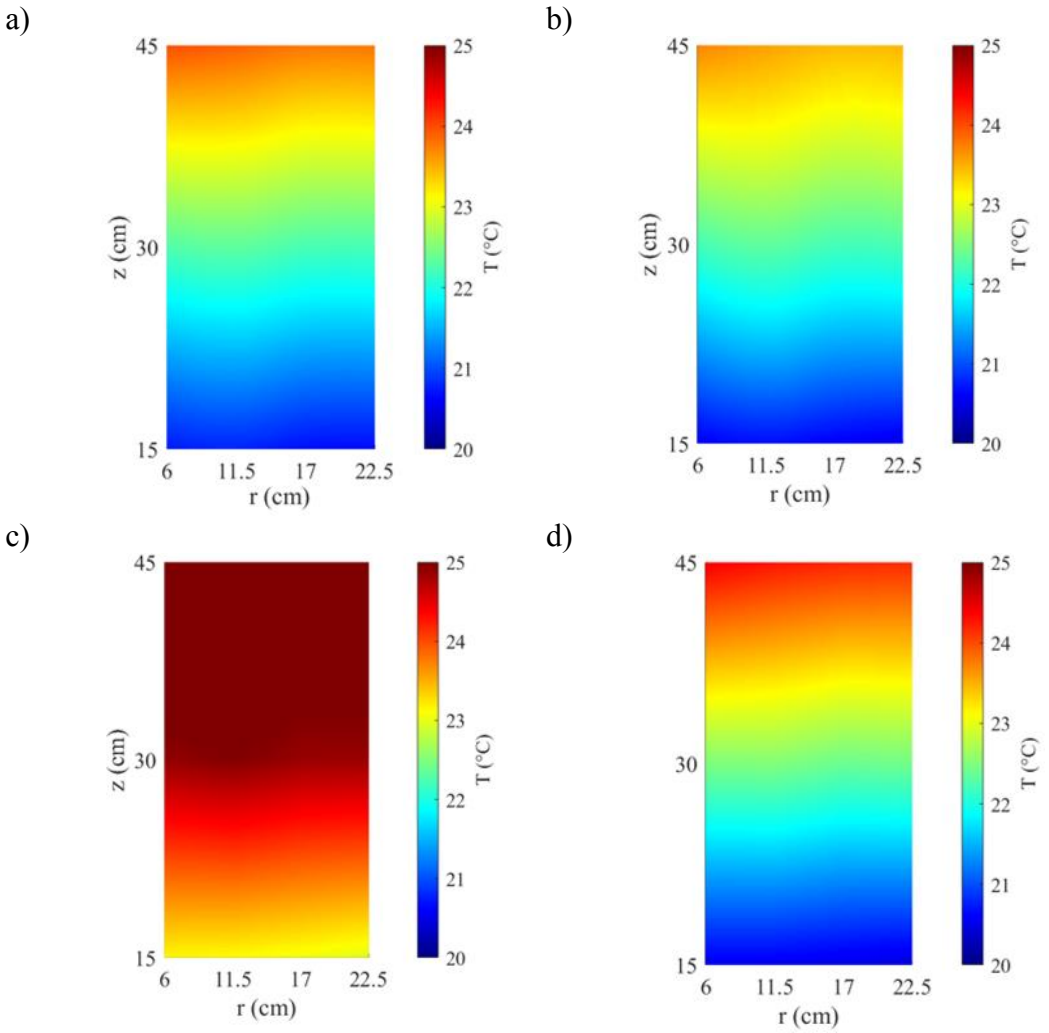

***Figure 7.6**: Temperature space distribution: a) Jacket cooling system at 3 h; b) Ideal heat pipe system at 3 h; c) Jacket cooling system at 5.5 h; d) Ideal heat pipe system at 5.5 h.*

Cooling system	σ
Jacket	± 1.24
Ideal heat pipe	± 1.23

***Table 7.1**:σ for the cases of jacket and ideal heat pipe without product mixing*

Results with product mixing

The distribution of the mean temperature of the three levels of thermocouples in the case of product mixing is shown as a function of time in Figure 7.7 for both the cooling systems. It is possible to note that the mixing action helped to prevent an excessive thermal stratification for both the cases, allowing to obtain a more homogeneous product temperature distribution. However, for the jacket case, it is still possible to observe greater temperature oscillations respect to the case of the ideal heat pipe: this behavior is ascribable to the intermittent activation of the cooling system for the classical configuration and produces a great variation of the temperature of the entire mass of the product during the entire time of the test.

With the mixing of the product, the value of temperature uniformity σ, calculated as reported in Eq. (2), reports some differences between the two cases: for the cooling jacket case it reaches about ± 0.99 °C (Table 7.2), while for the ideal heat pipe it reaches ± 0.31 °C.

Cooling system	$\boldsymbol{\sigma}$
Jacket	± 0.99
Ideal heat pipe	± 0.31

Table 7.2*: σ for cases of jacket and ideal heat pipe with product mixing.*

This parameter shows that with the application of product mixing, the ideal heat pipe could perform better than the cooling jacket in terms of uniformity of product temperature, keeping its better performances in terms of variation of the

temperature of the entire mass of the product during the entire time of the fermentation.

a) b)

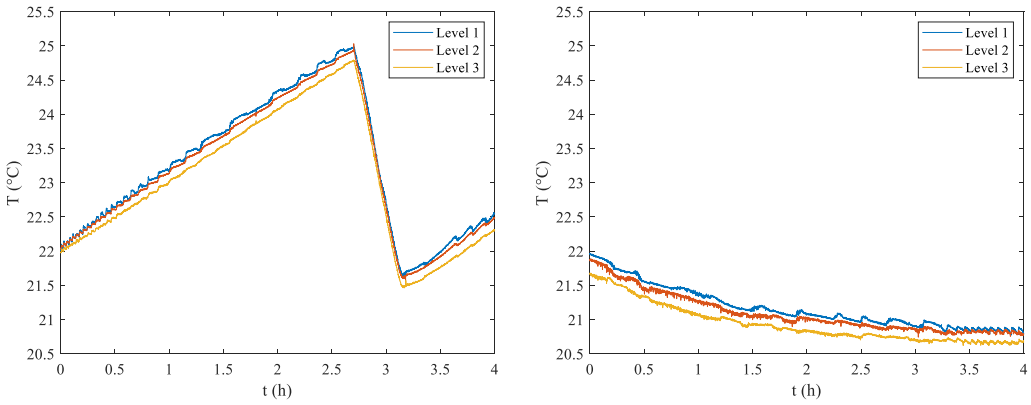

Figure 7.7:*Temperature distribution of the thermocouple levels for tests with 100W input power applying mixing of the product a) with the jacket cooling system; b) with the ideal heat pipe as cooling system*

7.5 Closure

Concluding, the application of the ideal heat pipe demonstrated to produce a lower axial thermal stratification inside the product both with product mixing and without it, and to reduce the variation of the temperature of the product during the whole time of fermentation. However, the best performances of the ITHP were reached when combined with the mixing action of the product. These results are confirmed also in terms of uniformity parameter and therefore in terms of suitable condition for the fermentation process inside the product. For this reason, it is possible to state that this kind of device associated to a stirring action could represent an interesting solution for the thermal control of the grape must during fermentation.

CHAPTER 8: Implementation of a real thermosyphon heat pipe (HP)

Since the ideal thermosiphon heat pipe showed a satisfactorily performance for temperature management in a fermentation tank, it was decided to continue the feasibility study considering the design and the realization of a real thermosyphon heat pipe.

As mentioned in par 6.3, during the realisation of a thermosyphon heat pipe, several aspects must be considered since they define the correct functioning and performance of the device. To this end, the first step in the design of the device included the selection of the correct realization materials. These choices were made according to the criteria necessitated by the scope and objectives set for the innovative device.

The second step involved the estimation of the device's possible thermal exchange limits in order not to compromise its functionality and user safety. Finally, as a last step, its thermal performances were evaluated.

8.1 Design and realization of a preliminary HP

Considering the purely food-related purpose of the innovative device, the choice of material to be used was bound by the mandatory regulations on materials for food contact [31]. For this reason, it was realised in aluminium that in addition to its compatibility with food contact, is characterised by high thermal conductivity (290 W/m K) and good structural resistance. The device was realised with a cylindrical shape, with an external diameter of 0.03 m, internal diameter of 0.02 m and its length was 0.8 m. To allow the correct positioning of the HP inside the fermenter, a centring flange was welded to its outer surface. Once inserted into the hole realized on the cap, in the HP the following sections are identifiable: the evaporator section (the part immersed in the product) 0.4 m long, the adiabatic section (the part between the liquid level and the cap of the fermenter) 0.2 m long and, finally, the condenser area (the part coming out from the cap of the fermenter) 0.2 m long (Figure 8.1a). R134a refrigerant was selected as working fluid because, at the exercise temperature range of 22°C-25 °C (the fermenting range considered), it reaches a non-excessive high absolute saturation pressure (about 6-8 bar).

At the top of the HP, it was realised the system for the fluid filling as it is possible to see in Figure 8.1a. Before the filling it is necessary to vacuumize the

device to avoid the presence of non-condensable gases that can alter the behaviour of the device. Valve V1 was connected to the vacuum system and valve V2 was maintained close: consequently, the loop and the tubes were vacuumed to below than 30 Pa by vacuum pump (AGILENT DS40M). The pressure was measured by a vacuum gauge (AGILENT 0531TC) and a controller (AGILENT RGC-150). Valve V1 was closed, the system was disconnected from the pump and the HP weight is measured in empty condition ($m_{RHTP,e}$).

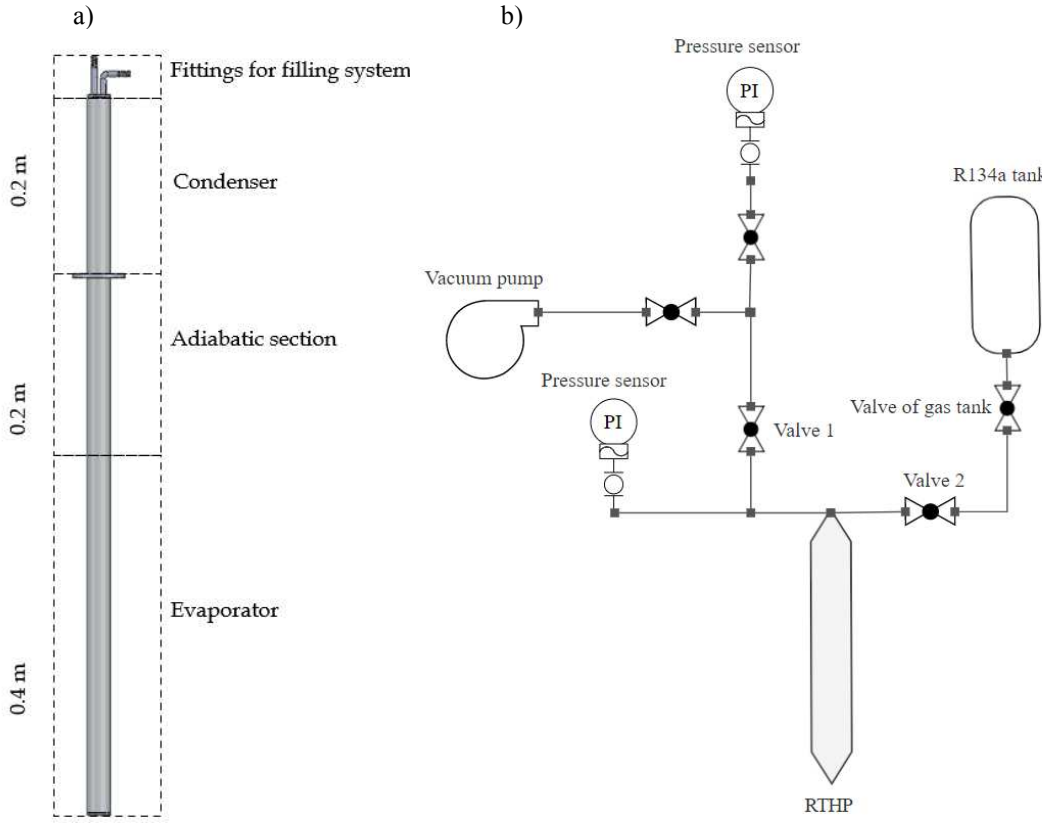

***Figure 8.1**: a) Schematic representation of the HP b) Schematic layout of filling system of HP*

The HP was then reconnected to the vacuum pump and, to the valve 2, the R134a container was connected maintaining its outlet valve close. Once the internal pressure reached another time a stable value of about 30 Pa, the valve 1 was closed, the vacuum pump disconnected, and the outlet valve of the gas tank was opened the refrigerant started to fill the device. Once the flow of refrigerant stopped, the valve 2 and the outlet valve of the refrigerant tank were closed to fully disconnect the HP from the charging system. The weight of the filled HP was measured ($m_{HP,fi}$) and the filling ratio (FR) of the HP was calculated as follows:

$$FR = \frac{m_{HP,fi} - m_{HP,em}}{V_{tot} \cdot \rho_l} \% \qquad (4)$$

where V_{tot} is the internal volume of the HP and ρ_l is the density of R134a in liquid phase.

8.2 Verification of the heat transfer limits of the HP

The heat transfer limits, as anticipated in paragraph 1.2.4, represent physical thresholds, exceeded which the operation of the heat pipe would be compromised, generating malfunctions of the device and consequently the collapse of its performance. For this reason, it seems appropriate to evaluate these limits for the designed device. However, since it is a thermosyphon heat pipe, the limits regarding the effect of capillarity will be neglected, indeed no wick or porous structure are present inside the realized device and for this reason the boiling limit and the capillary limit were not considered. Moreover, the viscous limit

was also neglected, since it is mostly common in the application of heat pipes in cryogenic conditions, where the working fluid viscosity increase a lot due to very low temperature and the vapour pressure differences between evaporator and condenser could be very low [19]. Consequently, the limits considered are the sonic limit and the entrainment limit:

- Sonic limit (q_{sl}): this limit is reached when the vapor, which flows from the evaporator to the condenser, reaches the velocity of the sound and the thermal flux cannot be increased further. Each increase in the heat flow to the evaporator corresponds to a decrease in the performance of the device. The minimum heat flux due to the sonic limitation will occur at the minimum operating temperature, that, in this case, corresponds to the lower limit of the optimal range of temperature for the grape must in fermentation: 22°C (see par 1.2.3). The sonic limit, q_{sl} [W/m2] is calculated as follow:

$$q_{sl} = \rho_v H \sqrt{\frac{\gamma R T_e}{2(\gamma + 1)}} \qquad (5)$$

where:

- ρ_v is the density of the vapour of R134 at 22°C [kg/m^3];
- H is the enthalpy of vaporization of R134a at 22°C [J/kg];
- γ the ratio between specific heats [-];
- R is the specific constant for R134a [J/(kg K)];
- T_e is the temperature at the condenser [K];

– In this case, the sonic limit q_{sl} corresponds to 4.18 · 108 W/m2. This value is several orders of magnitude greater if compared to the specific heat flux at the evaporator (q_e), calculated as follow [32]:

$$q_e = \frac{Q}{\pi\, D_{out}\, L_e} \qquad (6)$$

where:

- Q is the input power at the evaporator, generated by the fermentation [W];
- D_{out} is the external diameter of the evaporator of the thermosyphon heat pipe [m];
- L_e is the length of the evaporator of the thermosyphon heat pipe [m];

that corresponds to $2.65 \cdot 10^3$ W/m^2.

For this reason, the sonic limit can be considered respected.

– Entrainment limit (q_{el}): this limit represents the specific heat flow value to the evaporator (q_e) beyond which the steam flow towards the condenser begins to generate a tangential stress, between itself and the liquid returning to the evaporator, greater than the surface tension between the condensate and the wall of the device. This limit can be calculated as follow, considering the highest working temperature [32]:

$$q_{el} = \sqrt{\frac{2\pi\rho_v H^2 \sigma}{\sqrt{\pi D_{int}\left(\frac{D_{int}}{2} + L\right)}}} \quad (7)$$

where:

- ρ_v is the density of the vapour of R134 at 25°C [kg/m^3];
- σ is the surface tension of the liquid R134a at 25°C [m];
- D_{int} is the internal diameter of the thermosyphon heat pipe [m];
- L is the length of the thermosyphon heat pipe [m].

In this case, the entrainment limit q_{el} resulted of about $2.8 \cdot 10^5$ W/m^2 and, it resulted greater than the specific heat to the evaporator. For this reason also this limit can be considered respected.

8.3 Characterization of the performances of the HP

The thermal performances of the HP were characterised in terms of thermal equivalent resistance as defined in Eq. (1) while varying the power input provided at the evaporator varies. The heat load was provided by a wire thermal resistance wrapped around the cylindrical heat pipe for the whole evaporator section (see Figure 8.2a): it was connected to a DC power supply (JO POWER ALP6010) that allowed to apply electrical power in stepwise until the HP operating limits were reached.

a) b)

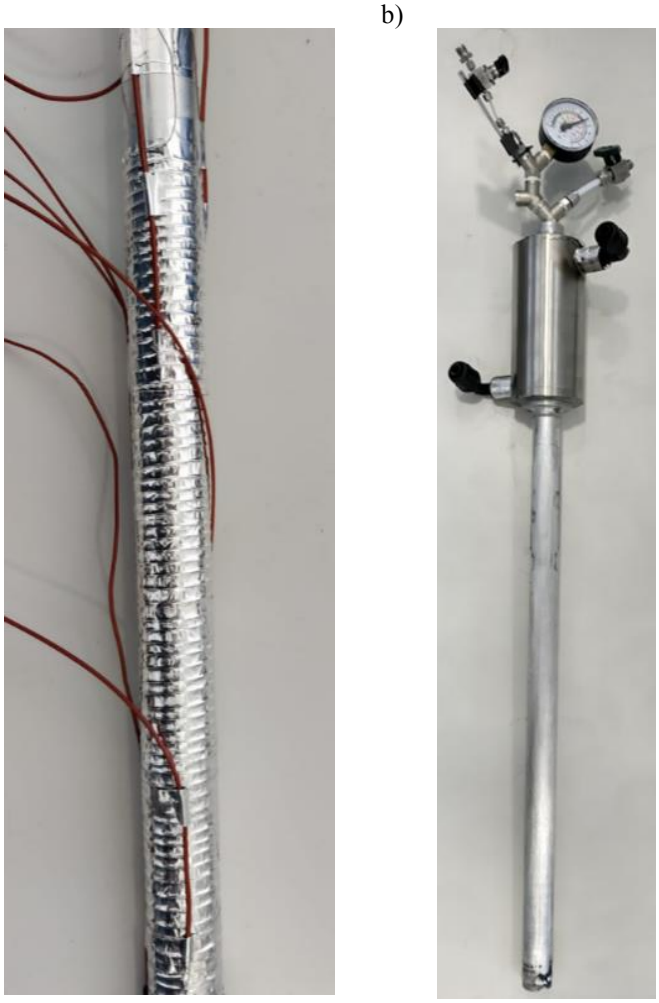

Figure 8.2*:a) Detail of the wire thermal resistance and thermocouples on the HP; b) HP with cooling jacket installed on the condenser*

Eight thermocouples were applied on the external wall of the HP to measure the temperature along the entire evaporative zone. The condenser section was realised with a shell in stainless steel (Figure 8.2b) were a cold fluid flowed around the external wall of the heat pipe: the adopted service fluid was water that was provided at 18 °C thanks to a chiller (Haake Kryo thermal 140). Providing a sufficiently high flow rate of the water inside the cooling jacket, it was

possible to keep constant the temperature at the condenser. Also for this step of the study, the value of 18°C has been chosen for the condenser section to simulate a standard environmental condition for the cellars were the fermenting stage is carried out. Thermocouples were placed at the water inlet and outlet section of the cooling jacket to check that the temperature remained constant. The entire external surface of the HP has been thermally insulated during the tests.

Five filling ratios, calculated as reported in Eq. (3), were tested: 0%, 20%, 30%, 50% and 70%, at different input power: from 0 W to 100W with steps of 5 W.

From the R_{eq} distributions as a function of the power input reported in figure 10 it is easy to notice that the best performance can be reached for the two lower percentage of filling that presented lower value of equivalent thermal resistance for the whole range of input power tested.

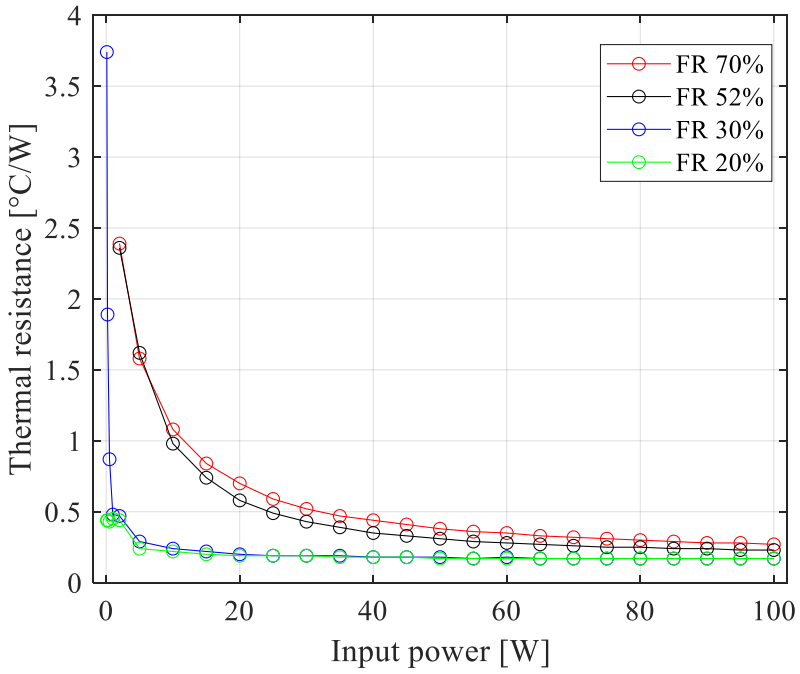

***Figure 8.3**:Equivalent resistance of the HP in function of the power input at the evaporator*

For the FR= 50 % and 70 %, R_{eq} reached an almost asymptotic trend at an input power of about 80 W, while for FR= 30 % and FR= 20 % the asymptotic distribution was already reached at an input power of about 10 W and moreover at lower R_{eq} values. This means that, under the considered conditions, the filling ratios of FR=20 % and FR= 30 % allowed the device to optimally operate, i.e. with a minimum R_{eq} value, in a wider range of input power than the other FR values, making it more modulable for the studied application. In the studied case, as already explained, a generation power of 100 W is considered as the maximum power value along the whole fermentation process and therefore lower values are generated most of the time throughout the process. Under these

considerations the fact that the FR=20 % and FR= 30 % guarantee the lowest values of R_{eq} for the wide range 10-100 W is a big plus point.

To better investigate the performance of the HP, it was also tested in his best setup (FR= 20%) inside the tank by simulating fermentation conditions: 100 l of water were used as the fermentation substrate, a 100 W immersion wire thermo-resistance was used to simulate the power generated by fermentation, the water temperatures inside the tank were measured using the acquisition system described before and the fluid was constantly mixed with stirring system. The temperature of the condenser of the HP was kept at 18 °C while the ambient was 19 °C and constant over the entire time of the test. The average temperatures of each level of thermocouples are reported in Figure 8.4 once the steady state has been reached. The temperature of the fermentation substrate, and so the one of the HP evaporator, reached about 29.4 °C, confirming that the RHTP is not able of dissipating the maximum power input while maintain the temperature of the product in the optimal prescribed range during the fermentation process.

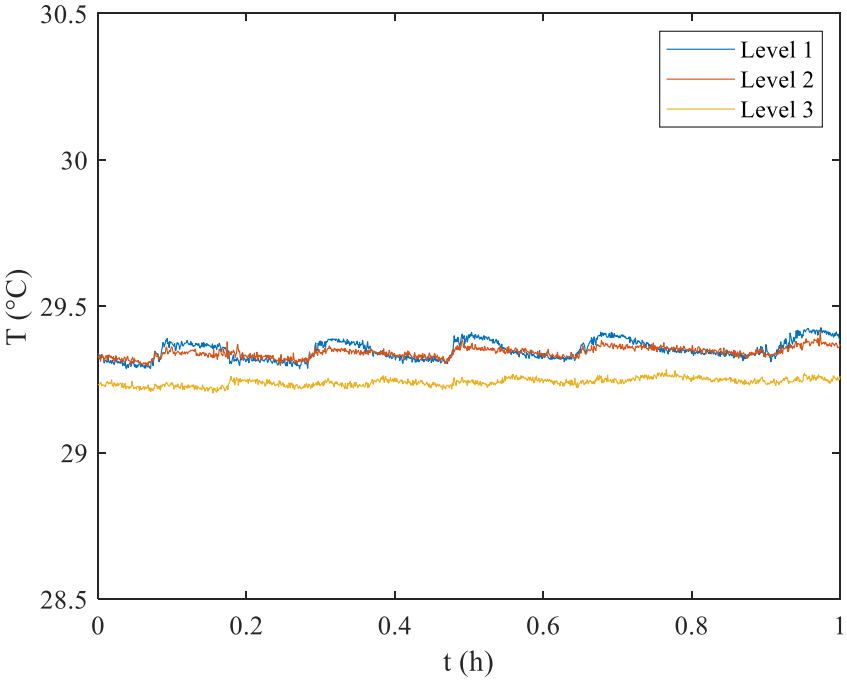

***Figure 8.4**:Temperature distribution of the thermocouple levels for the test of HP (FR= 20%) inside the tank*

The HP showed that, once the stationary thermal regime conditions have been reached, it can guarantee a very good temperature uniformity inside the product; in fact the three levels of thermocouples didn't show a substantial axial stratification inside the must (i.e. less than 0.1°C). To confirm this, it is possible to observe that the value of σ (**Table 8.1**:σ for the case of real thermosyphon heat pipe with product mixing.Table 8.1) is very limited and around ± 0.08 °C. Moreover, if this value is compared to the one achieved by the cooling jacket under product mixing conditions (Table 7.2), it is possible to note that the new device reached a value ten time less than the one reached by the cooling jacket. For this reason, it is possible to affirm that the HP could have the potentiality of

guaranteeing a lower stratification of the temperature during the fermentation phase reaching better performances respect to the cooling jacket from this point of view. This aspect could guarantee a reduced thermal stress for microorganisms involved in fermentation consequently improving the final quality of the product.

Cooling system	σ
Real Thermosyphon heat pipe with product mixing	± 0.08

Table 8.1*:σ for the case of real thermosyphon heat pipe with product mixing.*

However, it is possible to observe that, for the current configuration, the fluid temperature exceeded the upper limit of the optimal range considered for these tests (25 °C) highlighting that the current device is thermally undersized for the application studied here. Such a temperature of the grape wort would not be acceptable for fermentation purpose and would affect the yeast yield and the quality of the final product.

8.4 Closure

The results of the application of the innovative thermal control system for the fermentation phase, based on heat pipe technology, in terms of temperature uniformity and temperature stability of the must during the entire process, can be considered positive. However, the thermosyphon heat pipe proved to not be correctly thermally dimensioned, not allowing the temperature of the fermenting

substrate to be kept within the set ranges. For this reason, to obtain a fully functional device, the correction of its thermal performances is needed.

To this end, two main modes of operation can be identified: either redefine the design of the device from the beginning in order to reduce its overall thermal resistance or consider the possibility of applying several thermosyphon heat pipes in parallel in order to obtain a total equivalent thermal resistance adequate for keeping the temperature of the product in the correct range. In the following paragraph, both the two strategies will be discussed in detail.

CHAPTER 9: Solutions for achieving the correct thermal sizing of the innovative cooling system

9.1 Solution 1: calculation of the optimal number of HPs

To calculate the optimal number of THPs to be employed in the considered tank, it is useful to investigate and characterise the thermal interaction of the tank with the environment. Considering negligible in the studied case the effect of heat conduction in the metal wall and radiation between the tank and the environment, to quantify the heat dissipated to the environment by the tank, it is sufficient to quantify the convective heat transfer coefficient h. To calculating this parameter, two tests were executed.

The first test involved the heating of the water inside the tank, initially at room temperature, by means of a 100 W wire immersion thermal resistance while the second test regarded the cooling back to room temperature of the same water by natural convection. During both tests, the water temperatures were acquired as specified before, in addition, the ambient temperature was measured with two other thermocouples. Continuous stirring of the water inside the tank was applied to reduce the radial or axial thermal gradients. The energy balance equations for the cooling and heating tests can be written as reported in Eq. 8 and Eq. 9, respectively.

$$mc_p \frac{dT_c}{d\tau} = hA(T_e - T_c) \quad (8)$$

$$mc_p \frac{dT_h}{d\tau} = \dot{Q}_{el} - hA(T_h - T_e) \quad (9)$$

where T_c is the mean temperature of the whole product in the cooling test while T_h in the heating test, T_e is the temperature of the environment and $\dot{Q}_{el}$ is the input power of the wire resistance, if it is present.

In the system constituted by Eqs. (8-9), there are two unknown quantities that are the two products $h \cdot A$ and $m \cdot c_p$ where h is the convective heat transfer on the external side of the tank, A is the external surface of the tank. Regarding the variables m (mass) and c_p (specific heat), they are referred to the system composed by the union of the tank and of the water inside it. The temperature of the tank is supposed to be equal to that of the fluid.

The average product temperature inside the tank was calculated by dividing the internal volume into 12 circular crowns of a rectangular cross-section whose representative temperature is considered equal to the one measured by the thermocouple there placed (Figure 9.1).

The water temperature inside the fermenter was calculated as follows:

$$T_f = \frac{\sum_{i=1}^{12} T_{cr,i} V_{cr,i}}{V} \quad (10)$$

Where i is the i-th circular crown, $T_{cr,i}$ is the temperature measured by the thermocouple placed in the i-th circular crown, $V_{cr,i}$ is the volume of i-th circular crown and V is the volume of the product inside the tank.

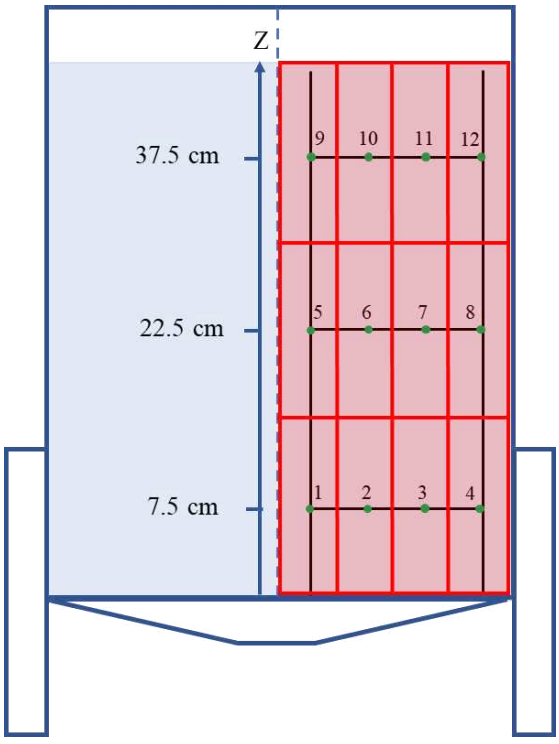

***Figure 9.1**:Rectangular sections (in red) of the 12 circular crowns with their respective thermocouples.*

To express, the two unknowns $h \cdot A$ and $m \cdot c_p$, Eq. 8 can be rewritten as follows:

$$\frac{mc_p}{hA} = (T_c - T_e)\frac{d\tau_c}{dT_c} \quad (11)$$

Substituting it in Eq. 6, it is possible to obtain:

$$hA = \frac{\dot{Q}_{el}}{(T_c - T_e)\frac{d\tau_c}{dT_c}\frac{dT_{f,h}}{d\tau_h} + (T_h - T_e)} \quad (12)$$

From Eq. 12, it is now possible to compute the value of $h \cdot A$, that in specific it is equal to 3.39 W °C^{-1}. This value was then used in Eq. 11 to compute also the $m \cdot c_p$ parameter, that is 450 kJ °C^{-1}.

The calculated value can be considered acceptable; indeed, if we consider the lateral and the bottom external surfaces of the tank as the heat transfer area with environment A (1.79 m^2), the convective heat exchange coefficient h is approximately 1.89 W m^{-2} °C^{-1}. This value can be considered acceptable if compared to the one obtained using the correlation proposed by Rogers and Mayhew [33]: ~ 2.17 W m^{-2} °C^{-1}.

Once the $h \cdot A$ parameter was estimated, it was possible to use it for computing the theoretical amount of heat transferred by the system (composed by tank + water) to the environment and the heat load dissipated by the HP. For this purpose, it is possible to write the energy balance of the system during the heating test as follows:

$$mc_p \frac{dT_h}{d\tau_h} = \dot{Q}_{el} - \ hA(T_h - T_e) - \ \dot{Q}_{HP} \qquad (13)$$

where $hA(T_h - T_e)$ is the amount of heat exchanged by the tank with the environment by natural convection and $\dot{Q}_{THP}$ is the amount of power dissipated by the HP:

$$\dot{Q}_{HP} = \dot{Q}_{el} - \ hA(T_h - T_e) \qquad (14)$$

and, substituting in Eq. 14 the test conditions (par. 1.3.3), $\dot{Q}_{THP}$ results about 64.74 W.

Then, it is possible to introduce an effective thermal resistance of the Heat Pipe defined as follows:

$$R_{eq,eff} = \frac{T_p - T_{cond}}{\dot{Q}_{HP}} \qquad (15)$$

where T_p is the product temperature in the fermenter and T_{cond} is the temperature at the condenser of the HP. Substituting the experimental values obtained in par 1.3.3 in Eq. 15, $R_{eq,eff}$ was computed to be about 0.18 °C/W.

The $R_{eq,eff}$ obtained in the test simulating the fermentation process slightly differs from the resistance value R_{eq} found in the bench test (0.17 °C/W) for the same power input.

However, this increase in $R_{eq,eff}$ can be explained by the presence of an additional thermal resistance in the test simulating the fermentation process,

compared to the bench tests: in this case, since the evaporator of the HP is immersed in water for the entire duration of the test, a convective thermal resistance on the external side of its wall must be considered.

Finally, to determine the number of HPs that are needed for the optimal thermal management of the fermentation process in the considered tank, the energy balance can be rewritten as follow:

$$\dot{Q}_f - hA\left(T_p - T_e\right) - \frac{N_{HP}\left(T_p - T_{cond}\right)}{R_{eq,eff}} = 0 \qquad (16)$$

where N_{HP} is the number of HPs, and it is unknow and $R_{eq,eff}$ is a function of the calculated input power to the evaporator section $\dot{Q}_{THP}$. In the energy balance equation, $\dot{Q}_{THP}$ corresponds to the term $\dot{Q}_f - hA\left(T_p - T_e\right)$, in specific $\dot{Q}_f$ is the thermal power developed by fermentation while $hA\left(T_p - T_e\right)$ are the heat power losses to the environment.

Finally, considering the environmental and the condenser conditions of the tests for simulating a real fermentation condition, proposed in par. 1.3.3, it has been possible to calculate the number N of HPs required to maintain the desired temperature of the product (T_p). In the above-cited fermenting conditions, for keeping the product temperature T_p at about 23.5°C (considered the optimal temperature in this case study, see section 1.2.3), the number of HPs needed N is equal to 3.

9.2 Solution 2: development of a model of the HP for its thermal sizing inside the fermenter

To correctly size the device from the thermal point of view, the equivalent resistance R_{eq}, defined as reported in Eq.1, must be considered once again, evaluating some boundary conditions imposed by the application of the device to a fermenter for the wine industry: the use of a heat pipe in a fermenter, with the aim of regulating the temperature of the must during the fermentation process, is subject to non-negligible operational constraints dictated by the operational requirements of the fermentation phase itself. These constraints are necessary to guarantee the success of the production process and, consequently, the quality of the final product.

In specific, the ambient temperature of the wine cellar is defined by the weather, by the season and by the location of the building where the fermentation takes place. It can therefore be said that this parameter tends to be imposed depending on the production conditions to which the process is subjected and can hardly be managed and varied significantly. For this reason, the ambient temperature, and thus the temperature at which the heat pipe condenser will be located (T_c), is to be considered as constrained. Moreover, the heat released from the fermentation is defined by the amount of glucose inside the grape must and the kinetics of the yeast metabolism during the entire process. It may be subject to slight variations during the time span of fermentation, but generally this parameter is also to be regarded as bound to non-modifiable characteristics of the

process. For this reason, also Q is to be considered as constrained. Finally, the temperature at the evaporator T_e, and so the temperature corresponding to the one of the fermenting product, is of great importance in order to ensure optimal metabolic activity of the yeast involved in this biochemical reaction. For this reason, it cannot be considered as a free parameter and therefore it is to be regarded as constrained according to the production process characteristics considered. In specific, this temperature is selected by the producer depending on the type of wine produced and on the organoleptic features wanted in the final product.

It is therefore clear that, considering the parameters Q and T_c as fixed by the process conditions, the way to obtain a desired product temperature (T_e), is to work on the only parameter not related to the process: R_{eq}. It is a function of the construction characteristics of the heat pipe and function of the power Q, and for this reason it must be deeply investigated in order to understand how to act to design it. For this purpose, a thermal model of the thermosyphon heat pipe applied to the wine fermentation was built as reported inFigure 9.2, where it is possible to see the contribution of the different thermal resistances and their connection. Considering the heat entering the heat pipe, it is possible to schematise its path through a succession of thermal resistances, for creating a model describing the operation of the thermosyphon.

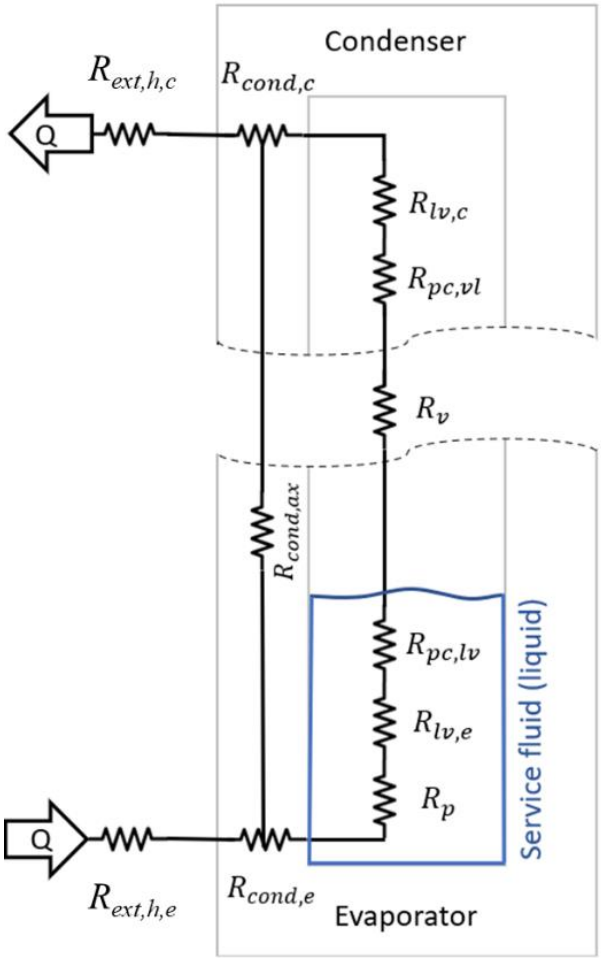

***Figure 9.2**: Complete resistor network*

These resistances can be expressed as follow:

– *External convective resistance at the evaporator* ($R_{ext,h,e}$): it is the resistance due to the external fluid convection at the evaporator. This value can be expressed ad follow:

$$R_{ext,h,e} = \frac{1}{h_{ext,e}\, A_e} \qquad (17)$$

where $h_{ex,e}$ and A_e are respectively the convection coefficient of water at the evaporator and the exchange area.

– *Wall conduction resistance at the evaporator* ($R_{cond,e}$): it is the resistance due to the wall layer of the heat pipe considering the radial direction. It can be calculated as follow:

$$R_{cond,e} = \frac{\ln\left(\frac{r_{ext}}{r_{in}}\right)}{2\pi\lambda\, l_e} \quad (18)$$

where r_{ex} and r_{in} are the outer and inner radius, λ is the conductivity of the material, and l_e the length of the evaporator.

Wall axial conduction resistance ($R_{cond,ax}$): it is the resistance for the heat flow in the axial direction of the heat pipe through the wall, and can be expressed as follow:

$$R_{cond,ax} = \frac{l_{HP}}{\pi\lambda(r_{ext}^2 - r_{int}^2)} \quad (19)$$

where, l_{HP} is the length of the thermosyphon heat pipe. It is usually three orders of magnitude greater than the radial resistance, so the amount of heat that tends to flow axially through the wall of the heat pipe can be neglected. Almost all of the heat power flows radially through the surface and heats the internal fluid. In fact, this thermal resistance is positioned parallelly to all the successive ones in Figure 9.2 (in series with each other) that characterise the inner part of heat pipe.

Pool boiling resistance (R_p): it represents the boiling resistance of the fluid in the thermosyphon evaporator. The heat flow, after passing through the wall layer, enters the evaporator, where it warms up the liquid held in a small bath at the bottom of the device. For this resistance, it is possible to use a formulation like those used for convection, as follow:

$$R_p = \frac{1}{h_{int}\, A_{int}} \qquad (20)$$

where the subscript int denotes the values inside the heat pipe in the pool area.

– *Thermal Resistance of the Evaporator Film ($R_{lv,e}$):* once passed the aluminium wall, the heat flux invests the liquid fluid either on the base in the pool or, if the pool does not cover the entire height of the evaporator (as in this case), the film layer of condensed liquid that is descending from the cold side towards the hot side. Considering the fluid's properties and the film thickness, this resistance can be expressed as follow [19]:

$$R_{lv,e} = \frac{0.235\, q_e^{1/3}}{D_i^{4/3} g^{1/3} l_e \left(\frac{h_{lv}\lambda_l^3 \rho_l^2}{\mu_l}\right)^{1/3}} \qquad (21)$$

where q_e is the power entering the evaporator, h_{lv} is the latent heat, λ_l is the conductivity of the liquid, ρ_l its density and μ_l its viscosity.

- *Phase change resistance ($R_{pc,lv}$ and $R_{pc,vl}$):* after passing through the liquid film, the heat flow encounters another resistance caused by the liquid-to-vapour phase transition interface. This contribution occurs in an identical manner both passing from liquid to vapour in the evaporator and, in the opposite way, passing from vapour to liquid inside the condenser. Usually, these two resistances are not considered because they are extremely low, on the order of 10^{-5} °C W^{-1}. Therefore, these two contributions can be considered negligible.
- *Thermal Resistance of flowing vapour (R_v):* the movement of the vapour creates an extremely low resistance, of the order of 10^{-8} °C W^{-1}, and therefore also this contribution is eliminated from the final balance.
- *Thermal Resistance of the Condenser Film ($R_{lv,c}$):* it is due to the thickness of the film of the condensate on the internal wall of the condenser. For this case too, it can be used the empirical formula written in Eq.6, substituting the value of q_e with the power provided to the condenser q_c, that in this case it was considered to be equivalent to the one at the evaporator:

$$R_{lv,c} = \frac{0.235\, q_c^{1/3}}{D_i^{4/3} g^{1/3} l_e \left(\frac{h_{lv}\lambda_l^3 \rho_l^2}{\mu_l}\right)^{1/3}} \qquad (22)$$

- *Wall conduction resistance at the condenser ($R_{cond,c}$): i*t is the same resistance exposed in Eq. 18 but considering the geometrical dimension of the condenser.
- *External convective resistance at the condenser ($R_{ext,h,c}$): i*t is the final resistance of the model, and it represents the resistance at the external side of the condenser. In this case it can be figured like a convective resistance, as follow:

$$R_{ext,h,c} = \frac{1}{h_{ext,c}\, A_{ext,c}} \qquad (23)$$

where $h_{ex,c}$ and A_c are the convective coefficient of the fluid on the external side of the condenser and the external heat exchange area of the condenser, respectively.

Finally, it is possible to write the final balance equation of the model, using Eqs. 2-8, excluding the contributes identified as negligible (i.e., $R_{cond,ax}$, $R_{pc,lv}$, $R_{pc,vl}$, R_v). The model, in its general form, can be written as follow:

$$R_{eq} = R_{ext,h,e} + R_{cond,e} + R_p + R_{lv,e} + R_{lv,c} + R_{cond,c} + R_{ext,h,c} \qquad (24)$$

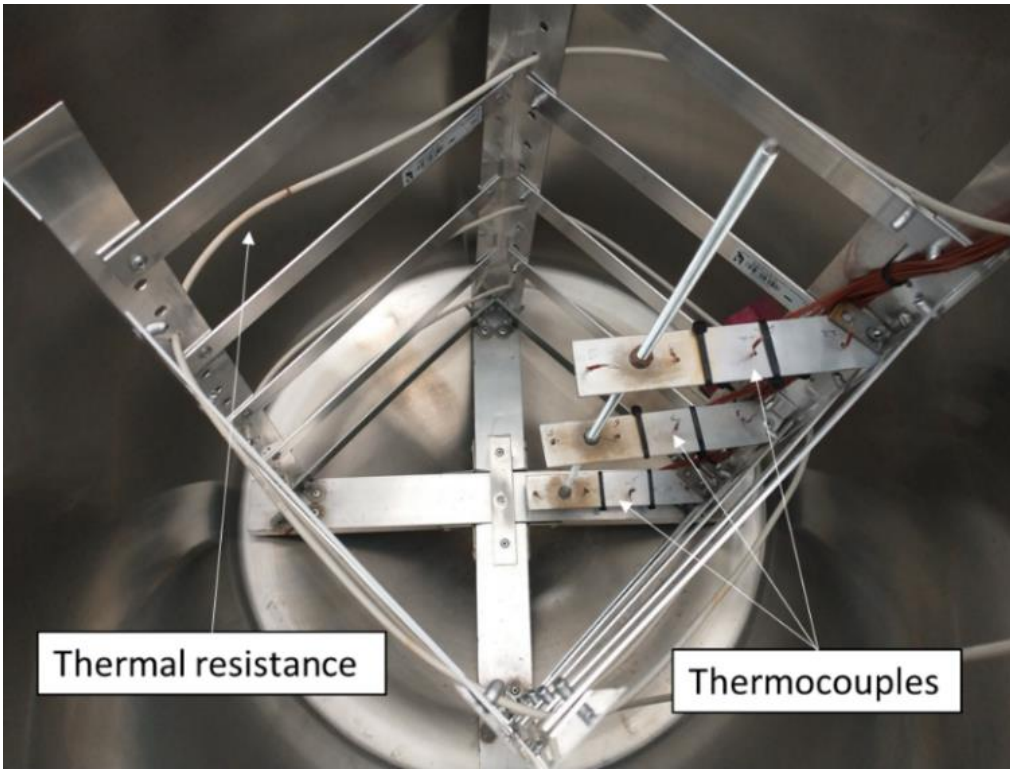

Figure 9.3*: inside picture of the fermentation tank used for simulating the fermentation for the validation of the model*

For the validation of the thermal model, the test simulating the fermenting condition performed in paragraph 7.3 was considered. The test was performed until the reaching of the steady state condition of the water inside the tank. With this experiment it was possible to obtain an experimental value of the R_{eq} for the thermosyphon heat pipe for the comparison with the one calculated with the proposed model to allow the validation of the model itself. In Figure 9.4 it is possible to observe the average temperature inside the product in steady state condition, and it is possible to observe that it is stable around 29.35°C. This temperature corresponds to the temperature of the evaporator T_e and it is possible to

substitute it inside the definition of R_{eq} (Eq. 1) together with the real temperature of the condenser T_c= 18°C and the real value of Q= 64.74 W, obtaining a value for the experimental R_{eq} of $1.75 \cdot 10^{-1}$ °C W^{-1}.

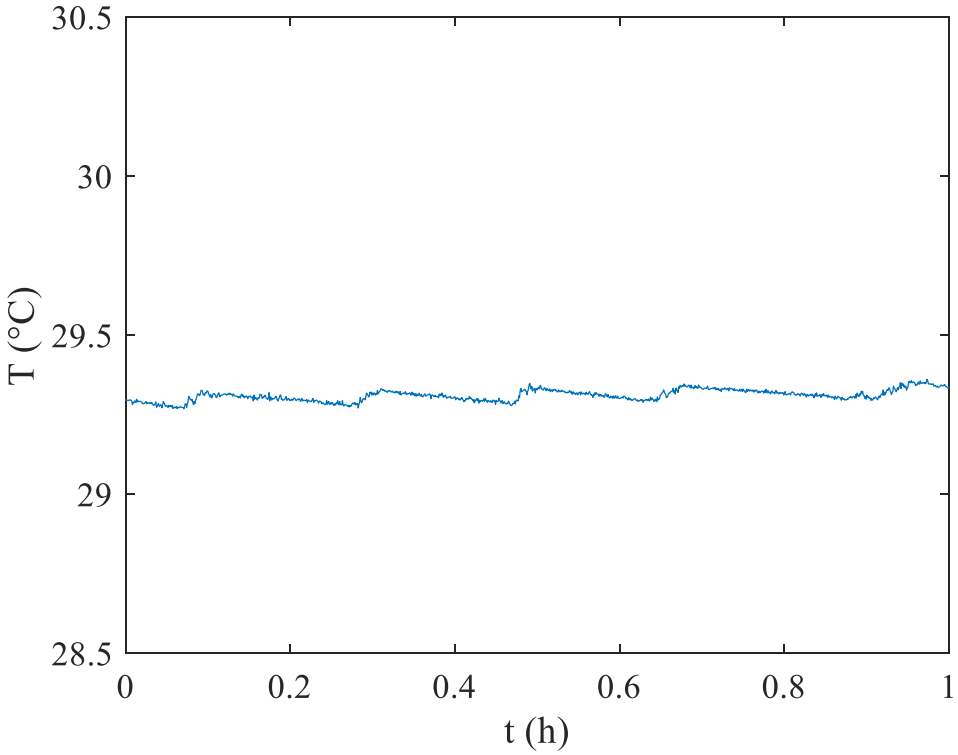

Figure 9.4*:average temperature of the product inside the fermenter tank*

By the proposed numerical model, the equivalent resistance of the thermosyphon heat pipe under investigation is calculated, starting from the computation of the values of the different thermal resistances.

– *External convective resistance at the evaporator ($R_{ext,h,e}$):* the value of the external area of the thermosyphon heat pipe evaporator is of 0.38 m^2. It is substituted to the A_e term in Eq. 17, and it was a forced

convection condition for the water outside the evaporator due to the stirring system ($h_{ext,e}$ can be assumed equal to 500 $Wm^{-2}K^{-1}$). In this way, $R_{ex,hs}$ resulted 0.053 °C W^{-1}.

- *Wall conduction resistance at the evaporator ($R_{cond,e}$) and at the condenser ($R_{cond,c}$):* substituting the geometrical values in Eq.18 and considering the thermal conductivity of the aluminium of about 210 $Wm^{-1}K^{-1}$, the parameter $R_{cond,e}$ and $R_{cond,c}$ result in the order of magnitude of 10^{-4} °C W^{-1}. For this reason, in this case, they can be considered negligible.
- *Pool boiling resistance (R_p):* in Eq. 19 it is possible to assume a value of 10^5 $Wm^{-2}K^{-1}$ for h_{int} and, substituting all the geometrical values of the thermosyphon heat pipe, it is possible to state that R_p is equal to $3.3 \cdot 10^{-2}$ °C W^{-1}.
- *Thermal Resistance of the Evaporator Film* ($R_{lv,e}$): considering h_{lv}=173.09 KJ kg^{-1}, ρ_l=1187 kg m^{-3} and λ_l= 0.079 W m^{-1} K^{-1} of the refrigerant R134a at the temperature of the evaporator, and the geometrical values of the evaporator section, it is possible to obtain a value of $R_{lv,e}$ equal to $2.4 \cdot 10^{-2}$ °C W^{-1}. In this case, to simplify the model, the surface area wetted by the pool boiling was neglected, considering the entire internal area of the evaporator as the film surface.
- *Thermal Resistance of the Condenser Film* ($R_{lv,c}$): repeating the passages used for calculating $R_{lv,e}$ but using and the geometrical values of

the condenser, it is possible to obtain a value of $R_{lv,c}$, that in this case is equal to $4.8 \cdot 10^{-2}$ °C W^{-1}.

- *Convective resistance at the condenser ($R_{ext,h,c}$):* since the condenser is kept at a constant temperature of 18°C by its cooling jacket, it is possible to state that in this case it is in temperature-imposed condition and, for this reason, its thermal resistance can be neglected.

Substituting in Eq. 24 the values obtained in the previous steps, and excluding the ones neglected during the calculation, it is possible to compute the theorical value of R_{eq}, that corresponds to $1.65 \cdot 10^{-1}$ °C W^{-1}.

This value is in accordance with the one obtained experimentally. In fact, the two values differ by 5.7 % and, for this reason, the model can be considered quite accurate for the estimation of the equivalent resistance of a thermosyphon heat pipe used in these conditions and it is possible to state that it is validated,

Considering the fermenting condition defined in par. 1.3.3: a temperature at the condenser T_c of 18°C and the net input power released by the fermentation Q_{HP} of about 64.74 W, it is possible to define the optimal equivalent resistance $R_{eq,opt}$ that a single HP should have for keeping the product at the temperature T_p of 23.5°C (and consequently the evaporator at the same temperature T_e) using the Eq.1. In this case $R_{eq,opt}$ corresponds to $8.5 \cdot 10^{-2}$ °C/W.

Observing the equations defining the thermal resistances of the HP, it is possible to state that there are several parameters that could be acted upon to change the equivalent resistance R_{eq} of the device to make it correspondent to $R_{eq,opt}$.

They mainly include the physical properties of the materials used in the construction of the device, such as the material of the pipe and the filling fluid, or the geometric characteristics of the heat pipe itself. Assuming to not change the working fluid and the material of the pipe, it appears evident that the geometrical parameters of the device are those on which to act.

For example, the adoption of an inner diameter of the pipe of 0.036 m of and an outer diameter of 0.04 m, would lower the equivalent resistance value R_{eq} to $8.4 \cdot 10^{-2}$ °C/W, making the device compatible with the intended use.

CHAPTER 10: Development of an innovative tool for estimating the heat release curve during wine fermenting processes

10.1 The estimation of heat release during oenological fermentation

As reported above, in wine fermentation processes, the temperature of the fermenting substrate is of fundamental importance as it can directly activate and regulate the microbial kinetics of the yeast responsible for the process [34] and consequently the fermentation kinetics too, [35]. Moreover, it can regulate the yeast metabolism, which determines both the production of primary and secondary molecular compounds during the process, determining the nature and the amount of volatile compounds synthesized [36] and consequently the organoleptic quality of the final product.

For these reasons, an accurate thermal control of the fermentation substrate is necessary to obtain a high-quality wine. To complicate this task is the exothermic character generally possessed by alcoholic fermentation reactions: during the fermentation phase, each mole of glucose in the grape must, releases a quantity of heat equal to approximately 106.3 kJ. This phenomenon could raise the temperature of the grape must, affecting the metabolism of the yeasts involved in fermentation or even reaching temperatures that could be lethal to them [35].

In this view, the precise knowledge of the curve of heat release during the entire time of fermentation, and therefore, also the estimation of the amount of heat that is to be removed from the grape juice during the fermenting phase for keeping an ideal temperature of the product, could be an important tool to facilitate and improve the design and the sizing of fermentation tanks and their thermal control systems in general in the oenological field.

In the literature some authors have proposed models for estimating the heat developed by alcoholic fermentation: Wiliams [30] proposed and validated a correlation between the sugar concentration of the must and the heat developed by fermentation. Colombiè [34] proposed an estimation model based on correlations and validated it with experimental data. Lòpez [37] proposed an experimentally validated mathematical model for estimating the kinetics of heat production during fermentation.

However, it is well known that a number of factors influences the extent to which the temperature of the must inside the tank rises, for example: the physico-

chemical properties of the must during alcoholic fermentation in tanks (like the glucose concentration), the initial fermentation temperature, the fermentation kinetics, the fluid-dynamics conditions inside tanks due to the mechanical actions of the ascension of CO2 bubbles produced during the process and the possible temperature gradients (especially in red wine making processes), [34]. All these factors could contribute to the heterogeneity and extreme variability of the fermentation processes, making the amount and the curve of heat release during fermentation closely linked to the specific fermentation conditions. For this reason, it is usually quite difficult to estimate in advance the amount of heat produced and the one to be removed during this stage of production and, specific models, due to their too restricted conditions of validation, could not be perfectly suited to any specific alcoholic fermentation circumstances that can be adopted by different wine producers in their cellars.

To fill this gap, in this chapter an estimation algorithm for determining the heat release curve vs time during fermentation in wine make processes is developed and validated. The estimation procedure of the power generated adopted in this work is based on the solution of the inverse problem, by adopting directly the experimental grape must temperature distribution as input data.

10.2 Experimental setup and estimating model

For the validation of the estimating model, a fermentation inside a small fermenter tank in AISI 316L with an internal volume of 100 l (detailed description in chapter 2) was considered. The heat generation during fermentation was

simulated using 2 immersion thermoelectric resistances: one of 40 W and the other one of 100 W. In this way it was possible to reproduce a change in input power generation during the tests, simulating the change in the microbial kinetics that usually occurs during an alcoholic fermentation. To simplify the model, water was used as substitute of the fermenting substrate as grape must is principally composed of it. The wire thermoelectric resistances were spirally disposed inside the tank using the mechanical support structure described in chapter 2, in order to have the most possible uniform heat generation inside the tank.

Considering that the concentration of glucose in a grape must for vinification can reach 1.7 mol/l and, considering that each mole of glucose fermented by the yeast can release heat up to about 106.3 kJ, it is possible to state that in the first two days of fermentation, i.e. those where the metabolic activities of the yeast are at the maximum level, 1 W/l is released in the grape must.

However, over the course of a week-long fermentation, it is possible to say that this value of power released per litre of grape must represents the maximum peak attainable by the process, since the metabolic kinetics of the yeast are not constant throughout the fermentation time, and are mainly concentrated in its first few days: most of the heat is released in 48-72 hours (~80-90%), while the rest of the fermentation time the power generated is approximately 20-40% of the initial peak, [2], [37].

In view of this, a variable input power in the product was considered: 2 values were selected for the initial heat peak and for each, 2 duration times. In specific,

the power inputs of the peak were: the theoretical one of 100 W and 140 W (+40%), while the time durations of every peak were: 1 h and 2 h. The input power for the remaining time of the fermentation was kept at about 40W. The total time of every single simulation of fermentation was of 3.5 h, excluding the initial period when the input power was not present.

During the validation tests, the temperature of the product inside the tank was acquired in the same modality as in chapter 2.

The aim of the work was to estimate the power input power inside the product, starting from the experimental temperatures measured during the tests. The description of the estimation procedure starts with the modelling of the direct heat-transfer problem, proceeds by applying the Tikhonov regularisation method and concludes with the estimation of the power input over the time of fermentation. The energy balance equation of the system can be written as follow:

$$\dot{Q}_f(\tau) = m\, c_p \frac{dT}{d\tau} + hA(T(\tau) - T_e(\tau)), \qquad (25)$$

$$T(\tau = 0) = T_i$$

where $\dot{Q}_f$ [W] is the power input generated inside the product, T [°C] is the average temperature of the product, measured by the 12 thermocouples, T_e [°C] is the environment temperature, τ [s] is the time, term h [W m^{-2} °C^{-1}] is the convective heat transfer on the external side of the tank, A is the external surface of the tank. Regarding the variables m (mass) and c_p (specific heat) they are referred to the system composed by the union of the tank and of the water inside it.

If for the direct problem of this situation, the value of $\dot{Q}_f$ is known (cause) while the value of dT(effect) is unknown, for the inverse problem the condition is the exact opposite: dT (effect) is experimentally measured while $\dot{Q}_f$ (cause) is unknown.

In view of this, the equation of the energy balance of the system could be rewritten as follow:

$$\dot{Q}_f(\tau) - hA(T(\tau) - T_e(\tau)) = m\, c_p \frac{dT}{d\tau} = \dot{Q}_{acc} \qquad (26)$$

introducing the term $\dot{Q}_{acc}$ [W] that corresponds to the net heat input power accumulated by the product inside the tank during the test.

In this case, $\dot{Q}_{acc}$ represent the terms that is estimated and, for this reason, as suggested by Beck et al. [38] and Dennis et al [39], because the inverse problem is linear with respect to it, the problem can be written in the discrete domain as follows:

$$T = \dot{Q}_{acc}\, X + T_{\dot{Q}_{acc}=0}, \qquad (27)$$

where X is the sensitivity matrix and $T_{\dot{Q}_{acc}=0}$ is a constant term that correspond to the average temperature of the product in case of null $\dot{Q}_{acc}$.

The sensitivity matrix X of N x N dimension and the vector $T_{\dot{Q}_{acc}=0}$ of dimension N, with N that is the total number of acquisitions, can be numerically written as follow:

$$X = \begin{bmatrix} \frac{\Delta\tau}{m\,c_p} & 0 & 0 & \dots & 0 \\ \frac{\Delta\tau}{m\,c_p} & \frac{\Delta\tau}{m\,c_p} & 0 & \dots & 0 \\ \vdots & \vdots & \vdots & & 0 \\ \frac{\Delta\tau}{m\,c_p} & \frac{\Delta\tau}{m\,c_p} & \frac{\Delta\tau}{m\,c_p} & \dots & \frac{\Delta\tau}{m\,c_p} \end{bmatrix} \quad (28)$$

$$T_{\dot{Q}_{acc}=0} = \begin{bmatrix} T_i \\ T_i \\ \vdots \\ T_i \end{bmatrix} \quad (29)$$

In the inverse formulation, the computed temperature distribution T is forced to match the experimental temperature distribution Y, by tuning the value of $\dot{Q}_{acc}$. The matching of the two temperature distributions (the computed and the experimentally one) could be easily performed under a least square approach. However, the ill-posed nature of the problem, makes the least square solution dominated by noise, and for this reason the Tikhonov regularization method is adopted; this approach has been successfully used in the inverse heat-transfer literature [40] making possible to reformulate the original problem as a well-posed problem that consists of minimizing the following objective function:

$$J(\dot{Q}_{acc}) = \left\| Y - \dot{Q}_{acc}\,X - T_{\dot{Q}_{acc}=0} \right\|_2^2 + \lambda^2 \left\| L\,\dot{Q}_{acc} \right\|_2^2, \quad \dot{Q}_f > 0, \quad (30)$$

where $\|\cdot\|_2^2$ stands for the square of the 2-norm, λ is the regularization parameter, L is the derivative operator and T is the average temperature of the product measured by imposing a given $\dot{Q}_{acc}$. Finally, since the choice of a proper regularisation parameter requires a good balance between the size of the residual

norm and the size of the solution norm (semi norm), the L-curve method proposed by Hansen and O'Leary [41] was used.

Finally, for improving the estimation model, it was calculated also the amount of heat released by convection from the fermenter to the environment using the value of hA parameter reported in chapter 2 and, tarting from the estimated value $\dot{Q}_{acc}$, it was possible to calculate the value of the power generated by the fermentation $\dot{Q}_f(\tau)$, as follow:

$$\dot{Q}_f(\tau) = hA(T(\tau) - T_e(\tau)) + \dot{Q}_{acc} \quad (31)$$

10.3 Results

To validate the estimation model, the non-constant yeast kinetic of fermentation was reproduced simulating 4 different fermenting conditions. Observing the comparison of the real input power curve and the estimated one in function of the time for the two tests carried out with peak input power of 100 W (Figure 10.1a and Figure 10.1b), it is possible to state that the estimation model is able to satisfactorily reconstruct the trend of the curve of the input power supplied to the product during the simulation of the fermentation process. It can be observed that the course and slopes of the curve are satisfactorily reproduced both at the beginning and at the end of the process. To better describe the behaviour of the estimation curve, the mean percentage error of the estimation $\overline{Err_Q}$ is considered and it is calculated as follow,

$$\overline{Err_Q} = \frac{\sum_{i=1}^{n} \frac{Q_{real,i} - Q_{estimated,i}}{Q_{real,i}}}{n} \%, \quad (32)$$

with *n* that is the total number of acquisitions. From the analysis of this parameter, for the tests with peak input power of 100 W, it is possible to confirms what stated above. In specific it is possible to note that the highest value for $\overline{Err_Q}$, of about 18.06 % (Table 10.1), is reached when the peak input power duration time was of 2 h, while for the test with peak input power duration time of 1 h the value of $\overline{Err_Q}$ reached 9.19 %. These values confirm another time that the model is able to reproduce the behaviour of the curve of power generated during the fermentation. Moreover, analysing and matching these values with Figure 10.1, it is possible to notice that the major discrepancy between the curves of the estimated input power and the experimental ones occurs at the moments of power switching for each test and it is possible to affirm the error calculated at these moments contributes to increase the value of $\overline{Err_Q}$ for every test.

However, if we consider a real fermentation process, the heat power generated inside the grape must generally does not change so sharply, so the need to estimate power input in such a sharp change in input power could be considered not necessary for the application of this model and the error of estimation in that phase could be considered negligible. In this case, the estimation error $\overline{Err_Q}$ would be further reduced, strengthening the validation of the model.

These validation conditions were chosen as they represent the most challenging ones for the estimation system. Nevertheless, the model proved to be able to

estimate the power generated during fermentation with good accuracy in the test with an input peak power of 100 W.

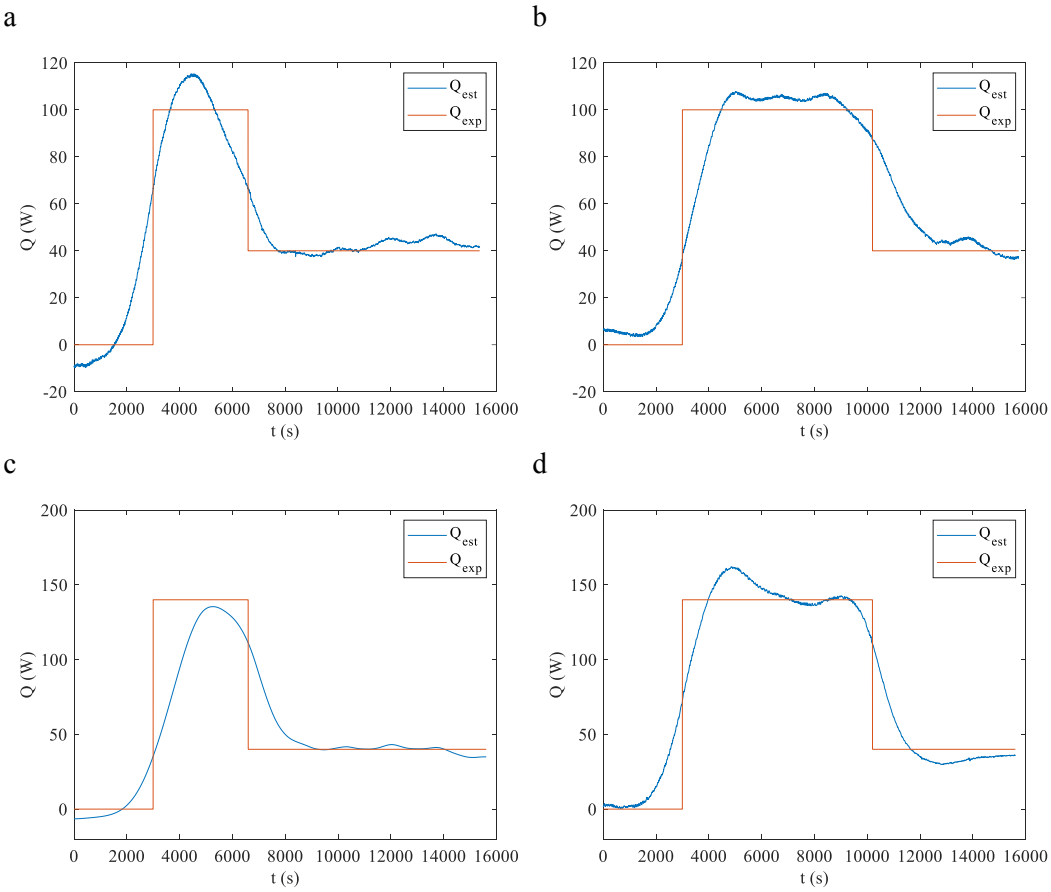

Figure 10.1: *comparison between the real input power and the estimated one for the case: a) 100 W-1 h; b) 100 W-2 h; c) 140 W-h; d) 140 W-2 h.*

Observing the comparison of the real input power curve and the estimated one in function of the time also for the tests with the peak input power of 140 W in Figure 10.1c and Figure 10.1d, it is possible to state that the model was able to estimate quite accurately the trend of the power input curve inside the product during the fermentation simulation although it seems that an increased difference between the peak and the rest of the input power during the test, quite increased

the error in estimation. In specific, the highest value of $\overline{Err_Q}$ was of 19.95 % (Table 10.1: $\overline{Err_Q}$ of every test.) and it was reached in the test with the duration time of the peak input power of 1 h, while for the tests with the duration of the peaks input power of 2 h, it was 15.34 %.

Peak input power	**100 W**		**140 W**	
Duration time of the peak input power	**1 h**	**2 h**	**1 h**	**2h**
$\overline{Err_Q}$	9.82 %	18.06 %	19.95 %	15.34 %

***Table 10.1**: $\overline{Err_Q}$ of every test.*

However, also in these cases, it is possible to state what observed for the other two tests: the major discrepancy between the estimated and real input power curves occurs at the moments of the input power switches and, in those moments, it could be considered negligible reducing the average error of estimation. To confirm the goodness of the model developed, in **Figure 10.2**: comparison between the average experimental temperature of the product inside the tank and the estimated temperature obtained by solving the direct problem using the estimated input power for the case: a) 100 W – 1 h; b) 100 W – 2 h; c) 140 W – 1 h; d)Figure 10.2, it is possible to observe the comparison between the average experimental temperature of the product inside the tank, measured during the tests, and the simulated temperature obtained by solving the direct problem using the power estimated by the model itself. It is possible to observe that the simulated temperature perfectly reproduces the real one. Indeed, the maximum percentage error of the estimation, calculated as follow:

$$Err_T = \frac{T_{real,i} - T_{estimated,i}}{T_{real,i}} \% \quad (33)$$

reached 1.15 % in the case with a peak power input of 140 W and duration of 1 h.

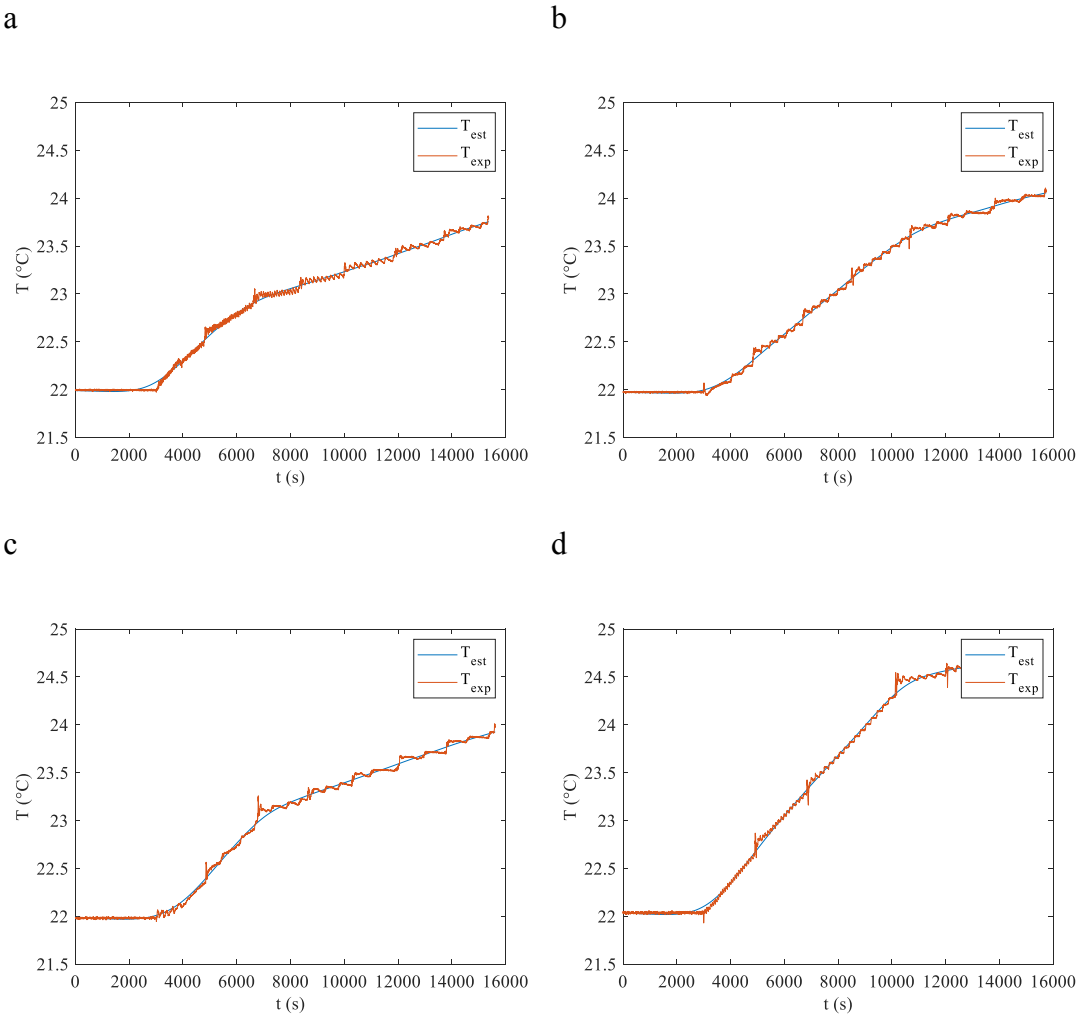

***Figure 10.2**: comparison between the average experimental temperature of the product inside the tank and the estimated temperature obtained by solving the direct problem using the estimated input power for the case: a) 100 W – 1 h; b) 100 W – 2 h; c) 140 W – 1 h; d)*

CHAPTER 11: Conclusions

The presented research represents the feasibility analysis for the implementation of a new control system of the grape must temperature during the fermentation process in wine making industries. The proposed system is based on heat pipe technology, and its applicability to the wine making industry was studied, prior by using an ideal thermosyphon heat pipe and then using a real one. The control of fermentation temperature in the wine-making process is of fundamental importance and quite tricky since the reactions that occur during this phase are exothermic and they are strongly influenced by the temperature in terms of efficiency and organoleptic quality of the final products obtained.

First, to investigate the applicability of this kind of device to control the temperature of the grape must during the fermentation stage, an ideal thermosyphon heat pipe was considered to achieve the best possible thermal performance and to substantiate the practicability of the project. Moreover, an ad hoc fermenter vessel was devised and built to allow the comparison of the performance of the

conventional cooling system (cooling jacket) for the fermentation process with the new temperature monitoring apparatus based on the ITHP. It showed that, in terms of temperature uniformity, it could improve the performance compared to the refrigeration shell, especially in mixing conditions. Moreover, it was observed that the new device produced a lower oscillation of the product temperature during the entire fermentation.

Then, a real thermosyphon heat pipe (HP) was designed and realised. It was made in aluminium and filled with refrigerant R134a. Its thermal performances were characterized in terms of equivalent thermal resistance as a function of the input power to the evaporator (10W- 100W) for four different filling ratios (FR: 20, 30, 52, and 70%). It was observed that the best performances were obtained for FR = 20% and FR=30% with a R_{eq} of about 0.17 °C/W and, additionally, it was tested simulating inside a small-scale fermenter tank, observing that it was thermally undersized. For this reason, two strategies were implemented to achieve the correct thermal sizing of the device.

In the first solution a specific test procedure was proposed whereby it was possible to estimate the number of devices needed to guarantee the optimal thermal range for fermentation (22-25°C). In particular, in the considered fermenting conditions, three THPs are needed.

In the second solution, a model for calculating the thermal behaviour of an HP applied to a fermenter tank for wine production was developed. The model proposed was based on a network of resistances that describes the operation of

the device. The model was validated by means of an experimental test that involved the HP installed in the small-scale fermenter reproducing the fermenting process conditions. During the experiment, it was possible to calculate the experimental thermal equivalent resistance and successively it was compared to the one obtained with the theoretical model. The two values differ by only the 5.7%, confirming the validation of the model and its suitability for the thermal sizing of these kind of devices in these specific conditions.

Concluding, this work proved that this kind of device could represent an interesting alternative to traditional cooling systems, guaranteeing better or similar performances. It could represent a noteworthy upgrading in the temperature monitoring systems for the winery sector, since its implementation as an alternative to the refrigeration shell can diminish costs for the fermentation and for whole wine production and improve the homogeneousness of temperature of the product, permitting to attain higher quality products.

Moreover, a model for estimating the heat release curve during winemaking fermentation process has been developed and validated. For testing the model under realistic fermenting condition, a simulation of the non-constant kinetics of the yeast involved was performed. In specific, the model was validated simulating 4 different alcoholic fermentation situations in a fermenter tank of 100 l. Since the heat release is concentrated at the beginning of the fermentation process, a peak input power in the product was considered at the initial part of any tests: 2 values were selected for the initial peak of heat input power (100 W and

140 W) and for each, 2 duration times (1 h and 2 h). The results shown that the model satisfactorily reproduces the general trend of the power generated inside the product, both for tests with an initial peak of 100 W and those with an initial peak of 140 W. This result is also confirmed by the $\overline{Err_Q}$ values even if the model loses its efficiency and accuracy in the proximity of sudden changes in generated power. However, such a sharp change of the input power is uncommon during fermentation because the changes in microbial kinetics and heat generation are usually gradual and, for this reason, this type of error could be considered negligible in this kind of estimation.

Finally, the good performances of the model are confirmed also by the comparison between the average experimental temperature of the product inside the tank and the simulated one obtained by solving the direct problem with the estimated input power. For the temperature comparison a maximum percentage error Err_T of 1.15 % is reached. In view of the results achieved, it is possible to consider the model validated. A future step for this work will be to apply the model to a real case of alcoholic fermentation in order to refine it and make it a complete tool at the service of wine producers.

References

[1] Alfonso V. Carrascosa, Rosario Munoz, and Ramon Gonzales, *Molecular wine microbiology*. 2011.

[2] P. Ribéreau-Gayon, D. Dubourdieu, B. Donèche, and A. Lonvaud, *Handbook of Enology: Volume 1, The Microbiology of Wine and Vinifications*, vol. 1. 2006.

[3] G. Beltran, B. Esteve-Zarzoso, N. Rozès, A. Mas, and J. M. Guillamón, "Influence of the timing of nitrogen additions during synthetic grape must fermentations on fermentation kinetics and nitrogen consumption," *J. Agric. Food Chem.*, vol. 53, no. 4, pp. 996–1002, 2005, doi: 10.1021/jf0487001.

[4] F. M. Carrau, K. Medina, L. Farina, E. Boido, P. A. Henschke, and E. Dellacassa, "Production of fermentation aroma compounds by Saccharomyces cerevisiae wine yeasts: Effects of yeast assimilable nitrogen on two model strains," *FEMS Yeast Res.*, vol. 8, no. 7, pp. 1196–1207, 2008, doi: 10.1111/j.1567-1364.2008.00412.x.

[5] E. Jiménez-Martí, A. Aranda, A. Mendes-Ferreira, A. Mendes-Faia, and M. L. del Olmo, "The nature of the nitrogen source added to nitrogen depleted vinifications conducted by a Saccharomyces cerevisiae strain in synthetic must affects gene expression and the levels of several volatile compounds," *Antonie van Leeuwenhoek, Int. J. Gen. Mol. Microbiol.*,

vol. 92, no. 1, pp. 61–75, 2007, doi: 10.1007/s10482-006-9135-1.

[6] A. Mendes-Ferreira, C. Barbosa, V. Falco, C. Leão, and A. Mendes-Faia, "The production of hydrogen sulphide and other aroma compounds by wine strains of Saccharomyces cerevisiae in synthetic media with different nitrogen concentrations," *J. Ind. Microbiol. Biotechnol.*, vol. 36, no. 4, pp. 571–583, 2009, doi: 10.1007/s10295-009-0527-x.

[7] M. J. Torija *et al.*, "Effects of fermentation temperature and Saccharomyces species on the cell fatty acid composition and presence of volatile compounds in wine," *Int. J. Food Microbiol.*, vol. 85, no. 1–2, pp. 127–136, 2003, doi: 10.1016/S0168-1605(02)00506-8.

[8] M. Vilanova, M. Ugliano, C. Varela, T. Siebert, I. S. Pretorius, and P. A. Henschke, "Assimilable nitrogen utilisation and production of volatile and non-volatile compounds in chemically defined medium by Saccharomyces cerevisiae wine yeasts," *Appl. Microbiol. Biotechnol.*, vol. 77, no. 1, pp. 145–157, 2007, doi: 10.1007/s00253-007-1145-z.

[9] F. F. Bauer and I. S. Pretorius, "Yeast Stress Response and Fermentation Efficiency: How to Survive the Making of Wine - A Review," *South African J. Enol. Vitic.*, vol. 21, no. 1, pp. 27–51, 2019, doi: 10.21548/21-1-3557.

[10] G. H. Fleet, "Yeast interactions and wine flavour," *Int. J. Food Microbiol.*, vol. 86, no. 1–2, pp. 11–22, 2003, doi: 10.1016/S0168-1605(03)00245-9.

[11] C. Delfini and J. V Formica, “Wine microbiology: science and technology,” *Choice Rev. Online*, vol. 39, no. 04, pp. 39-2180-39–2180, 2001, doi: 10.5860/choice.39-2180.

[12] R. Jowitt, “Fermentation and biochemical engineering handbook — Principles, process design and equipmentEdited by Henry C. Vogel. Noyes Publications, New Jersey. 1983. 440 pp. + xv. Price: US$64,” *J. Food Eng.*, vol. 3, no. 2, pp. 162–163, 1984, [Online]. Available: http://linkinghub.elsevier.com/retrieve/pii/0260877484900372.

[13] L. Wang, “Energy efficiency technologies for sustainable food processing,” *Energy Effic.*, vol. 7, no. 5, pp. 791–810, 2014, doi: 10.1007/s12053-014-9256-8.

[14] S. Rainieri, F. Bozzoli, L. Cattani, and G. Pagliarini, “Experimental investigation on the convective heat transfer enhancement for highly viscous fluids in helical coiled corrugated tubes,” *J. Phys. Conf. Ser.*, vol. 395, no. 1, 2012, doi: 10.1088/1742-6596/395/1/012032.

[15] F. Bozzoli, L. Cattani, S. Rainieri, and G. Pagliarini, “Estimation of local heat transfer coefficient in coiled tubes under inverse heat conduction problem approach,” *Exp. Therm. Fluid Sci.*, vol. 59, pp. 246–251, 2014, doi: 10.1016/j.expthermflusci.2013.11.024.

[16] M. Rinaldi, M. Malavasi, M. Cordioli, and D. Barbanti, “Investigation of influence of container geometry and starch concentration on thermal treated in-package food models by means of Computational Fluid

Dynamics (CFD)," *Food Bioprod. Process.*, vol. 108, pp. 1–11, 2018, doi: 10.1016/j.fbp.2017.12.003.

[17] Da-Wen Sun, *Thermal Food Processing New Technologies and Quality Issues*. .

[18] G. Huminic, A. Huminic, I. Morjan, and F. Dumitrache, "Experimental study of the thermal performance of thermosyphon heat pipe using iron oxide nanoparticles," *Int. J. Heat Mass Transf.*, vol. 54, no. 1–3, pp. 656–661, 2011, doi: 10.1016/j.ijheatmasstransfer.2010.09.005.

[19] M. B. H. Mantelli, *Thermosyphons and Heat Pipes: Theory and Applications*. 2021.

[20] S. W. Chi, "Heat pipe theory and practice: a sourcebook," *Series in thermal and fluids engineering*. p. 242, 1976.

[21] A. Franco and S. Filippeschi, "Experimental analysis of Closed Loop Two Phase Thermosyphon (CLTPT) for energy systems," *Exp. Therm. Fluid Sci.*, vol. 51, pp. 302–311, 2013, doi: 10.1016/j.expthermflusci.2013.08.013.

[22] E. Sadeghinezhad, A. R. Akhiani, H. S. C. Metselaar, S. Tahan Latibari, M. Mehrali, and M. Mehrali, "Parametric study on the thermal performance enhancement of a thermosyphon heat pipe using covalent functionalized graphene nanofluids," *Appl. Therm. Eng.*, vol. 175, no. April, p. 115385, 2020, doi: 10.1016/j.applthermaleng.2020.115385.

[23] D. Jafari, A. Franco, S. Filippeschi, and P. Di Marco, "Two-phase closed

thermosyphons: A review of studies and solar applications," *Renew. Sustain. Energy Rev.*, vol. 53, pp. 575–593, 2016, doi: 10.1016/j.rser.2015.09.002.

[24] A. Bahmanabadi, M. Faegh, and M. B. Shafii, "Experimental examination of utilizing novel radially grooved surfaces in the evaporator of a thermosyphon heat pipe," *Appl. Therm. Eng.*, vol. 169, no. May 2019, p. 114975, 2020, doi: 10.1016/j.applthermaleng.2020.114975.

[25] W. Srimuang and P. Amatachaya, "A review of the applications of heat pipe heat exchangers for heat recovery," *Renew. Sustain. Energy Rev.*, vol. 16, no. 6, pp. 4303–4315, 2012, doi: 10.1016/j.rser.2012.03.030.

[26] H. Jouhara, T. Nannou, H. Ghazal, R. Kayyali, S. A. Tassou, and S. Lester, "Temperature and energy performance of open refrigerated display cabinets using heat pipe shelves," *Energy Procedia*, vol. 123, pp. 273–280, 2017, doi: 10.1016/j.egypro.2017.07.240.

[27] N. Panyoyai, P. Pathike, T. Wongsiriamnuey, T. Khamdeang, and Y. Tanongkankit, "Drying Characteristics of Paddy Dried by Thermosyphon Heat Pipe Heat Exchanger," *J. Sci. Technol. MSU*, vol. 35, no. 6, pp. 658–664, 2016, [Online]. Available: http://content.ebscohost.com/ContentServer.asp?T=P&P=AN&K=121258374&S=R&D=asn&EbscoContent=dGJyMNHX8kSeprc40dvuOLCmr0%2Bep7VSsKu4S6%2BWxWXS&ContentCustomer=dGJyMPGut1C3rLZNuePfgeyx44Hy7fEA.

[28] L. Ketteringham and S. James, “Use of high thermal conductivity inserts to improve the cooling of cooked foods,” *J. Food Eng.*, vol. 45, no. 1, pp. 49–53, 2000, doi: 10.1016/S0260-8774(00)00043-1.

[29] C. James, M. Araujo, A. Carvalho, and S. J. James, “The heat pipe and its potential for enhancing the cooking and cooling of meat joints,” *Int. J. Food Sci. Technol.*, vol. 40, no. 4, pp. 419–423, 2005, doi: 10.1111/j.1365-2621.2004.00943.x.

[30] L. A. Williams, “Heatrelease in alcoholic fermentation: A critical reappraisal.,” *Am. J. Enol. Vitic.*, vol. 33, no. 3, pp. 149–153, 1982.

[31] E. Kampa, T. Dworak, C. Laaser, and R. Vidaurre, “European regulations,” *Green Sustain. Pharm.*, no. 1935, pp. 253–277, 2010, doi: 10.1007/978-3-642-05199-9_17.

[32] D. Reay, P. Kew, and R. McGlen, *Heat Pipes. Theory, Design and Applications*. 2014.

[33] G. Rogers and Y. Mayhew, *Engineering thermodynamics work and heat transfer.*, vol. 7, no. 2. 2014.

[34] S. Colombié, S. Malherbe, and J. M. Sablayrolles, “Modeling of heat transfer in tanks during wine-making fermentation,” *Food Control*, vol. 18, no. 8, pp. 953–960, 2007, doi: 10.1016/j.foodcont.2006.05.016.

[35] A. M. Molina, J. H. Swiegers, C. Varela, I. S. Pretorius, and E. Agosin, “Influence of wine fermentation temperature on the synthesis of yeast-derived volatile aroma compounds,” *Appl. Microbiol. Biotechnol.*, vol.

77, no. 3, pp. 675–687, 2007, doi: 10.1007/s00253-007-1194-3.

[36] M. J. Torija, N. Rozès, M. Poblet, J. M. Guillamón, and A. Mas, “Effects of fermentation temperature on the strain population of Saccharomyces cerevisiae,” *Int. J. Food Microbiol.*, vol. 80, no. 1, pp. 47–53, 2003, doi: 10.1016/S0168-1605(02)00144-7.

[37] A. López and P. Secanell, “A simple mathematical empirical model for estimating the rate of heat generation during fermentation in white-wine making,” *Int. J. Refrig.*, vol. 15, no. 5, pp. 276–280, 1992, doi: 10.1016/0140-7007(92)90042-S.

[38] J. Beck, “Beck, J.,” *Inverse Heat Conduction Ill-posed problems*. pp. 137-157,179-180,198-211, 2011.

[39] B. H. Dennis and G. S. Dulikravich, “Simultaneous determination of temperatures, heat fluxes, deformations, and tractions on inaccessible boundaries,” *J. Heat Transfer*, vol. 121, no. 3, pp. 537–545, 1999, doi: 10.1115/1.2826014.

[40] F. Bozzoli, L. Cattani, S. Rainieri, F. S. Viloche Bazán, and L. S. Borges, “Estimation of the local heat-transfer coefficient in the laminar flow regime in coiled tubes by the Tikhonov regularisation method,” *Int. J. Heat Mass Transf.*, vol. 72, pp. 352–361, 2014, doi: 10.1016/j.ijheatmasstransfer.2014.01.019.

[41] D. O. P.C. Hansen, “The use of the L-curve in the regularization of discrete ill-posed problems,” vol. 14, no. 6, pp. 1487–1503, 1993.

PART III: CORRUGATED PIPES FOR FOOD INDUSTRY

List of figures

***Figure 12.1**: Scraped surface heat exchanger* *202*

***Figure 12.2**: twisted tape [5]* *204*

***Figure 12.3**: coiled pipe [5]* *205*

***Figure 12.4**: geometrical parameter of corrugation* *207*

***Figure 13.1**: Corrugated pipe tested: a) H32, b) H16, c) T32 and d) T16* *215*

***Figure 13.2**: schematic representation of the setup for average analysis* *216*

***Figure 13.3**: setup for the estimation of the local heat transfer with IR camera* *220*

***Figure 13.4**: schematic representation of the two references placed at the extremities of the pipe with the division of the areas of interest for every picture acquired* *221*

***Figure 13.5**: example of six IR raw pictures, obtained around the pipe, before the unwrapping and merging operations.* *222*

***Figure 13.6**: for every IR raw image (A, B, C, D, E and F) example of: 1) wrapped pictures with the illustration of the cutting borders for obtaining the 2) central portions with which executing the following merging operation.* *224*

***Figure 13.7**: example of a reconstructed external surface after merging operation.* *225*

***Figure 13.8**: a) Geometrical domain with coordinate system; b) a portion of the test section 226*

***Figure 14.1**: Nu as function of Re 231*

***Figure 14.2**: Nuz as function of dimensionless abscissa $z*$ for the cases a) Re=4000, b) Re=10000 and c) Re= 16000. ..... 233*

***Figure 14.3**: friction factor f and efficiency η as function of Re 236*

***Figure 14.4:** schematic position of corrugations and flow direction in the tested pipes a) H32 b) H16 c) T32 and d) T16 ..... 237*

***Figure 14.5**:not filtered temperature distribution at Re=4000 for a) H32 b) H16 c) T32 d) T16 ..... 238*

***Figure 14.6**: filtered temperature distributions at Re=4000 for a) H32 b) H16 c) T32 d) T16 ..... 239*

***Figure 14.7**: Restored internal convective h heat transfer distribution at Re= 4000 for a) H32 b) H16 c) T32 d) T16 ..... 242*

***Figure 14.8:** Restored internal convective h heat transfer distribution at Re= 10000 for a) H32 b) H16 c) T32 d) T16 ..... 243*

***Figure 14.9**: Restored internal convective h heat transfer distribution at Re= 16000 for a) H32 b) H16 c) T32 d) T16 ..... 244*

***Figure 14.10:** Local Nu at $\alpha=\pi$ as function of z at Re=4000 for a) H32 b) H16 c) T32 d) T16 ..... 247*

***Figure 14.11**:Local Nu at $\alpha=\pi$ as function of z at Re=10000 for a) H32 b) H16 c) T32 d) T16 ..... 248*

***Figure 14.12**: Local Nu at α=π as function of z at Re=16000 for a) H32 b) H16 c) T32 d) T16 ..... 249*

CHAPTER 12: Wall corrugation in pipes for food heat exchanger

12.1 Heat transfer enhancement

As mentioned in the introduction, in food industry the most of heat treatments involves fluid food matrix, for this reason improving convection is a well-established research topic in this sector, and the ever-increasing cost of energy and raw materials is generating a great deal of interest in this regard.

In heat exchangers for the food industry, the increase in heat exchange can be achieved through different techniques. These techniques can be classified according to whether an external energy supply is required or not.

When the technique requires an external energy input to increase the heat transfer in the heat exchanger, the technique is called 'active'. Otherwise, it is referred to as 'passive'.

Among the active techniques, the most widely used can be listed as follow:

- Use of mechanical aids: in this category they are included all devices in which the application of a mechanical action produces an improvement in heat transfer. The most adopted solutions in the food industry are scraped surfaces heat exchanger. Scraped surfaces (Figure 12.1) consist of a pipe in which there is a rotor equipped with a series of blades that 'scrape' the fluid from the wall, ensuring that the boundary layer is broken, and the fluid is remixed, thus improving heat transfer. This strategy is commonly used when high viscous food fluids are treated, and heat transfer rate is limited by very low *Re* number.

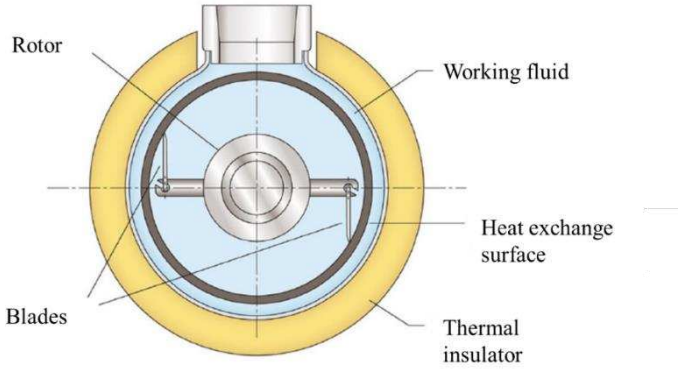

***Figure 12.1**: Scraped surface heat exchanger*

- Application of vibrations. Vibration phenomena induce an unsteady motion of the fluid that enhances heat transfer [1]. Usually, vibrations are supplied to the boundary surface or to the fluid itself

and they are produced by means of a mechanical actuator on the duct walls or directly to the fluid, respectively.

- Electrostatic fields: an electric field characterised by a high potential difference and a low current is applied to the fluid. One of the objectives of this approach is to convert electrical energy into kinetic energy. Several studies have reported high effectiveness of this type of technique [2].

Among the passive technique, it is possible to list:

- Treated surfaces: usually, with this technique, a micro-scale modification is applied on the surface finishing or coating of the heat exchange areas. This type of surface finish, or coating, can be continuous or discontinuous, and are mainly used for promoting boiling or condensation phenomena [3].
- Extended surfaces: classical example of this technique is the use of finned surfaces. Finns enhance the heat transfer as they increase the exchange surface area and disturb the fluid flow [3].
- Vortex generation: this technique is aimed to produce a secondary recirculation of the axial flow within the duct. Several devices can be used for this purpose and twisted tape are the most common ones. They (Figure 12.2) are metal strips that are twisted back on themselves; these devices are produced in many different shapes

and sizes and are used inside heat exchangers to improve heat transfer without excessively increasing pressure drops [4].

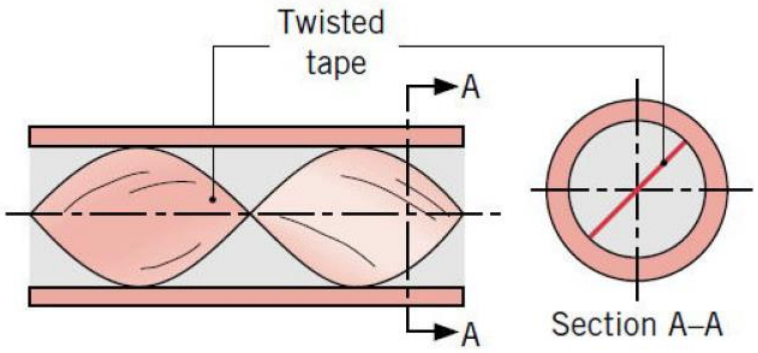

***Figure 12.2**: twisted tape* [5]

- Corrugated surfaces: corrugated surfaces are one of the most widely used heat transfer enhancement methods, especially inside pipes and ducts. The heat transfer enhancement mechanism consists of breaking the fluid-dynamic and thermal boundary layer by generating vortices and turbulence that produce an increase in thermal performance [6].
- Curved pipes (Figure 12.3): usually their geometrical 'spiral' shape allow the generation of secondary flows that generate an increase in the heat exchanged [5].

Certainly, passive strategies are very attractive as their functioning aimed to an increase in the thermal efficiency of the device in which they are installed, does not require any external energy input. Furthermore, the main strategies

listed above are relatively simple to design and realise, inexpensive and easy to implement in devices already manufactured or in use by users. However, relying mainly on modifications to the geometries or internal surfaces of heat exchanger components, such as pipes, they can represent a handicap from a fluid-dynamic point of view. In fact, the expedients used for increasing the exchange surface area, or for increasing the turbulence of the fluids flowing in contact with these surfaces, represent obstacles for the fluids themselves in terms of friction and pressure drops, which, in some cases, cannot be neglected forcing the user to use more energy to flow the treated fluids. Such modifications, moreover, if carried out in fields where drainability and/or cleanability and/or sterilizability are required, such as in the food, pharmaceutical or biotechnological sector, may represent a divergence from the main hygienic design criteria adopted. Among the listed strategies, the one that best overcomes these problems is the corrugated walls. In fact, this strategy can be realised by limiting the pressure drops generated and guaranteeing the hygienic characteristics of the device.

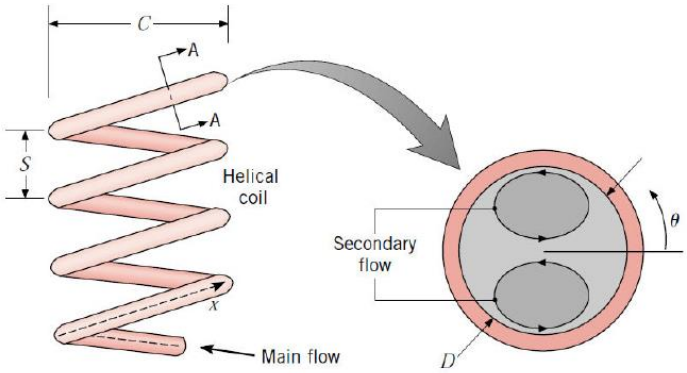

***Figure 12.3**: coiled pipe [5]*

12.2 Corrugated pipes

Wall corrugated tubes certainly represent the most preferred passive solution in heat exchangers industrial applications [7]. The application of corrugated surfaces in shell and tube heat exchangers is very common since it's very easy their implementation on the wall of the pipes constituting this heat transfer equipment. In literature [8]–[13] it has been shown that this kind of technique promotes a significant increase in the thermal performance in comparison to devices using smooth pipes and many correlations have been proposed for any flow regime.

The corrugation on pipes can be realized with different strategy and shapes: internally grooved pipes [14], axially corrugated pipes [15], converging and diverging pipes [16], [17], dimpled pipes [18], spirally corrugated pipes [19]–[22] and wavy channeled pipes [9], [23].

One of the most adopted solutions in food industry is the inner corrugation. To better describe this type of corrugation geometry, it is important to illustrate some of its characteristic parameters (Figure 12.4):

- Corrugation pitch (p), this is the distance between one corrugation crest and the next one; it must be evaluated considering a straight line and two points at the same level. This parameter has a great effect on the degree of turbulence in the flow.
- Depth (e) or corrugation height depending on whether it is an inner or outer corrugation.

- d_o and d_i are the external and internal diameter of the pipe, respectively.
- α is the inclination angle of the corrugation with respect to the longitudinal axis of the pipe.

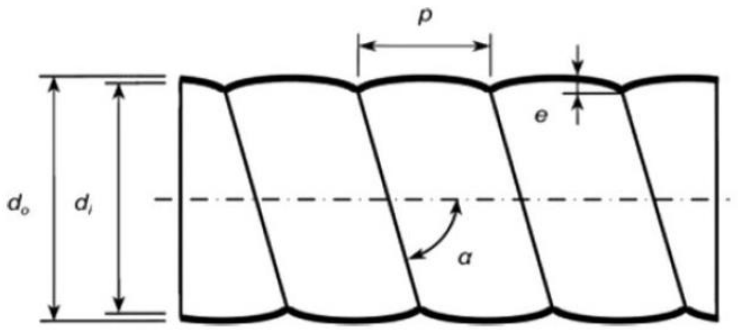

***Figure 12.4**: geometrical parameter of corrugation*

Commonly in literature the mainly adopted types of inner corrugation: longitudinal, transverse, and helical one.

- Longitudinal corrugation: in this type of corrugation, the internal corrugation grooves run parallel to the longitudinal axis of the pipe. This kind of corrugation has been deeply studied in literature: S.Kareem et al. [7] performed a characterisation of pipelines using oil as a test fluid.

  Saha et al. [24], for Reynolds values between 20 and 1000, demonstrated an increase in heat transfer between 15 % and 30 % in comparison to the smooth tube at the same pumping power of the pump. Always Saha [25] considers a rectangular-section duct with

combined internal longitudinal corrugation and with twisted tape type inserts, reporting an increase of up to 45% in heat exchange rate if compared to the two techniques individually, associated to a reduction up to 30% of the power absorbed by the pump.

Another study conducted by Saha [26] considered a rectangular-section pipe longitudinally corrugated with twisted tape. Using air as working fluid ($10^4 < Re < 10^5$), the author reports an improvement up to 55% in heat transfer for the same mechanical power absorbed by the test system, if compared to the case without twisted tape.

– Transverse corrugation: for this geometry, the inner groove is perpendicular to the longitudinal axis of the pipe. This kind of corrugation has been deeply studied in literature: Inagaki and Ozawa [27], tested four titanium tubes with different transverse corrugations, with a pitch and depth of corrugation of 0.3 - 3.5 mm and 4 - 5.5 mm, respectively; using water with Reynolds values between 15000 and 65000 as test fluid. They recorded an increase of about 2.5 times in heat transfer rate compared to the case of smooth pipes, proposing a correlation relating Prandtl number, Schmidt number and friction coefficient. Moreover, the study conducted by Poredos et al. [28] on transverse corrugated ducts for conveying air, evaluated the increase in heat transfer from 65% up

to 90% for Reynolds between 4000 and 24000. Meng et al. [29] report a correlation for the evaluation of the Nusselt number for elliptical section pipes with transverse corrugation, obtained from experimental tests with water and oil for Reynolds values between 500 and 100000.

– Helical corrugation: for the helical geometry, the groove appears as a continuous line that wraps around the pipe with an angle of inclination α. Helical corrugation is the most studied in literature and it is possible to find various experimental correlations attesting its effectiveness in increasing heat exchange. Rainieri et al. [13] considered a helical corrugation with a pitch between 10 and 18 mm and a corrugation depth between 1 and 1.5 mm, using ethylene glycol as test fluid in the Reynolds range $200 < Re < 2000$; they observed an increase in heat transfer between 1.1 and 6 times. Barba et al. [30] proposed a correlation to evaluate the Nusselt number for helical corrugated pipes in which working fluid flows at $100 < Re < 800$. Zimparov et al. [31] showed an increase in heat transfer between 177% and 273% using helical corrugation in comparison to a smooth pipe, using water with Reynolds between 10000 and 60000 as the test fluid; they also proposed a correlation for the cases considered. Dong et al. [32] used water and oil as working fluid, with $6000 < Re < 93000$ and $3200 < Re < 19000$, respectively. They

observed an increase in heat transfer of up to 120%. The use of a "w" corrugation profile, proposed in the analysis by Cui et al. [33], produces an increase in heat exchange rate of up to 160% compared to the case of a smooth pipe. Correlations are proposed to evaluate Nusselt number for this particular corrugation profile. Finally, various studies by Rainieri, Farina and Pagliarini [13], Rainieri and Pagliarini [19] evaluated the heat transfer increase on different types of helical corrugated pipes under imposed heat flow wall conditions. Newtonian and non-Newtonian fluids were tested in laminar and turbulent regimes, and the following results were obtained: for low values of the Reynolds number, the flow is maintained in a laminar regime and the effect of the increase in heat exchange is negligible; the increase in the Reynolds number leads to the development of the turbulent transition at lower values than would be required in a smooth duct, resulting in an increase in heat exchange of up to 600%.

The ability of corrugated pipes to promote the transition to turbulent regime, and thus to promote an enhancement in heat transfer performances of heat exchangers, has made them a very appreciated in the food industry, especially in cases where the fluid to be treated has a very high viscosity and consequently it is difficult to achieve turbulent flowing regimes with the only aid of pump thrust.

Secondly, when designing of devices for the food industry, the aspect of cleanability is necessarily to be considered and, from this point of view, the most of heat exchanger for food industry are designed to be cleaned in-place and the self-drain ability feature is required to not retain food or chemical residues. Following the European Hygienic Engineering and Design Group (EHEDG) guidelines [34], only geometries with insert with a curvature radius bigger than 3 mm are acceptable. This characteristic is easy to meet in corrugated pipe and, for this reason, this kind of enhancement technique is the most preferred in food industrial applications. Moreover, this kind of tubes can be quite easily manufactured by a continuous cold rolling process [4], and their realization cost is relatively low. As reported above, corrugated pipes have been deeply studied in the literature and it has been found out that corrugations act as a disturbance source in the main flow, promoting an early transition to turbulent regimes that significantly enhances the thermal performances of the tube section and limiting the pressure drop augmentation if compared to other passive techniques, such as the ones based on insert devices [35].

It is clear that, for this sector, the study of the effect of corrugation on the heat transfer in pipes represent a powerful tool in the design of increased energy-efficient and effective heat exchangers in unit operations on foodstuffs such as pasteurization and sterilization.

Nevertheless, in the current literature, the thermal enhancement performance of corrugation in straight pipe, in general, has been mainly evaluated only from

an average point of view, considering only the heat transfer performance averaged over the entire heat transfer surface area.

In this work, helical and transverse corrugations have been investigated. This kind of geometries have been experimentally studied both considering the heat transfer performance from an average point of view and investigating the local heat transfer enhancement. The local analysis of the convective heat transfer coefficient is of great interest for some specific industrial processes, such as the case of sterilization and pasteurization treatments of food, in which the occurrence of an irregular distribution of the temperature on the internal side of the corrugation wall, could compromise their effectiveness. Its estimation procedure was based on the solution of the Inverse Heat Conduction Problem (IHCP) within the wall domain using the temperature distribution on the external wall as input data and in which the convective heat transfer coefficient distribution at the fluid-internal wall interface is considered to be unknown. To acquire the temperature of the external side of the wall, a high precision cooled infrared camera was used, in this way it was possible to obtain highly spatially resolved temperature map of the external side of the corrugation.

CHAPTER 13: Average and local analysis of the effect of different corrugations on pipes wall in turbulent regime

13.1 Pipes tested

In the present work, 4 different corrugated straight pipes in stainless steel type AISI 304 were tested. They were characterized by a length of 3.0 m, an internal diameter (D_i) of 14 mm and a wall thickness of 1.0 mm.

Two pipes have a wall helical corrugation with depth *(e)* of 1 mm, one (called H16) with corrugation periodicity (p) of 16 mm (Figure 1) and the other one (called H32) with corrugation periodicity (p) of 32 mm. Two pipes have a wall transverse corrugation with depth *(e)* of 1.5 mm, one (called T16) with corrugation periodicity (p) of 16 mm and the other one (called T32) with corrugation periodicity (p) of 32 mm.

In addition, also a smooth pipe was tested as reference. Its length was 3.0 m, the internal diameter (D_{env}) was of 14 mm and the wall thickness was 1.0 mm.

The total length of every corrugated pipe is subdivided as follows: the first section is 1 metre long and it allows the complete thermodynamic development of the flow, after this section there is a heating section of 1.84 m, created by applying two steel fin electrodes which were connected to a power supply, type HP 6671A, working in the ranges 0–8 V and 0–220 A. The heat flux generated by Joule effect on the pipes wall was considered uniform along the heat transfer section. The pipes were thermally insulated on their entire length with a double layer of expanded polyurethane for the minimization of the heat losses to the environment.

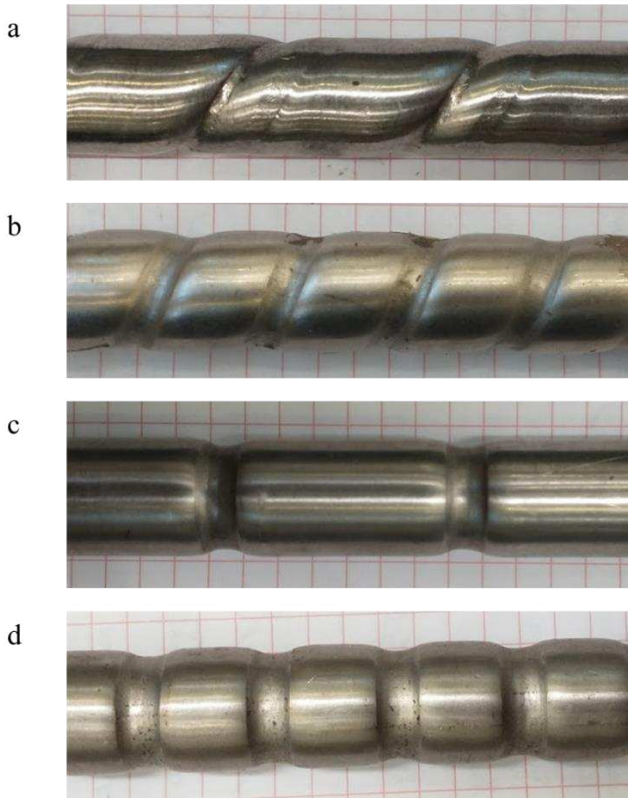

***Figure 13.1**: Corrugated pipe tested: a) H32, b) H16, c) T32 and d) T16*

13.2 Experimental setup for average analysis

The average performances of the tested pipes were evaluated by inserting the corrugated pipes horizontally in a specially designed setup, schematically reported Figure 13.2. The test rig is composed by a volumetric pump that conveys the working fluid from the holding tank to a heat exchanger fed with city water. With this passage the temperature of the working fluid at the inlet section of the corrugated pipe tested was kept constant. Once the working fluid exits from the corrugated pipe, it re-enters in the holding tank for restarting the cycle.

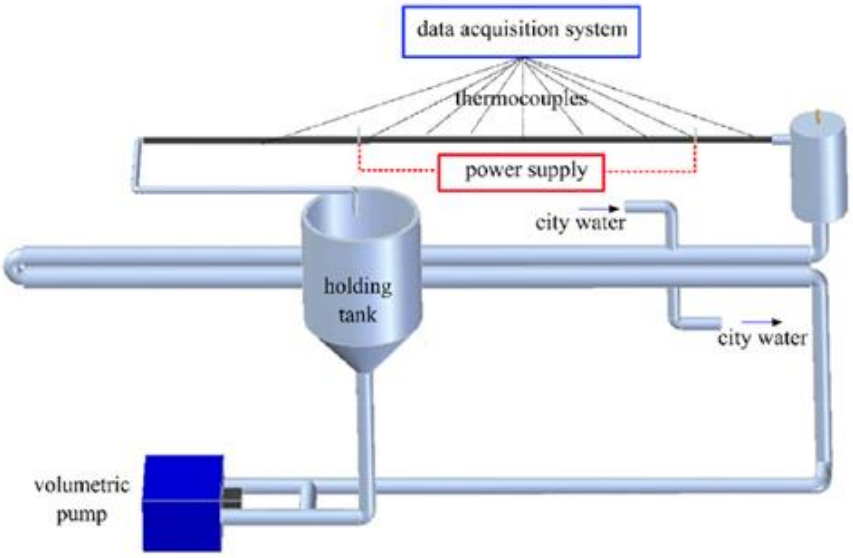

***Figure 13.2**: schematic representation of the setup for average analysis*

The temperature of the tube wall and the temperature of the fluid at the inlet and outlet sections was measured using forty T-type thermocouples, calibrated and connected to a multichannel ice point reference (type KAYE K170-50C). The external wall temperature was measured placing the probes on the external tube's surface along different axial and circumferential positions, in the heated zone, in order to estimate the average temperature of each section. For each axial distance considered, two diametrically opposed thermocouples were placed one on the upper surface and one on the lower surface. To estimate the internal wall temperature, the steady-state heat conduction problem related to heat generation in the tube wall was solved. For determining the inlet and outlet temperatures, the probes were placed on the tube's wall before and after the heated section, respectively. The bulk temperature at any location in the heat transfer section

was calculated from the power supplied to the tube, assumed to be distributed uniformly per unit length over the heat transfer surface area. Volumetric flow rates were obtained by weighing the quantity of product exiting by the test section and relating it to the time taken. Finally, the data acquisition system was composed of a high precision multimeter (type HP 3458A) connected to a switch control unit (type HP 3488A) driven by a Personal Computer. Pressure drop throughout the corrugated pipe was measured by a Rosemont® 3051S differential pressure transducer in isothermal conditions. Temperatures were acquired for 5 min. with a frequency of 0.33 Hz once steady state was reached for *Re* values of $4 \cdot 10^3$ up to $16 \cdot 10^3$. The experimental setup allowed to measure the Nusselt number along the axial coordinate, considering it uniform along the cross section and its average value in the wall heated section, as follow:

$$Nu_z = \frac{h_z \cdot \mathrm{D}_i}{\lambda} \qquad (1)$$

$$Nu = \frac{1}{L_H} \int_0^{L_H} Nu_z dz \qquad (2)$$

where λ is the fluid thermal conductivity, z the axial coordinate, L_H the length of the heated section while the local convective heat transfer coefficient h_z is defined as follow:

$$h_z = \frac{q}{(T_w - T_b)} \qquad (3)$$

where T_w is the circumferentially averaged wall temperature obtained by averaging the values measured by the thermocouple on the wall pipe, T_b is the bulk fluid temperature, q is the heat exchanged per unit of area, assuming the surface equal to the pipe envelope cylinder area. The bulk temperature was used for evaluating product properties. The Nusselt number value has been evaluated by varying the Reynolds number, which is defined as follows:

$$Re = \frac{\rho \cdot v \cdot \mathrm{D}_i}{\mu} \qquad (4)$$

being ρ and μ the density and the dynamic viscosity of the product, v the mean fluid velocity over the tubes and D the pipe diameter.

13.3 Experimental setup for local analysis

The local analysis performed in this part of the thesis is based on the solution of the inverse problem described at the end of the paragraph 12.2, and, in specific, it was carried out using a filtering technique for the stabilization of its solution, as introduced in Chapter 3. Specifically, for the local heat transfer estimation, a small portion of thermal insulating layer was removed in every pipe in order to make accessible the external tube wall to a thermal imaging camera. The length of the portion of thermal layer removed was selected in order to shoot a complete rotational period of the corrugation. This wall portion was coated with a thin film of opaque paint with uniform and known emissivity. The surface temperature distribution of the wall was acquired adopting a IR camera FLIR

SC7000, with a 640 x 512 pixels sensor with a tabulated sensitivity of 20 mK at 303 K and accuracy of ±1 K. To measure the temperature distribution on the whole test section surface, multiple images were acquired, moving the infrared camera around the tube's axis (Figure 13.3).

For every pipe, images were acquired at $Re = 4 \cdot 10^3$, 10^4 and $1.6 \cdot 10^4$ once the thermal steady state condition was reached. To reduce acquisition noise, the acquisition time of each image was set to 3s using a frame rate of 25 Hz, so that each image obtained is the result of averaging 75 frames.

The camera was fixed on a support, as sketched in Figure 13.3, to keep the optic in normal position respect the tube axis and minimizing perspective artifacts and involuntary movements. In the present experimental setup, the limited viewing angle, less than ± 30°, allows to consider the surface of the pipe as a diffuse grey emitter [36]. The effective emissivity of the painting used for coating was estimated by shooting the same target at different known temperatures, and its value was about 0.95.

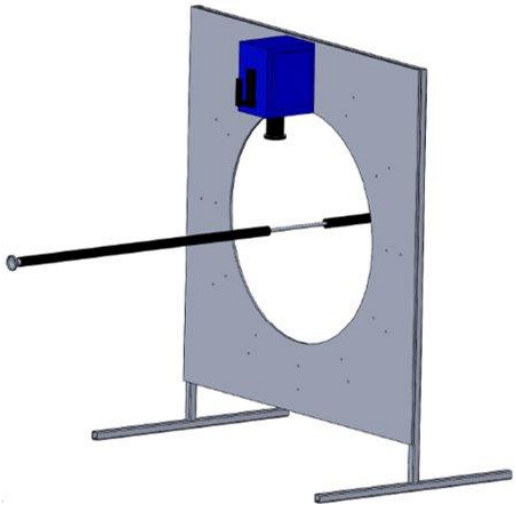

***Figure 13.3**: setup for the estimation of the local heat transfer with IR camera*

The image processing for obtaining a total picture of the temperature distribution on the pipe wall was tricky because the observed target surface is not flat, but cylindrical. For this reason, in this paper, the image processing procedure adopted is the one validated by Bozzoli et al. [20]. This procedure allowed to rectify the optical deformations on the collected images caused by surface curvature. The acquired images, thanks to adequate position references fixed on the tube wall, were then processed to obtain continuous temperature map on the tube wall. The references were positioned at the extremities of the surface captured by the camera and allows to identify the interest areas (1/6 of the total external surface of the pipe) of every picture obtained (Figure 13.4).

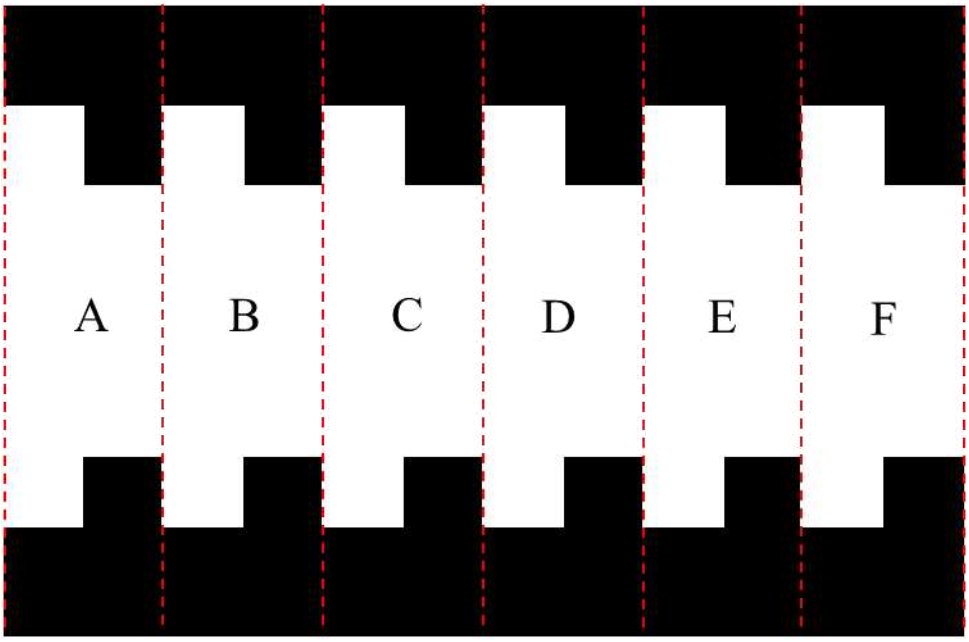

***Figure 13.4**: schematic representation of the two references placed at the extremities of the pipe with the division of the areas of interest for every picture acquired*

The first step of the procedure consists in the acquisition of six IR raw pictures around the external surface of the corrugated pipe (Figure 13.5).

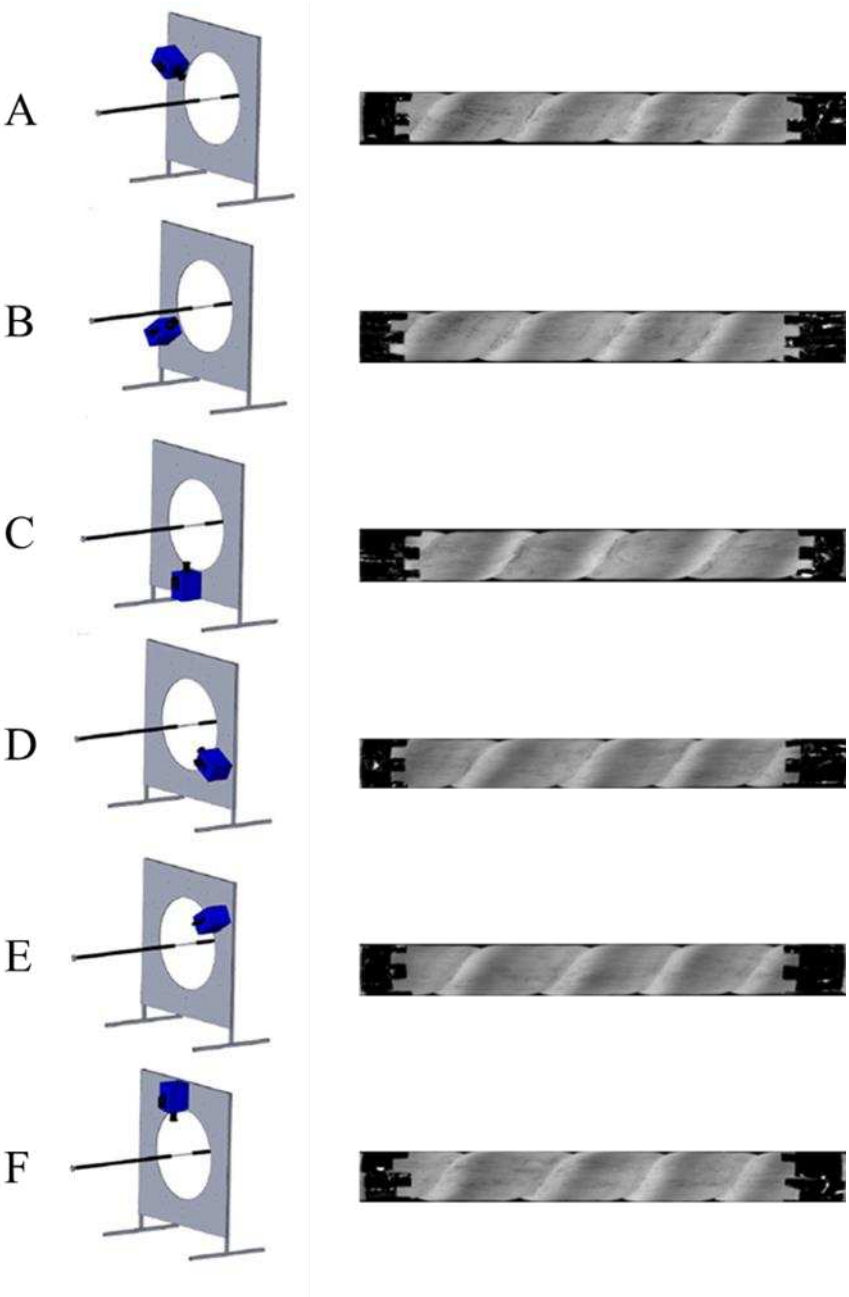

***Figure 13.5**: example of six IR raw pictures, obtained around the pipe, before the unwrapping and merging operations.*

Assuming the camera far enough from the pipe, from the coordinates (x, y) of a point of a picture in planar reference system, it is possible to obtain the corresponding coordinates in the cylindrical coordinates system using the following equations:

$$\begin{cases} z = \Omega\, y + z_0 & (5) \\ \alpha = \arctan\left(\frac{x}{\Psi}\right) + \alpha_0 & (6) \end{cases}$$

where Ψ, x, z_0 and α_0 are parameters defined by the camera lenses and camera relative position [37], [38].

Using this system of equations (eq.5 and eq.6), it has been possible to unwrap the 6 IR raw pictures obtained with the infrared camera. Once completed this procedure, in all the wrapped images, the upper and bottom parts were cut as reported in Figure 13.6, in order to avoid the deformation on the extremities.

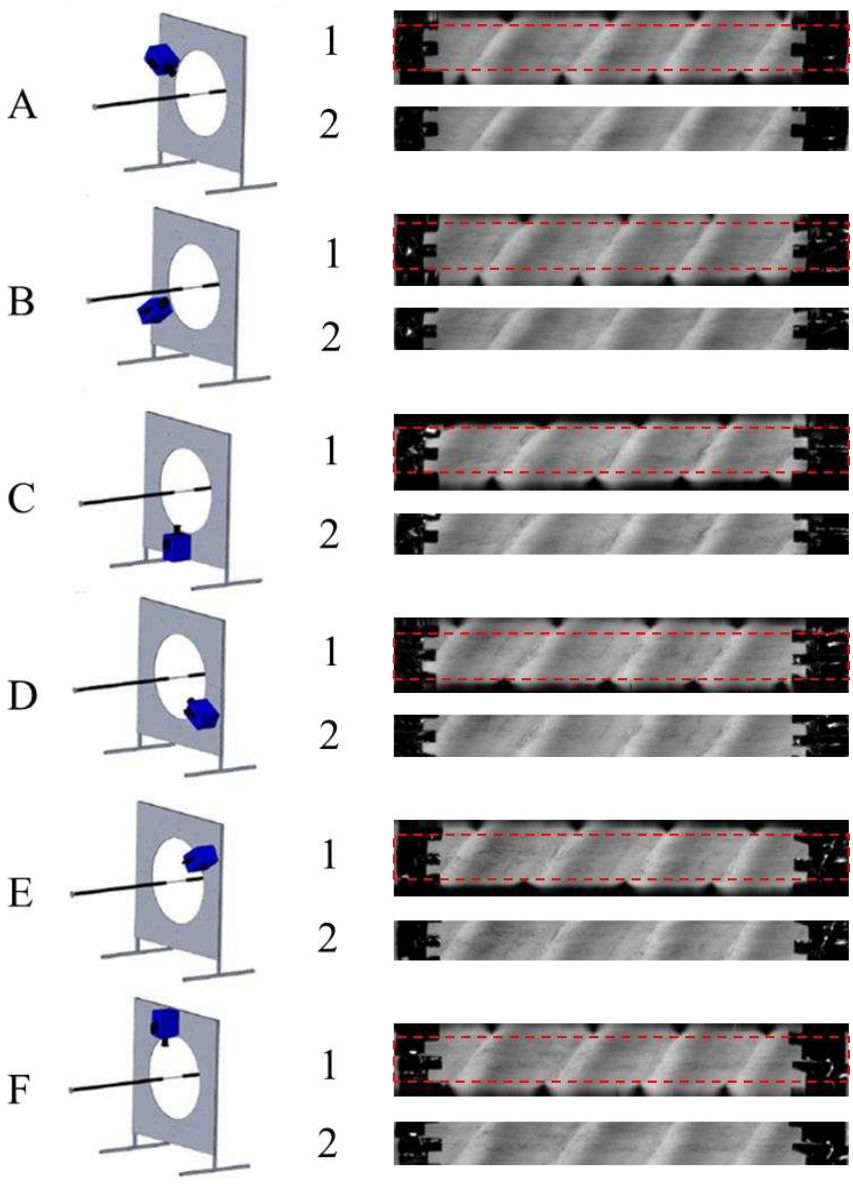

Figure 13.6*: for every IR raw image (A, B, C, D, E and F) example of: 1) wrapped pictures with the illustration of the cutting borders for obtaining the 2) central portions with which executing the following merging operation.*

Finally, for the reconstruction of the planar development of the external surface of the pipes, the obtained images are merged following the references placed at the extremities to obtain the relative areas of interest (Figure 13.7).

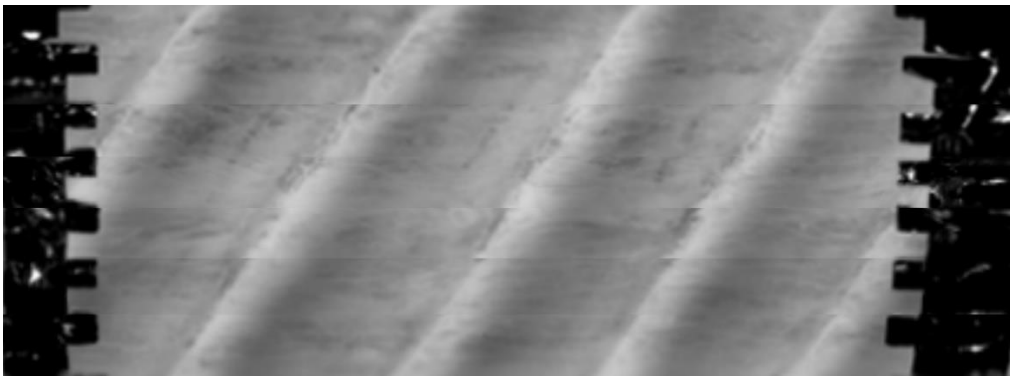

Figure 13.7*: example of a reconstructed external surface after merging operation.*

Starting from the obtained image of the temperature distribution of the whole tube portion captured by the IR camera, to evaluate the value of the local convective heat transfer coefficient, the IHCP in the wall domain was solved. The convective heat transfer coefficient distribution on the internal wall surface was considered unknown while the heat generated by Joule effect was known.

The heat conduction in the wall of a cylindrical pipe (Figure 13.8a) is the physical problem to consider. The balance equation describing the problem can be described with Eq.5, while the boundary conditions with Eq.6 and with Eq.7 for the external surface of the pipe and for the internal one, respectively:

$$k\nabla^2 T + q_g = 0; \quad (7)$$

$$-k\frac{\partial T}{\partial r_{r=r_{est}}} = \frac{(T - T_{env})}{R_{env}}; \quad (8)$$

$$-k\frac{\partial T}{\partial r_{r=r_{int}}} = h_{int}(T - T_b); \qquad (9)$$

where q_g is the heat generated per unit volume in the tube wall, k is the conductivity of the tube material, T_{env} is the surrounding environment temperature, R_{env} is the overall heat transfer resistance between the environment and the tube wall and T_b is the local fluid bulk temperature.

a)

b)

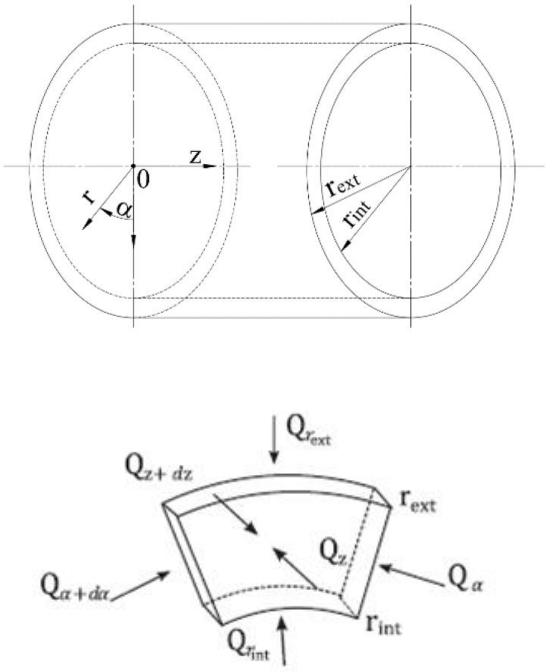

Figure 13.8*: a) Geometrical domain with coordinate system; b) a portion of the test section*

For the estimation procedure, the portion of the experimentally analysed section of the pipe was modelled as cylindrical shell with an infinitesimal sector as reported in Figure 13.8a, assuming that the temperature of its external surface

was equal to the temperature of the internal one, by means the thin-wall approximation:

$$T(\alpha, r, z) \cong T(\alpha, r_{int}, z) \cong T(\alpha, r_{ext}, z) \quad (10)$$

If the Biot number, that corresponds to the convective heat transfer coefficient multiplied by the thickness of the tube and divided by the tube wall thermal conductivity, is smaller than 0.1, then the thin-wall approximation is acceptable, [5]. For the cases analysed this condition was verified.

The steady state energy balance equation of the problem, considering the cylindrical sector as represented in Figure 13.8b can be written as follow:

$$Q_{\alpha+d\alpha} + Q_{\alpha} + Q_{r_{int}} + Q_{r_{ext}} + Q_{z+dz} + Q_z + Q_g \quad (11)$$

The heat flux on the α angular coordinates are expressed as:

$$Q_{\alpha} = \int_{r_{int}}^{r_{ext}} -\frac{k\partial T}{r\partial \alpha} dr dz = -\frac{k dT}{d\alpha} \ln\left(\frac{r_{ext}}{r_{int}}\right) dz \quad (12)$$

$$Q_{\alpha+d\alpha} = = -k\frac{\partial T}{\partial \alpha}\ln\left(\frac{r_{ext}}{r_{int}}\right) dz + k\frac{\partial^2 T}{\partial \alpha^2}\ln\left(\frac{r_{ext}}{r_{int}}\right) d\alpha dz \quad (13)$$

where r_{int} and r_{ext} are the interna and external radius of the pipe, respectively. For the radial coordinate *r,* the heat flux contribute can be expressed as follow:

$$Q_{r_{int}} = -h_{int}\,(T - T_{int}) r_{int}\, d\alpha\, dz \quad (14)$$

$$Q_{r_{ext}} = -\frac{(T - T_{env})}{R_{env}} R_{ext}\, d\alpha\, dz \quad (15)$$

Along the axial coordinates, the heat flux can be described as follow:

$$Q_z = \int_{r_{int}}^{r_{ext}} -\frac{k\partial T}{r\partial z}\frac{\pi r^2}{2\pi} d\alpha dr = -k\frac{\partial T}{\partial z}\left(\frac{r_{ext}^2 - r_{int}^2}{2}\right) d\alpha \quad (16)$$

$$Q_{z+dz} = -k\frac{\partial T}{\partial z}\left(\frac{r_{ext}^2 - r_{int}^2}{2}\right) d\alpha + k\frac{\partial^2 T}{\partial z^2}\left(\frac{r_{ext}^2 - r_{int}^2}{2}\right) d\alpha dz \quad (17)$$

Finally, the heat source can be defined as:

$$Q_g = q_g \left(\frac{\pi r_{ext}^2 - \pi r_{int}^2}{2\pi}\right) d\alpha dz = \frac{q_g}{2}\,(r_{ext}^2 - r_{int}^2)\, d\alpha dz \quad (18)$$

Substituting Eqs. (10-16) in Eq. (9), the energy balance equation can be rewritten, isolating the convective heat transfer of the internal wall, as follow:

$$h_{int} = \frac{k\cdot\ln\left(\frac{r_{ext}}{r_{int}}\right)\cdot\frac{\partial^2 T}{\partial \alpha^2} + \frac{k}{2}(r_{ext}^2 - r_{int}^2)\cdot\frac{\partial^2 T}{\partial z^2} - \frac{r_{ext}}{R_{env}}(T - T_{env}) + \frac{q_g}{2}(r_{ext}^2 - r_{int}^2)}{r_{int}\cdot(T - T_b)} \quad (19)$$

Since noise is present in the raw images of the surface temperature distribution, the Eq.17 gives unreliable results [39]. Its peculiarity of second derivative operator makes it very sensitive to small perturbations in the input data due to the well-known destructive effect of the noise [40].

A good strategy to overcome this issue is the application of a Gaussian filtering procedure to the raw temperature data in order to eliminate high-frequency components, behaving then like a regularization function. The

effectiveness of the Gaussian filtering in this kind of approach was experimented by many authors [39], [41], [42]. The function of the filter in a 2-D frequency domain, can be expressed as follows:

$$H(u,v) = e^{-(u^2+v^2)/2u_c^2} \quad (20)$$

where u_c is the cutoff frequency, assumed equal along the *u* and *v* coordinates. In real situation the value of the optimal frequency of cut-off is unknown, it is necessary to choose a selection criterion for performing a successful regularization step. In the present work, the discrepancy criterion of Morozov [43] was selected. Following this criterion, the solution of the inverse problem can be considered accurate enough when the difference between the measured temperatures *Y* and the filtered ones Y_f is similar to the standard deviation of the measured temperatures *Y*. For this reason, the correct frequency of cut-off can be determined once the following condition is satisfied:

$$\frac{\|Y_f - Y\|_2^2}{N \cdot M} = \sigma_Y^2 \quad (21)$$

where *N·M* is the dimension of the matrix of the measured temperatures *Y* and σ_Y is the standard deviation of the noise, obtained measuring the surface temperature of the coil maintained in isothermal condition. In this way, the best approximation obtainable is in the order of the random error of the data affecting the measurements.

CHAPTER 14: Results

14.1 Average results

The first part of the investigation was aimed at measuring the average heat transfer performances of the corrugated pipe illustrated above, using the experimental setup described in paragraph 2.2. The heat transfer effect of corrugations has been evaluated considering also the penalising pressure drop of the tested geometries. For comparing the global thermal performances of the tested geometries, the Nusselt number (*Nu*) as a function of *Re* for all the tested pipes is reported in Fig. 3a. In the same plot it is reported also the distribution of the Nusselt number for a smooth tube experimentally obtained together with the correlation of Dittus-Boelter for smooth tubes in turbulent regime [5]. The satisfactory correspondence between the measured values for the smooth tube and the Dittus-Boelter correlation demonstrates the appropriateness of the experimental set up.

In Figure 14.1, it is possible to note that the best thermal performances are given by the transverse corrugations (T16 and T32), obtaining a *Nu* about 3 times higher than the smooth one and 1.5 times than the H32. Moreover, it is possible to note that the pitch seems to be influent only in the case of helical geometry, where the smallest one (H16) promotes a greater thermal increasing effect respect to the biggest one (H32), especially for high Re number. Anyway, every geometry of corrugation showed a better thermal transfer rate if compared to the smooth pipe, showing its effectiveness in enhancing thermal performances.

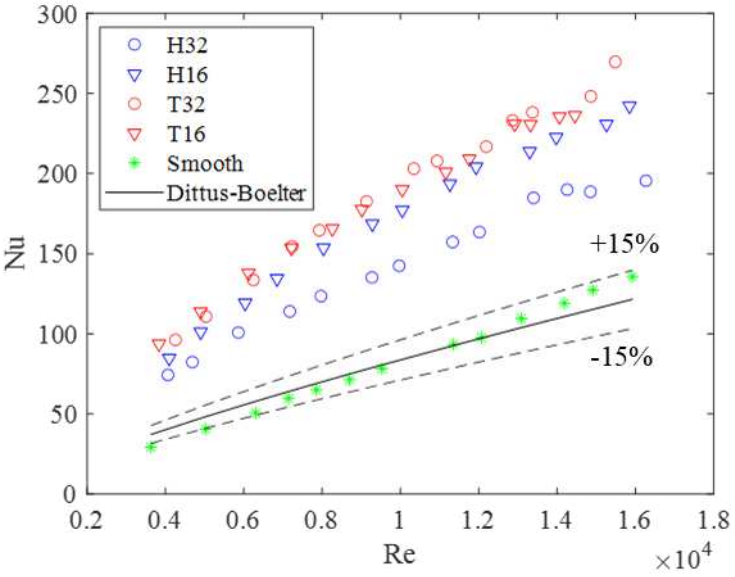

***Figure 14.1**: Nu as function of Re*

To deeply analyse the effect of corrugation geometry on the thermal exchange, the behaviour of the axial Nusselt number Nu_z in function of the dimensionless abscissa, calculated as reported in Eq.19, is shown for every corrugated pipe and for the smooth one in Figure 14.2, taking as example the cases of Re= 4000, Re= 10000 and Re= 16000.

$$z^* = \frac{z}{Re \cdot Pr \cdot D} \qquad (22)$$

It is possible to observe that in the fully developed condition, the Nu_z and so the thermal effect of the corrugation, resulted quite constant along the dimensionless abscissa for all the pipes. Moreover, it is possible to note that the results observed for the global behaviour are confirmed: in all the reported cases, the transverse corrugation generates the greatest increase in thermal performances: for this type of corrugation, the Nu_z is about 3 times larger than for the smooth pipe, while for the helical geometry the thermal increase is about 1.5 time. Also in this case, observing Figure 14.2, it is possible to note that for helical geometry the small pitch (H16) seems to have a greater thermal increasing effect respect the big one (H32), especially at high Re number. Conversely, no significative differences are observable between different pitches in the transverse geometry (T32 and T16).

These results seems to confirm in turbulent condition what Rainieri and Pagliarini [19] observed for laminar condition: transverse corrugation achieved the best thermal results, showing the best thermal enhancement power in straight pipes.

a)

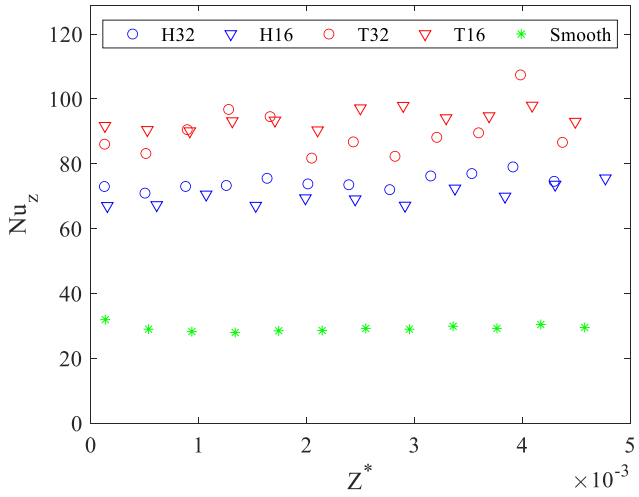

b)

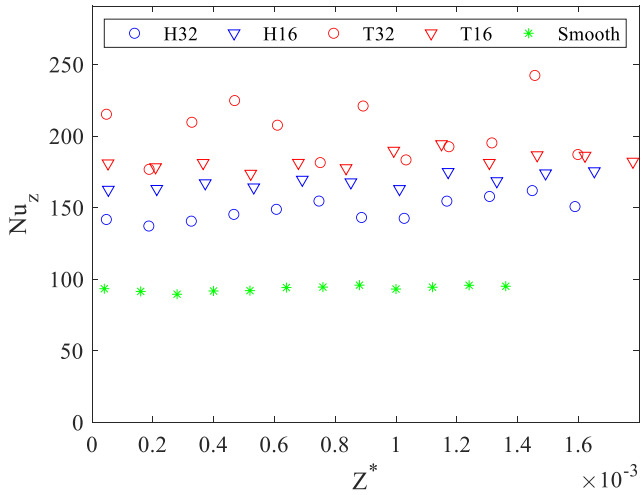

c)

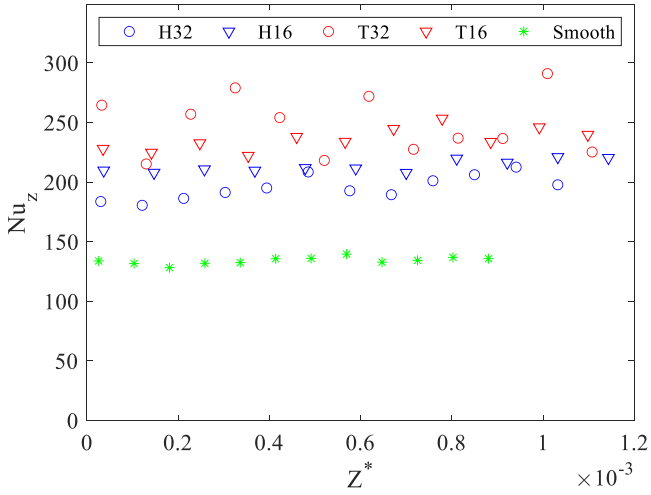

***Figure 14.2**: Nu_z as function of dimensionless abscissa z^* for the cases a) Re=4000, b) Re=10000 and c) Re= 16000.*

Moreover, in Figure 14.3a, the pressure drop in terms of Darcy friction factor (*f*) has been evaluated in function of the Re number for all the pipes. The Darcy friction factor was calculated as follow:

$$f = \frac{\Delta p}{\rho} \cdot \frac{D}{L} \cdot \frac{2}{v^2} \quad (23)$$

where Δp is the pressure drop along the pipe and *L* is the length of the pipe. It is possible to observe that for Re < $8 \cdot 10^3$ the helicoidal geometry pipe guarantees a lower pressure drop than the transverse one, while starting from Re > $8 \cdot 10^3$ the two pipes seem to behave similarly. As expected, both the two corrugated pipe shown value of *f* higher than the smooth one. Finally, in order to evaluate the effect of the different geometries, both the thermal enhancement effect and the pressure drop caused by the corrugation were considered. For this purpose, a term describing the efficiency of the geometry (η) was introduced and calculated as follow:

$$\eta = \frac{\varepsilon_h}{(\varepsilon_f)^{1/3}}; \quad (24)$$

$$\varepsilon_h = \frac{Nu}{Nu_{smooth}}; \quad (25)$$

$$\varepsilon_f = \frac{f}{f_{smooth}}; \quad (26)$$

where the subscript *smooth* refers to the smooth pipe and ε_h is identified as the heat transfer enhancement and ε_f as the friction factor enhancement.

In Figure 14.3b it is possible to observe that in terms of efficiency η, for Re $< 10^4$ the transverse geometry performs always better than the helicoidal one, especially in the case with bigger pitch (T32). For this reason, it is possible to state that, although transverse corrugation generates a greater friction factor, its effect of enhancement on the thermal performances makes it the more efficient. On the contrary, the geometry H32 shows the worst efficiency in the entire range of *Re* tested.

For Re $> 10^4$ the efficiency η of all the pipe does not show significative differences with the exception of the geometry H32, that remains the geometry with the lowest efficiency.

a)

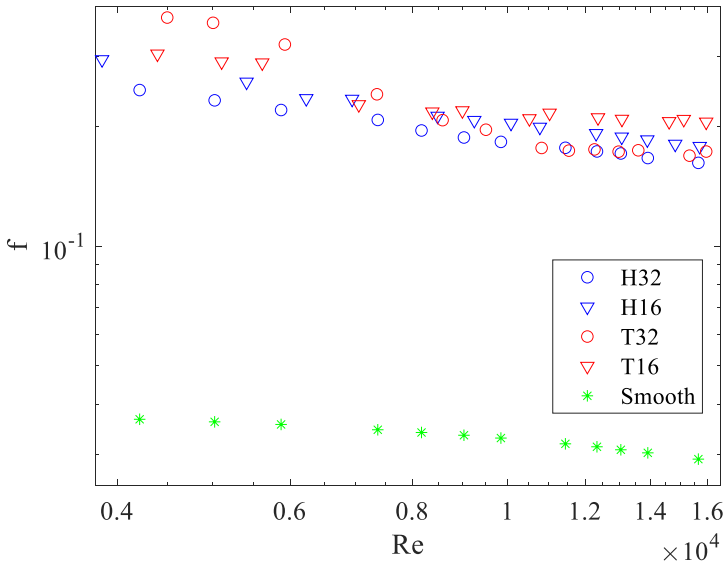

b)

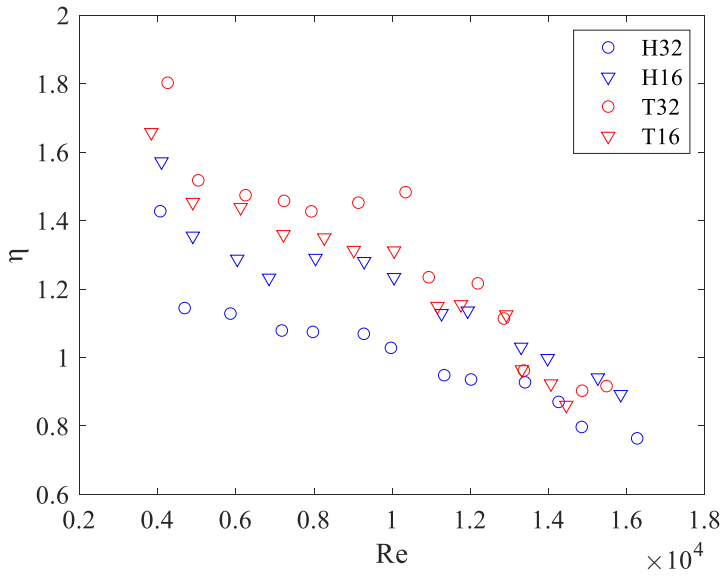

***Figure 14.3**: friction factor f and efficiency η as function of Re*

14.2 Local results

To help the reader in understanding the interpretation of the results obtained with the IR analysis, in Figure 14.4 the schematization of the developed portion of the pipe captured by the IR camera with the position of the corrugations on every pipe analysed during the local tests and the direction of the flow rate is reported.

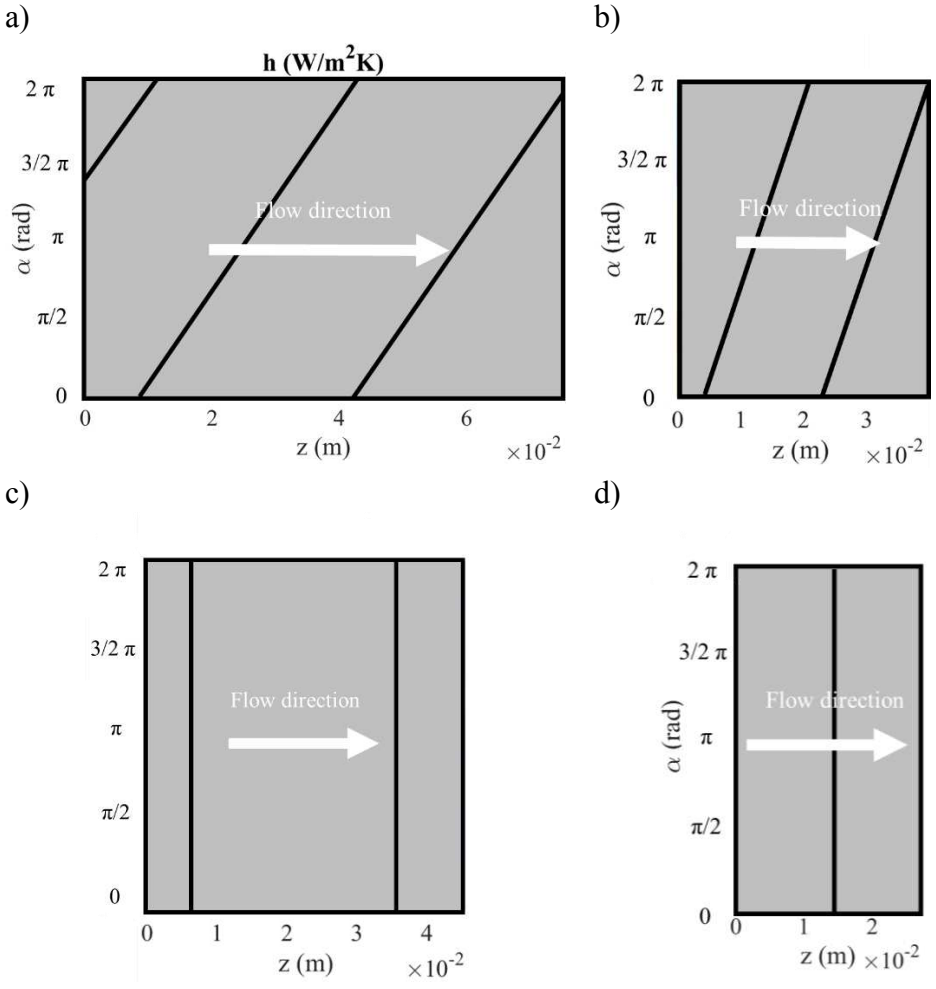

Figure 14.4: *schematic position of corrugations and flow direction in the tested pipes a) H32 b) H16 c) T32 and d) T16*

Starting from the temperature distribution of the external surface of the pipe and applying the inverse procedure described in chapter 2, it was possible to obtain the local heat transfer coefficient *h* on the internal wall of the pipe. An example of the not filtered (Figure 14.5) and filtered (Figure 14.6) temperature distributions on the external surface of the tested pipes for the cases with Re= 4000 is reported in Figure 14.6.

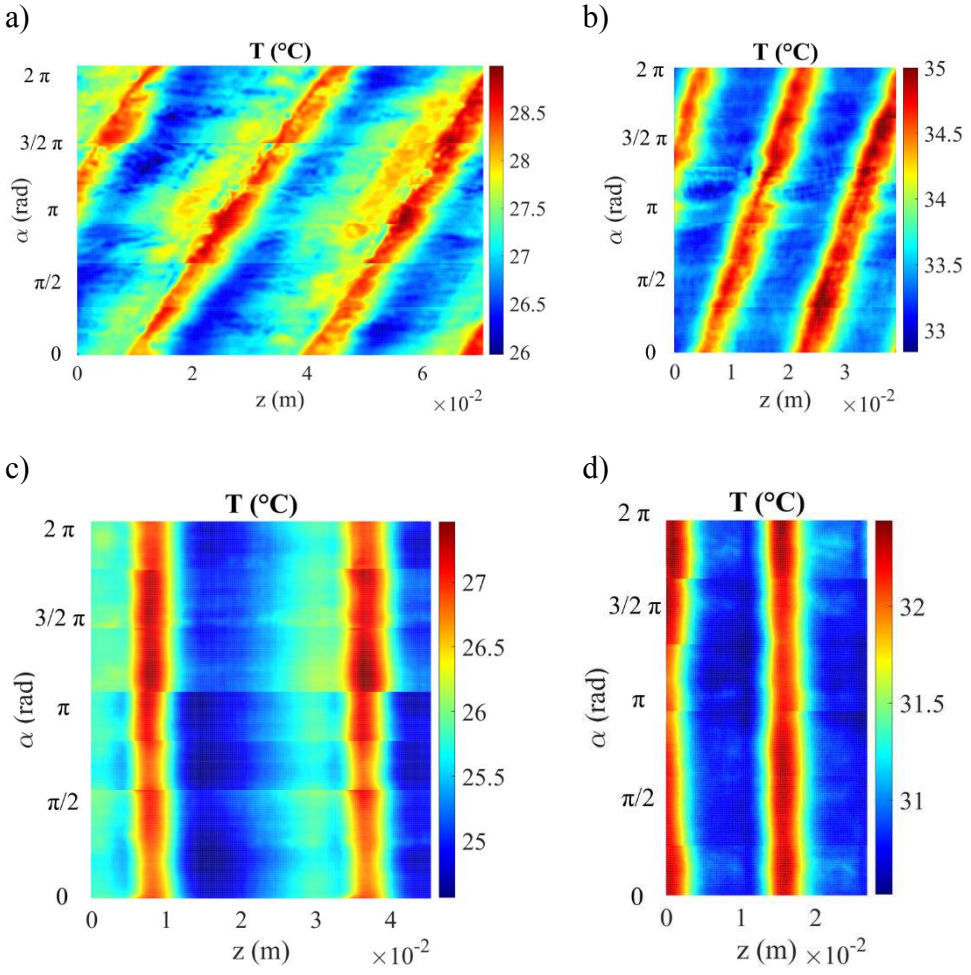

Figure 14.5*:not filtered temperature distribution at Re=4000 for a) H32 b) H16 c) T32 d) T16*

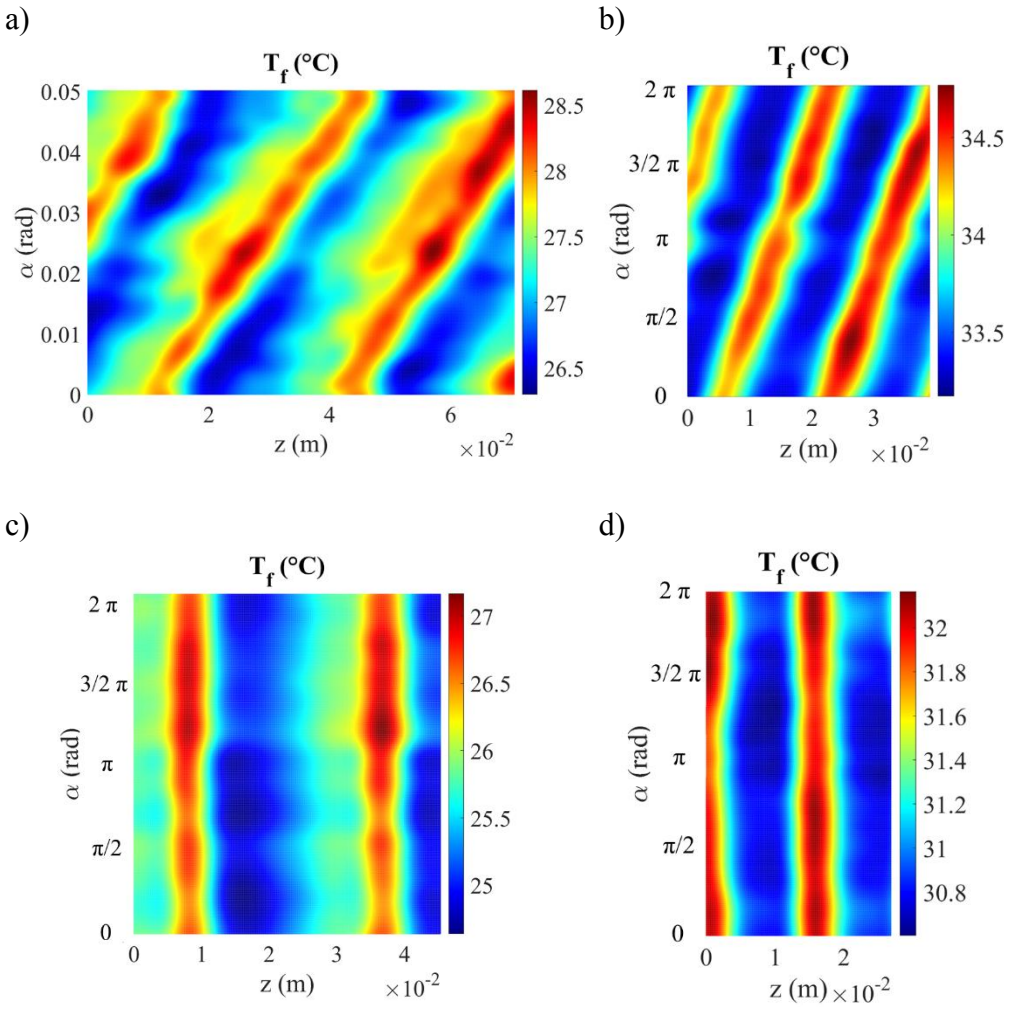

***Figure 14.6**: filtered temperature distributions at Re=4000 for a) H32 b) H16 c) T32 d) T16*

A careful analysis of Figure 14.6 shows how the corrugations locally influence the temperature distribution on the wall of the analysed pipes. Firstly, it is possible to state that every type of corrugation highly influences the temperature distribution on the pipe wall. In specific, if we take as example the case H32, it is possible to observe that, immediately after corrugation, following the direction of flow, the wall temperature reaches a maximum peak. Since, in this case, the higher the wall temperature, the lower the heat exchange between

fluid and wall, it is possible to state that immediately after the corrugation a reduction of the thermal exchange rate occurs.

This behaviour could be ascribed to a disruption of the boundary layer of the fluid in contact with the internal wall of the pipe due by the roughness of the corrugation, causing a local detachment effect of the fluid from the internal pipe wall itself. On the contrary, once the described effect of corrugation is overcome, following the fluid stream, the wall temperature suddenly reaches a minimum, witnessing an equally sudden increase in the rate of thermal exchange between fluid and wall. This phenomenon could be caused by the reattachment of the fluid to the inner wall of the pipe, whose impact locally causes an increase of the turbulence of the fluid. Finally, after reaching the minimum, the wall temperature tends to gradually increase until the next corrugation, where the phenomenon repeats from the beginning. This gradual rise in temperature of the fluid after reaching the minimum, could be promoted by the re-establishment of the fluid's original turbulent state, indeed, the smooth pipe section encountered by the fluid could act as a stabiliser for the fluid flowing state. The same behaviour is also attributable to the case T32.

Observing the temperature distribution for cases with smaller pitches (H16 and T16), the stabilizing effect between the corrugation seems to disappear. This phenomenon could be caused by the not sufficient distance between corrugations. In fact, if it is considered the length of smooth pipe required for the temperature to begin the gradual rise after reaching the minimum, it is

possible to observe that it is about 15 mm. In pipes with corrugation smaller pitches (H16 and T16), the distance between the end of one corrugation crest and the beginning of the crest of the next one is less than 15 mm, not allowing the stabilization effect and thus results in lower and more homogeneous temperatures that indicate an increased heat exchange ability in the pipe wall, confirming, under this point of view, their best thermal performances if compared to the pipes with bigger pitch and confirming also what above observed in average analysis.

More in general, it is possible to state that the corrugations, in any geometrical configuration tested, acts as “heat exchanger enhancer”, improving the thermal performances of a smooth pipe.

In Figure 14.7 the restored internal convective heat transfer coefficient h at $Re=4\cdot10^3$ are reported for all the pipes. The behaviour of h confirms what observed for the temperature distributions: immediately after the corrugation, following the fluid stream, the value of h reaches the minimum and then a maximum. In corrugations with a pitch of 32mm, h tends to decrease until the next corrugation after reaching a maximum, confirming the temperature behaviour observed previously for the same cases. This phenomenon is most evident for case T32. However, it is important to highlight that although the convective heat transfer coefficient reaches a minimum value immediately after corrugation, its value is still greater than the one obtainable in a smooth tube. It

would therefore be more correct to talk about a region where the effect of corrugation on *h* values is lower respect to subsequent areas.

Considering the pipes with corrugations pitches of 16 mm (H16 and T16), it is possible to observe that this intermediate decrease of *h* between corrugations is not present (confirming what above observed for temperature distributions), allowing to obtain on the entire surface between corrugations values of *h* close to the maximum ones and a greater homogeneity of the convective heat transfer distribution if compared to the ones obtained for H32 and T32.

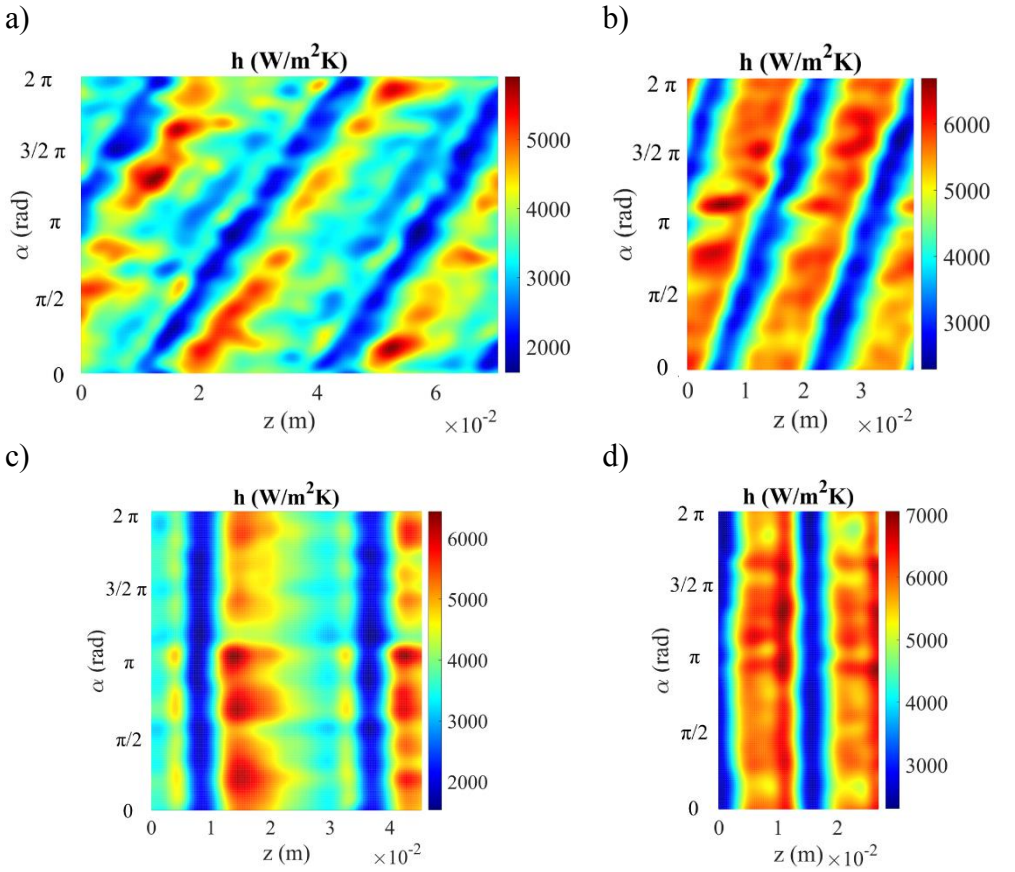

Figure 14.7*: Restored internal convective h heat transfer distribution at Re= 4000 for a) H32 b) H16 c) T32 d) T16*

Finally, it is possible to note that small pitches allowed to obtain maximum value of *h* slightly higher than the big pitches, promoting a greater heat transfer enhancement. The trend above described is respected also for the cases at Re= 10^4 (Figure 14.8) and Re= $16 \cdot 10^4$ (Figure 14.9).

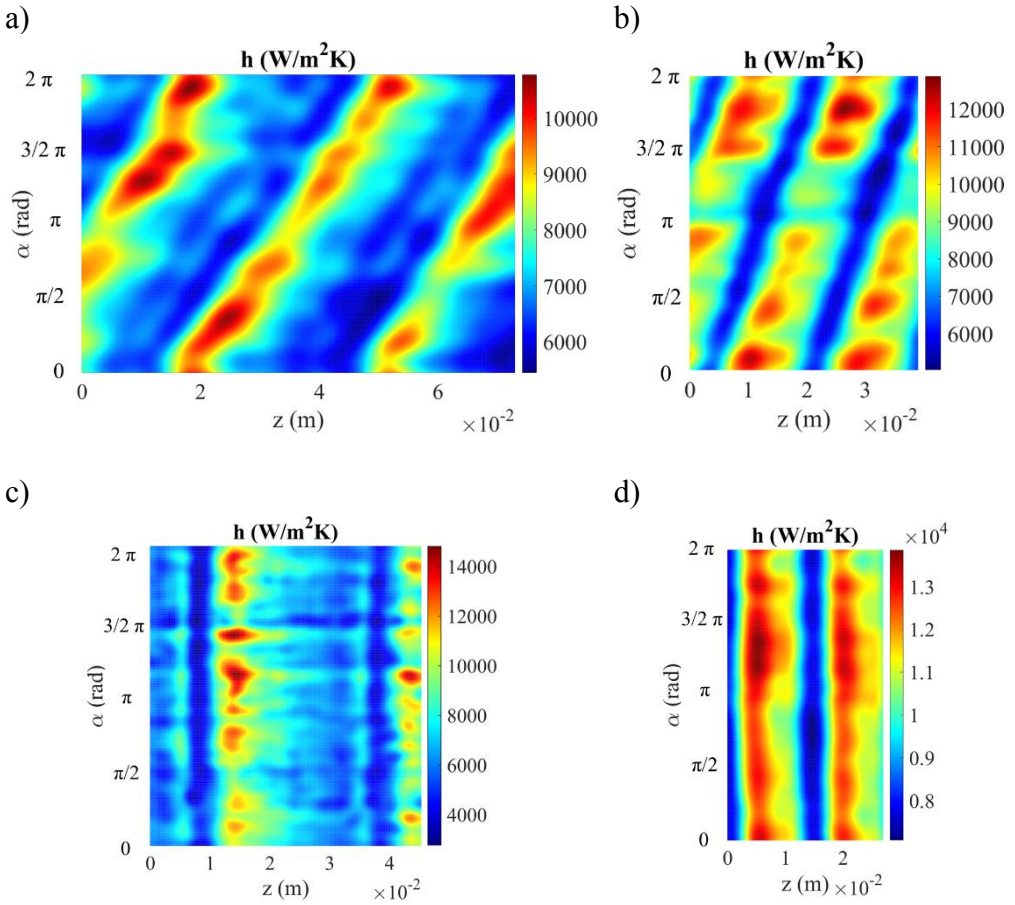

Figure 14.8: *Restored internal convective h heat transfer distribution at Re= 10000 for a) H32 b) H16 c) T32 d) T16*

It is possible to observe that, at the same value of *Re*, for both the helical and transverse geometry, the reduction of the corrugation pitch allows to obtain slightly higher values of *h*. Moreover, corrugations with smaller pitches (H16 an

T16), also in these cases, allow to maintain a more uniform distribution of the convective heat transfer coefficient in the internal side of the wall, confirming another time what observed above.

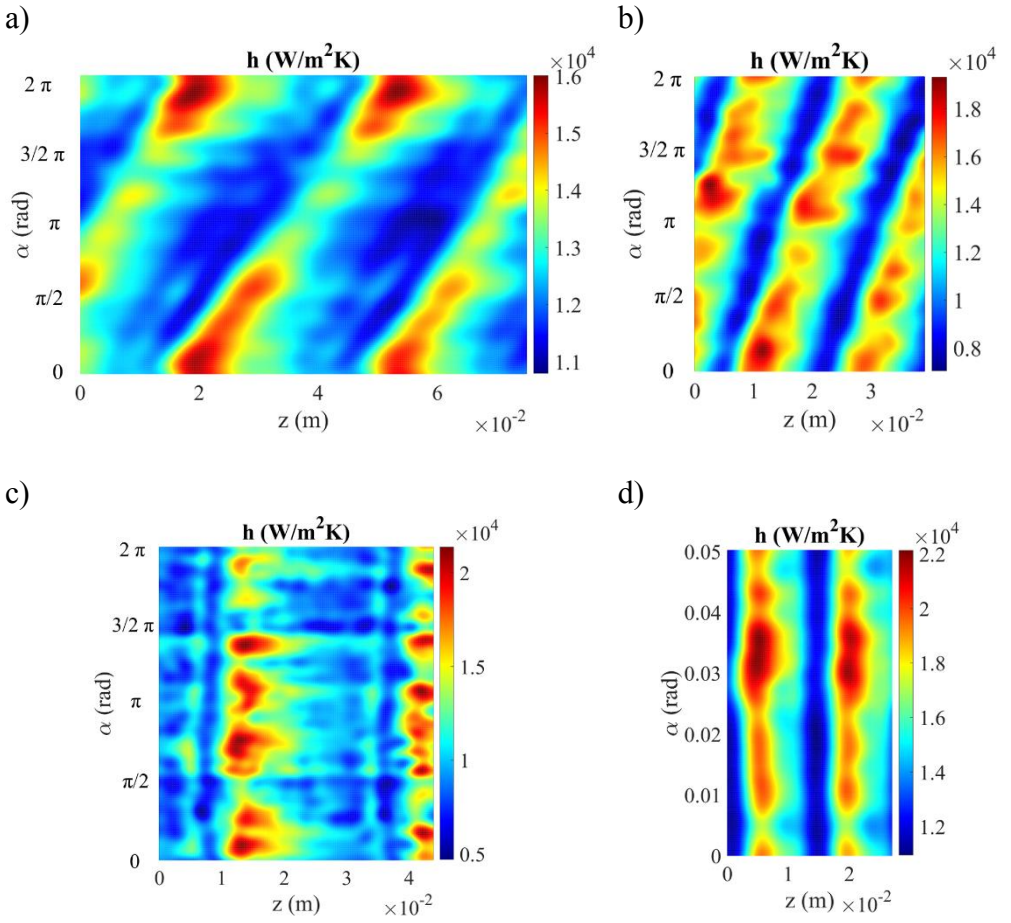

***Figure 14.9**: Restored internal convective h heat transfer distribution at Re= 16000 for a) H32 b) H16 c) T32 d) T16*

Concluding, transverse corrugation seems to perform better than helical in terms of enhancement of thermal performances. In fact, when comparing the internal convective heat transfer coefficient *h* obtained at the same Re and the same corrugation pitch, the transverse geometry shows always consistently

higher values. For pitch of 32 mm, *h* values of transverse corrugations showed an average increase 29% higher than helical one, while for pitch= 16mm of about 10%. Finally, in view of what above reported, it is possible to state that the results obtained by the local measurements of the surface temperature distribution and of the internal convective heat transfer coefficient *h* allow to confirm all the results obtained with the average measurements and confirms another time that corrugations can be considered an interesting strategy for the enhancement of the thermal performances of a tubular heat exchanger, also in turbulent conditions.

In Figure 14.10, Figure 14.11, Figure 14.12 is reported the local Nu in position $\alpha = \pi$ as function of z foe every pipe tested for the cases with $Re=4\cdot10^3$, $Re=10^4$ and $1.6\cdot10^4$, respectively.

The values of Nusselt reported can be considered in good accordance with the one reported in Figure 14.1, confirming the results achieved in both the analysis. Indeed, if the Nu values between corrugations are considered in Figure 14.10, Figure 14.11 and Figure 14.12, it is possible to observe that they are comparable to the ones in in Figure 14.1, that are measured in intermediate position between corrugation as well.

Comparing these images with the one reported in Figure 14.4, that reports the position of the corrugation on the pipes wall, it is possible to note that for all the cases, the local Nusselt number suddenly decreases after the corrugation, while it reaches its maximum value in the areas between the corrugations. With the

same Re and corrugation type, it is also possible to observe that for smaller corrugation pitch, the trend of the local Nusselt number appears smoother in the areas between corrugations, maintaining values that tend to be close to its maximum, while for the bigger pitches, it tends to gradually decrease until the subsequent corrugation, generating inhomogeneities in thermal performances. This behaviour confirms what was previously observed for the values of *h*.

Moreover, for both helical and transverse geometry, smaller pitches generate greater maximum values of local Nusselt number for same *Re*. Finally, for the same pitches and *Re*, transverse geometry seems to better perform from the thermal point of view, generating higher local Nusselt number in comparison to the helical geometry.

Finally, the local measurements, as well as the average ones, demonstrated that the corrugation, in every geometry tested, could be an effective tool in the enhancement of the heat transfer capability of the heat exchanger also in turbulent conditions. For this reason, their applicability can be considered also in cases where the food fluid is flowing in turbulent condition and an increase of the heat transfer capability of the process is required. Moreover, their ease implement-ability and their low cost, make corrugated pipes an appreciable tool both by food manufacturers in order to increase the performance of units already in use, and by machinery manufacturers as an energy and thermal optimisation solution for new equipment design.

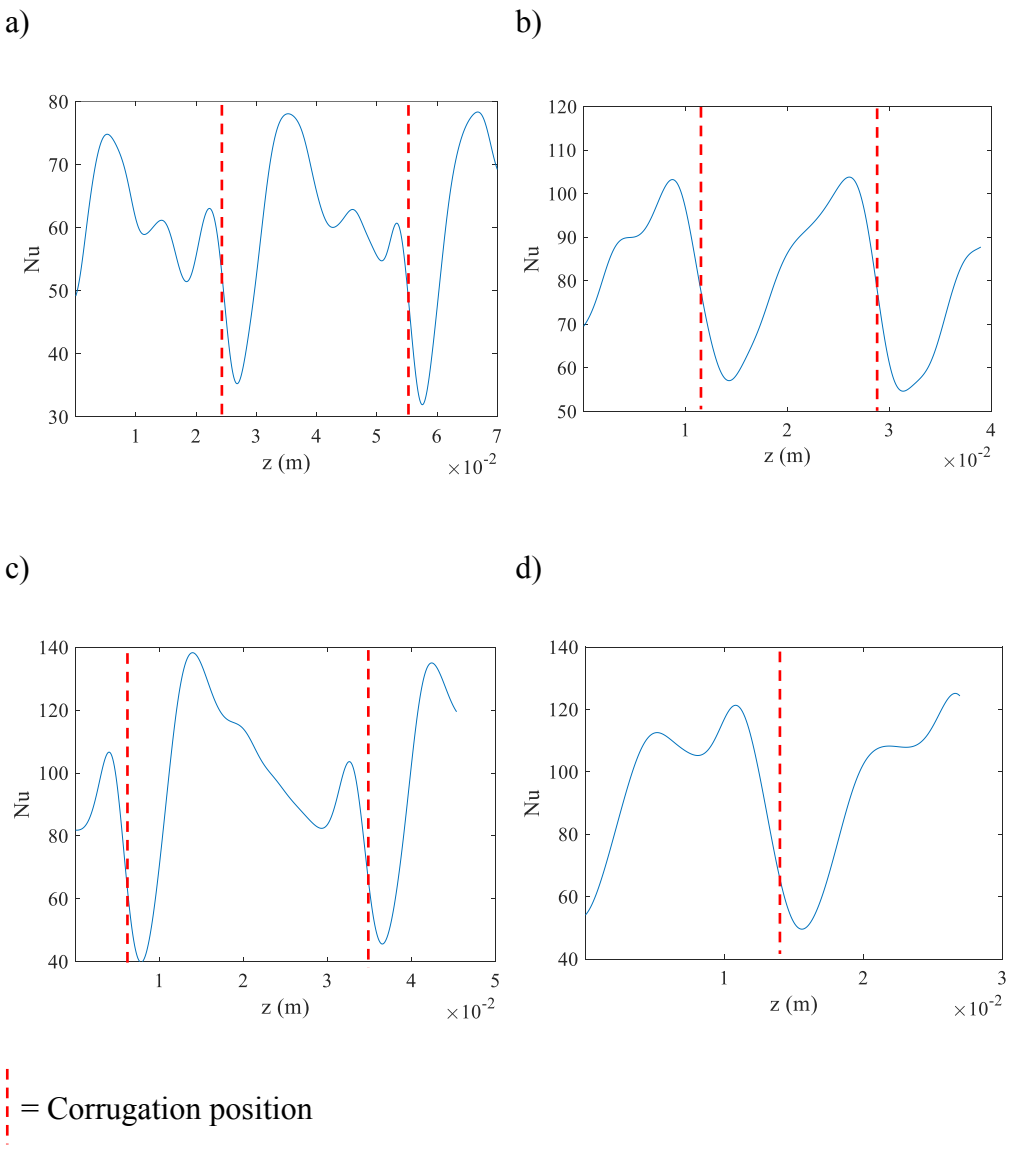

Figure 14.10: *Local Nu at α=π as function of z at Re=4000 for a) H32 b) H16 c) T32 d) T16*

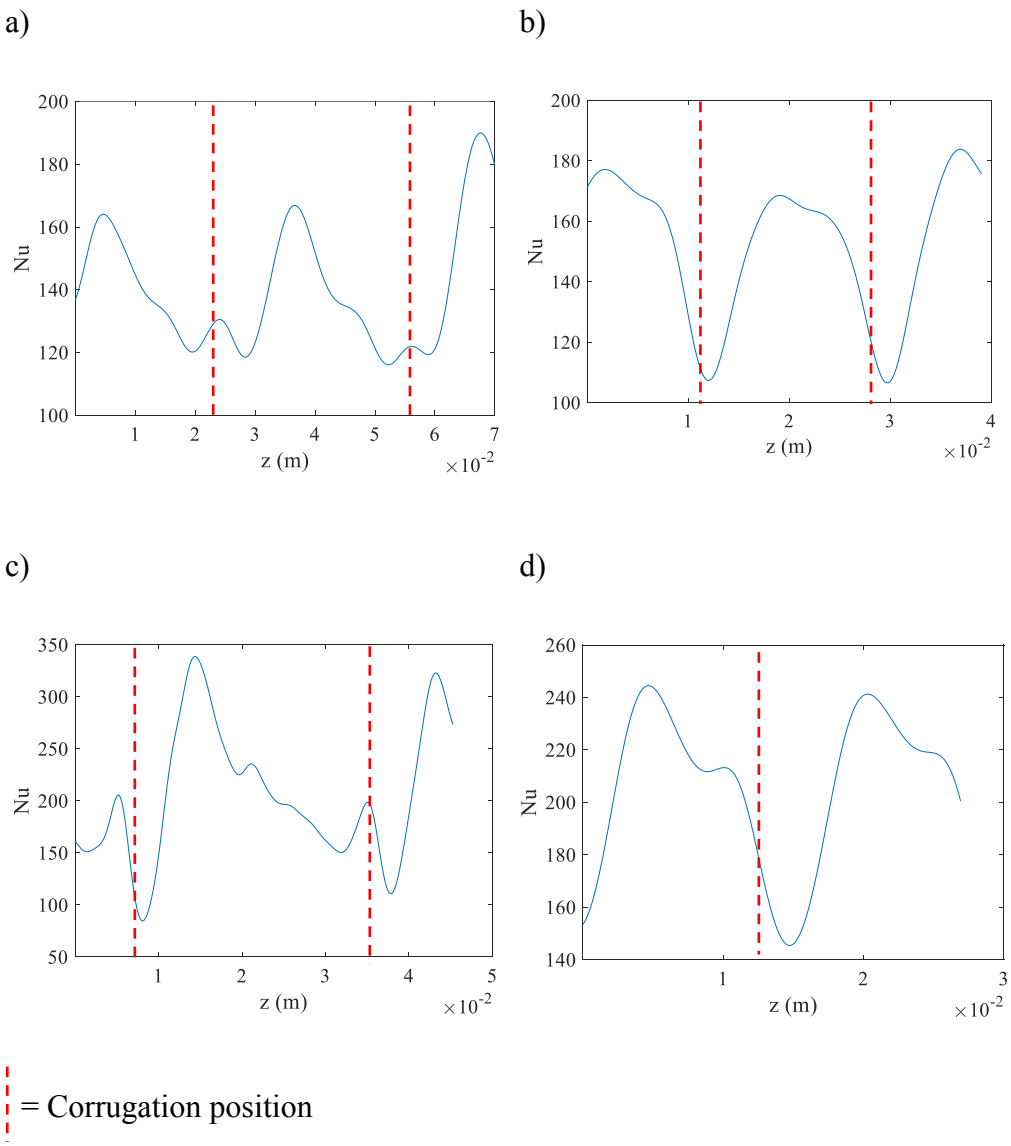

***Figure 14.11**:Local Nu at α=π as function of z at Re=10000 for a) H32 b) H16 c) T32 d) T16*

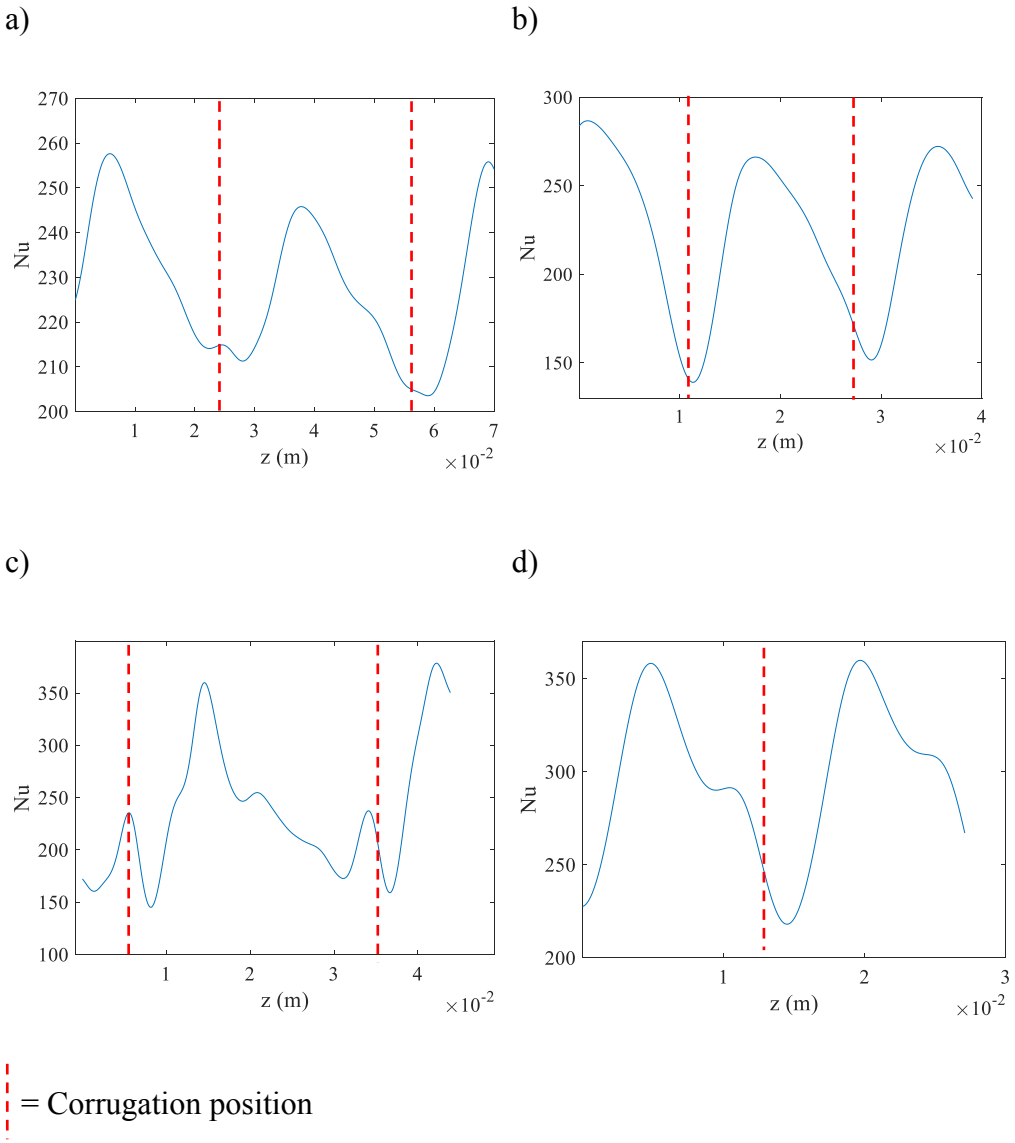

***Figure 14.12**: Local Nu at α=π as function of z at Re=16000 for a) H32 b) H16 c) T32 d) T16*

CHAPTER 15: Closure

In this part of the thesis, the effect on the thermal performances of different type of corrugation on the pipe wall have been characterized both from an average and a local point of view. In specific, two pipes with wall helical corrugation, one with corrugation pitch of 16 mm (H16) and one with corrugation pitch (H32), two pipes with wall transverse corrugation, one with corrugation pitch of 16 mm (T16) and one with corrugation pitch of 32 mm (T32) were tested.

Average analysis showed a value of *Nu* about 3 times higher than the smooth pipe, used as reference in these tests. Transverse corrugations showed also a better performance respect to the helicoidal one, specially respect to H32, showing Nu values about 1.5 time higher. For the transverse geometry, no significative differences were observed from the variation of the pitch of corrugation, while for helical geometry the reductio of the pitch seems to cause an increase in thermal performances. The evaluation of the effect of the different

geometries, both the thermal enhancement effect and the pressure drop caused by the corrugation showed that the transverse corrugation, in turbulent conditions, could represent the best solution since its efficiency η reached the higher values.

IR analysis allowed to deeply investigate the effect of corrugation from the local point of view. The corrugations generate an overall increase in the convective heat transfer coefficient on the inner wall of the pipe. However, this effect is less intense in the region of fluid that has just passed the corrugation, and then increases dramatically immediately afterwards. Furthermore, it could be seen that for corrugations with a larger pitch (H32 and T32), the coefficient *h,* once it has reached its maximum value after the corrugation, undergoes a gradual decrease until the next corrugation. Since in the geometries with a smaller corrugation pitch (H16 and T16), the distance needed by the fluid to reattach to the internal wall is higher than the distance between corrugation, this phenomenon disappears. In these cases, the absence of such behaviour generates greater homogeneity in the distribution of *h*. The local analysis also confirmed that the best performance from a thermal point of view is achieved by the transverse corrugation geometry and the smaller pitches, making the T16 geometry the best one.

Finally, once the radial coordinate α was fixed, it was also possible to observe the local trend of Nu values as a function of z, again confirming what was previously observed for *h*.

Concluding, in this analysis referred to the effect of the corrugation in turbulent regime, it is possible to state that the transverse corrugation showed the best performances. For helical corrugation, the difference in pitches seems to be relevant, favouring the geometry with the smaller one.

More in general, all the corrugations showed an increased heat transfer capability if compared to the smooth pipe, demonstrating their applicability in food industry when the enhancement of the efficiency of the heat exchangers is required, also in case of turbulent flow of the product treated.

References

[1] F. Carlsson, M. Sen, and L. Lofdahl, “Analytical studies of flow effects due to vibrating walls,” *J Fluid Mech*, 2002.

[2] L. Léal *et al.*, “An overview of heat transfer enhancement methods and new perspectives: Focus on active methods using electroactive materials,” *Int. J. Heat Mass Transf.*, vol. 61, pp. 505–524, 2013.

[3] R. L. Webb, *Principles of enhanced heat transfer*. 1994.

[4] A. Dewan, P. Mahanta, K. S. Raju, and P. S. Kumar, “Review of passive heat transfer augmentation techniques,” *Proc. Inst. Mech. Eng. Part A J. Power Energy*, vol. 218, no. 7, pp. 509–527, 2004.

[5] TheodoremL. Bergman Adrienne S. Lavine, *Fundamentals of heat and mass transfer*, vol. 7, no. 1. 2015.

[6] R. Kiml, A. Magda, S. Mochizuki, and A. Murata, “Rib-induced secondary flow effects on local circumferential heat transfer distribution inside a circular rib-roughened tube,” *Int. J. Heat Mass Transf.*, vol. 47, no. 6–7, pp. 1403–1412, 2004.

[7] Z. S. Kareem, M. N. Mohd Jaafar, T. M. Lazim, S. Abdullah, and A. F. Abdulwahid, “Passive heat transfer enhancement review in corrugation,” *Exp. Therm. Fluid Sci.*, vol. 68, pp. 22–38, 2015, doi: 10.1016/j.expthermflusci.2015.04.012.

[8] S. Rainieri and G. Pagliarini, “Convective heat transfer to orange juice in smooth and corrugated tubes,” *Int. J. Heat Technol*, vol. 15, no. 2, pp. 69–75, 1997.

[9] B. Ničeno and E. Nobile, “Numerical analysis of fluid flow and heat transfer in periodic wavy channels,” *Int. J. Heat Fluid Flow*, vol. 22, no. 2, pp. 156–167, 2001, doi: 10.1016/S0142-727X(01)00074-1.

[10] A. M. Guzman and C. H. Amon, “Dynamical flow characterization of transitional and chaotic regimes in converging–diverging channels,” *J. Fluid Mech.*, vol. 321, pp. 25–57, 1996.

[11] G. Wang and S. P. Vanka, “Convective heat transfer in periodic wavy passages,” *Int. J. Heat Mass Transf.*, vol. 38, no. 17, pp. 3219–3230, 1995, doi: 10.1016/0017-9310(95)00051-A.

[12] A. García, J. P. Solano, P. G. Vicente, and A. Viedma, “The influence of artificial roughness shape on heat transfer enhancement: Corrugated

tubes, dimpled tubes and wire coils," *Appl. Therm. Eng.*, vol. 35, no. 1, pp. 196–201, 2012, doi: 10.1016/j.applthermaleng.2011.10.030.

[13] S. Rainieri, A. Farina, and G. Pagliarini, "Experimental investigation of heat transfer and pressure drop augmentation for laminar flow in spirally enhanced tubes," *Proc. 2nd Eur. Therm. 14th UIT Natl. Heat Transf. Conf. Ed.*, pp. 203–209, 1996.

[14] K. Bilen, M. Cetin, H. Gul, and T. Balta, "The investigation of groove geometry effect on heat transfer for internally grooved tubes," *Appl. Therm. Eng.*, vol. 29, no. 4, pp. 753–761, 2009, doi: 10.1016/j.applthermaleng.2008.04.008.

[15] C. Chen, Y. T. Wu, S. T. Wang, and C. F. Ma, "Experimental investigation on enhanced heat transfer in transversally corrugated tube with molten salt," *Exp. Therm. Fluid Sci.*, vol. 47, pp. 108–116, 2013, doi: 10.1016/j.expthermflusci.2013.01.006.

[16] E. Bellos, C. Tzivanidis, K. A. Antonopoulos, and G. Gkinis, "Thermal enhancement of solar parabolic trough collectors by using nanofluids and converging-diverging absorber tube," *Renew. Energy*, vol. 94, pp. 213–222, 2016, doi: 10.1016/j.renene.2016.03.062.

[17] G. Pagliarini, P. Vocale, A. Mocerino, and S. Rainieri, "Second principle approach to the analysis of unsteady flow and heat transfer in a tube with arc- shaped corrugation," *J. Phys. Conf. Ser.*, vol. 755, no. 1, 2016, doi: 10.1088/1742-6596/755/1/011001.

[18] M. Li, T. S. Khan, E. Al-Hajri, and Z. H. Ayub, “Single phase heat transfer and pressure drop analysis of a dimpled enhanced tube,” *Appl. Therm. Eng.*, vol. 101, pp. 38–46, 2016, doi: 10.1016/j.applthermaleng.2016.03.042.

[19] S. Rainieri and G. Pagliarini, “Convective heat transfer to temperature dependent property fluids in the entry region of corrugated tubes,” *Int. J. Heat Mass Transf.*, vol. 45, no. 22, pp. 4525–4536, 2002, doi: 10.1016/S0017-9310(02)00156-4.

[20] F. Bozzoli, L. Cattani, and S. Rainieri, “Effect of wall corrugation on local convective heat transfer in coiled tubes,” *Int. J. Heat Mass Transf.*, vol. 101, pp. 76–90, 2016, doi: 10.1016/j.ijheatmasstransfer.2016.04.106.

[21] S. Rainieri, F. Bozzoli, L. Cattani, and G. Pagliarini, “Compound convective heat transfer enhancement in helically coiled wall corrugated tubes,” *Int. J. Heat Mass Transf.*, vol. 59, no. 1, pp. 353–362, 2013, doi: 10.1016/j.ijheatmasstransfer.2012.12.037.

[22] S. Rainieri, F. Bozzoli, L. Cattani, and G. Pagliarini, “Experimental investigation on the convective heat transfer enhancement for highly viscous fluids in helical coiled corrugated tubes,” *J. Phys. Conf. Ser.*, vol. 395, no. 1, 2012, doi: 10.1088/1742-6596/395/1/012032.

[23] Y. Hong, J. Du, S. Wang, and S. M. Huang, “Heat transfer and flow behaviors of a wavy corrugated tube,” *Appl. Therm. Eng.*, vol. 126, pp.

151–166, 2017, doi: 10.1016/j.applthermaleng.2017.07.135.

[24] S. K. Saha, S. Bhattacharyya, and P. K. Pal, “Thermohydraulics of laminar flow of viscous oil through a circular tube having integral axial rib roughness and fitted with center-cleared twisted-tape,” *Exp. Therm. Fluid Sci.*, vol. 41, pp. 121–129, 2012, doi: 10.1016/j.expthermflusci.2012.04.004.

[25] S. K. Saha, “Thermohydraulics of laminar flow through rectangular and square ducts with axial corrugation roughness and twisted tapes with oblique teeth,” *J. Heat Transfer*, vol. 132, no. 8, 2010.

[26] S. K. Saha, “Thermohydraulics of turbulent flow through rectangular and square ducts with axial corrugation roughness and twisted-tapes with and without oblique teeth,” *Exp. Therm. Fluid Sci.*, vol. 34, no. 6, pp. 744–752, 2010, doi: 10.1016/j.expthermflusci.2010.01.003.

[27] K. Hwang *et al.*, “Heat transfer and pressure drop characteristics of enhanced titanium tubes,” *Desalination*, vol. 159, no. 1, pp. 33–41, 2003, doi: 10.1016/S0011-9164(03)90043-9.

[28] P. Poredoš, T. Šuklje, S. Medved, and C. Arkar, “An experimental heat-transfer study for a heat-recovery unit made of corrugated tubes,” *Appl. Therm. Eng.*, vol. 53, no. 1, pp. 49–56, 2013, doi: 10.1016/j.applthermaleng.2013.01.004.

[29] J. A. Meng, X. G. Liang, Z. J. Chen, and Z. X. Li, “Experimental study on convective heat transfer in alternating elliptical axis tubes,” *Exp.*

Therm. Fluid Sci., vol. 29, no. 4, pp. 457–465, 2005, doi: 10.1016/j.expthermflusci.2004.04.006.

[30] A. Barba, S. Rainieri, and M. Spiga, "Heat transfer enhancement in a corrugated tube," vol. 1933, no. 02, 1933.

[31] V. D. Zimparov, N. L. Vulchanov, and L. B. Delov, "Heat transfer and friction characteristics of spirally corrugated tubes for power plant condensers—1. Experimental investigation and performance evaluation," *Int. J. Heat Mass Transf.*, vol. 34, no. 9, pp. 2187–2197, 1991.

[32] Y. Dong, L. Huixiong, and C. Tingkuan, "Pressure drop, heat transfer and performance of single-phase turbulent flow in spirally corrugated tubes," *Exp. Therm. Fluid Sci.*, vol. 24, no. 3–4, pp. 131–138, 2001, doi: 10.1016/S0894-1777(01)00047-4.

[33] H. Cui, X. Yuan, and Z. Yao, "Experimental investigation of heat transfer and pressure drop characteristics of w-type spirally fluted tubes," *Exp. heat Transf.*, vol. 16, no. 3, pp. 159–169, 2003.

[34] European Hygienic Engineering & Design Group, "Hygienic Design Principles," *EHEDG Guidel.*, vol. 8, no. March, p. 13, 2018, [Online]. Available: https://www.ehedg.org/guidelines/free-documents/?tx_ehedgguidelines_guidelines%5Bfiletodownload%5D=file%3A6700&tx_ehedgguidelines_guidelines%5Bguideline%5D=8&tx_ehedgguidelines_guidelines%5Btitel%5D=Hygienic design

principles&tx_ehedgguidelines_guidelines.

[35] L. Cattani, F. Bozzoli, S. Rainieri, and G. Pagliarini, "Experimental investigation on the convective heat transfer enhancement in tubes with cross-helix profile wall corrugation," *J. Phys. Conf. Ser.*, vol. 755, no. 1, 2016, doi: 10.1088/1742-6596/755/1/011001.

[36] T. Astarita and G. M. Carlomagno, *Infrared thermography for thermo-fluid-dynamics*. Springer Science & Business Media, 2012.

[37] B. Cyganek and J. P. Siebert, *An introduction to 3D computer vision techniques and algorithms*. John Wiley & Sons, 2011.

[38] K. Pavelka, S. Ruzicka, and Z. Bila, "Photo-Plan Creation of Cylindrical Objects," *Int. Arch. Photogramm. Remote Sens. Spat. Inf. Sci.*, vol. 42, p. 2, 2013.

[39] F. Bozzoli, L. Cattani, G. Pagliarini, and S. Rainieri, "Infrared image filtering applied to the restoration of the convective heat transfer coefficient distribution in coiled tubes," *Opto-Electronics Rev.*, vol. 23, no. 1, pp. 109–117, 2015.

[40] J. Beck, "Beck, J.," *Inverse Heat Conduction Ill-posed problems*. pp. 137-157,179-180,198-211, 2011.

[41] D. A. Murio, *The mollification method and the numerical solution of ill-posed problems*. John Wiley & Sons, 1993.

[42] F. S. V Bazán, L. Bedin, and F. Bozzoli, "Numerical estimation of convective heat transfer coefficient through linearization," *Int. J. Heat*

Mass Transf., vol. 102, pp. 1230–1244, 2016.

[43] V. A. Morozov, *Methods for solving incorrectly posed problems*. Springer Science & Business Media, 2012.

CHAPTER 16: Final remarks

The challenge of the thermal and energetic optimization of heat exchange processes can be considered a topic of great interest for the food industry, since they represent the most energetic demanding operations in this sector.

Therefore, in this thesis, solutions for achieving these goals in three different heat exchange processes of food production were proposed, validated, applied and the results produced by their application were analysed.

Specifically, in Part I, the problem of the characterization of the thermal performances of a triple-tube heat exchanger (TTHE) was addressed for creating a tool allowing correct thermal sizing of this kind of devices, promoting their enhanced thermal and energetic efficiency. To achieve this goal, the investigation was intended to enable a robust procedure of estimation of the heat transfer correlation for the product side Nusselt number, using an innovative approach for this kind of equipment: the parameter estimation.

The choice of developing and validating an algorithm for defining a correlation for heat transfer for a TTHE, instead the form of the correlation itself, was given by the specificity nature of the correlation to any application of the tested device. Validating the entire procedure of estimation, it is possible to have available a tool that could be applied to any other device for achieving the same goal. This procedure of estimation was validated through its application to both synthetic and experimental data acquired from TTHE for treating highly viscous fluid food, showing a great potential for achieving the proposed aim, since with a reasonable low number of experimental data it is possible to obtain a valid correlation for the Nusselt number on the product side.

For this work, it is possible to conclude that this innovative approach can be considered a powerful tool for obtaining TTHE with an enhanced thermal efficiency. Moreover, this technique can be used by the producer both for sizing new apparatus and eventually by the owner for modifying existing units to obtain better performances.

In the Part II of the thesis, the author focused on the thermal and energetic optimization of the alcoholic fermentation phase in oenological production. The alcoholic fermentation is an exothermic reaction and, during its proceeding, causes an increase of the temperature of the grape must. Since temperature is fundamental for a successful fermentation in terms of organoleptic quality of the wine, this increase in temperature is usually controlled by an external cooling jacket placed on the external wall of the fermenting tank, inside which a cooling

fluid flows conveyed by a pump. The classical temperature control method is thus totally active and, needs an external energy source, for this reason its replacement with a total passive one could represents a great solution to enhance the energy efficiency of the entire production. The author proposed the use of an innovative device based on the heat pipe technology for achieving this goal. The new solution was tested in a simulated fermentation phase, and it showed a great potential despite it thermal sizing was not perfect for the experimental case; indeed it allowed a more uniform temperature distribution inside the must during the entire simulation of the fermentation. Since the implementation of the new cooling device proved feasible, for improving it and obtaining its correct thermal sizing, the author proposed two strategies. The first one was based on the calculation of the number of heat pipes composing the innovative device while the second one allows the definition of the geometrical dimensions of a device based on a single heat pipe.

Finally, since the knowledge of the heat release curve during fermentation process could be fundamental for improving the thermal sizing of the new device and enhance the energy efficiency of the whole process of production, a tool for estimating it, based on the measurement of the grape must temperature and the solution of the relative inverse problem, was developed and validated.

In this case also, the proposed solutions for the enhancement of the energy efficiency and the effectiveness of the heat exchange phase showed a great potential. Another time, the innovative passive solutions proposed can be

considered an effectiveness and innovative strategy for achieving the goal prefixed.

Finally, in the Part III, the author focused on the analysis of the effect of 4 different corrugations in pipes for heat exchangers for food industry, under turbulent flow regime. Two pipes have a wall helical corrugation with depth of 1 mm, one (H16) with corrugation periodicity of 16 mm and the other one (H32) with corrugation periodicity of 32 mm. Two pipes have a wall transverse corrugation with depth of 1.5 mm, one (T16) with corrugation periodicity of 16 mm and the other one (T32) with corrugation periodicity of 32 mm.

The effects of the corrugation on the thermal exchange rate were studied under both the average point of view and the local one. For the local analysis, the IR measurements technique was adopted in order to obtain the distribution of the temperature on the external surface of the pipe. With this distribution, the inverse problem of heat transfer through the pipe wall was solved in order to obtain the local distribution of the convective heat transfer coefficient h on the internal side of the pipe wall.

The analysis performed allowed to state that all the corrugations showed increased thermal exchange capability if compared to the smooth pipe. In particular, the transverse corrugations, in the condition tested, have the best performances from the thermal and fluid dynamic point of view. Moreover, the local analysis showed that the use of smaller pitches allows to obtain a more

uniform distribution of enhanced *h* than the bigger one, increasing the thermal beneficial effects.

In conclusion, it is possible to state that, in all the three heat exchange processes of the food industry analysed, the innovative passive solutions, proposed to increase the thermal and energy efficiency of these operations, have shown positive results.

Both passive approaches used for the enhancement of the efficiency of the heat exchange in food processes, i.e., an improved characterisation of the thermal performance of existing devices, and the replacement of devices in use with new, more thermally and energy efficient ones, demonstrated a great flexibility and adaptability within the food industry panorama. Moreover, in the cases studied, this strategy could be considered as a “low cost” one, since the realization of the improvements showed can be obtained with very limited investments by the producers. In author opinion, these aspects make the solutions presented in this thesis a very interesting tool for optimising performance in the heat exchange field of the food industry, aimed on the one hand at the improvement of its energy efficiency to counteract the continuous energy rising cost, and on the other aimed at increasing the quality of the finished product.

The publications connected to the topics illustrated in this work are:

- Thermal characterisation of Triple Concentric Tube Heat Exchangers by applying parameter estimation: Direct problem implementation, Vocale, P., Malavasi, M., Cattani, L., Bozzoli, F., Pelacci, M., Rainieri, S., Journal of Physics: Conference Series, 2021, 1868(1), 012022.
- Thermal characterisation of triple tube heat exchangers by parameter estimation approach, Malavasi, M., Cattani, L., Vocale, P., Bozzoli, F., Rainieri, S., International Journal of Heat and Mass Transfer, 2021, 178, 121598.
- Thermal Performance Analysis of Triple Heat Exchangers via the Application of an Innovative Simplified Methodology Vocale, P., Malavasi, M., Cattani, L., Bozzoli, F., Rainieri, S. International Journal of Heat and Technology, 2022, 40(1), pp. 167–173.
- Development of an innovative temperature control system in a fermenter: Application to the case of the wine industry, Malavasi, M., Cattani, L., Bozzoli, F., Rainieri, S., Journal of Physics: Conference Series, 2022, 2177(1), 012036.
- Model Development of a Thermosyphon Heat Pipe for the Temperature Management in a Wine Fermenter Tank, Malavasi, M., Cattani, L., Bozzoli, F., Rainieri, S., Mathematical Modelling of Engineering Problems, 2022, 9(4), pp. 857–861.

Acknowledgements

Giunto a questo punto, è senza dubbio un piacere, ancor prima che doveroso, ringraziare chi mi è stato a fianco durante questi tre anni.

In primis, vorrei ringraziare i miei tutor Prof.ssa Sara Rainieri e Prof. Fabio Bozzoli per il mai assente supporto e incoraggiamento durante l'intero periodo di dottorato.

Un ulteriore ringraziamento è senza dubbio destinato all'azienda MBS s.r.l., specialmente nella figura di Gian Luca Bertoluzzi, per il supporto tecnico nell'attività sperimentale e alla regione Emilia-Romagna nell'ambito del "Piano triennale alte competenze per la ricerca e il trasferimento Tecnologico" per il supporto finanziario.

Un grazie speciale è per il Prof. Luca Cattani: mentore ma soprattutto amico.

Grazie anche all' Ing. Giampaolo Betta, con il quale ho condiviso lavoro, tempo e vita in questi tre anni e, al cui esempio, non ho mai dovuto, né voluto, rinunciare: un riferimento che può vantare tutta la mia stima.

Un grazie va anche al mio collega di percorso Luca Pagliarini, con il quale ho condiviso gioie e difficoltà.

Infine, certamente non per ordine di importanza, un ringraziamento, mai sufficientemente grande, è per i miei genitori, Ivana e Valter, esempio di vita e costante supporto in tutto ciò che faccio.